TẠP CHÍ KHOA HỌC
TRƯỜNG ĐẠI HỌC QUY NHƠN

QUY NHON UNIVERSITY
JOURNAL OF SCIENCE

KHOA HỌC TỰ NHIÊN VÀ KỸ THUẬT
NATURAL SCIENCES AND ENGINEERING

CONTENTS

Thuốc trừ sâu: mục tiêu, cơ chế hoạt động và đánh giá rủi ro

Yves Combarnous[1], Nguyễn Thị Mộng Điệp[2,*]

[1]Đơn vị Sinh lý sinh sản và Hành vi (PRC), INRAe, CNRS, Trường Đại học Tours, 37380 Nouzilly, Pháp
[2]Khoa Khoa học Tự nhiên, Trường Đại học Quy Nhơn, Thành phố Quy Nhơn, tỉnh Bình Định, Việt Nam

TÓM TẮT

Thuốc trừ sâu (chủ yếu là thuốc diệt cỏ, diệt côn trùng, sâu và diệt nấm) được sử dụng để tiêu diệt một số loài thực vật, động vật hoặc vi sinh vật có hại cho nông nghiệp. Do những điểm tương đồng cơ bản trong tất cả các sinh vật sống, việc tấn công mục tiêu là các loài không mong muốn mà không ảnh hưởng đến những loài khác, kể cả con người là một thách thức. Theo quan điểm này, việc xác định chính xác các phân tử hoặc cơ chế tấn công mục tiêu của thuốc trừ sâu là vô cùng quan trọng để đánh giá rủi ro và phát triển các chế phẩm thuốc trừ sâu hiệu quả, ít gây nguy hiểm đến cây trồng, động vật hoang dã và con người. Bài báo này sẽ trình bày ngắn gọn về các nhóm thuốc trừ sâu phổ biến, cơ chế hoạt động cũng như độc tính của chúng đối với mục tiêu và tác dụng phụ có thể xảy ra đối với các thành phần của môi trường như quần thể côn trùng và thực vật, không khí, nước hoặc hệ sinh vật đất.

Từ khóa: *Đa dạng sinh học, thuốc trừ sâu, thuốc diệt cỏ, thuốc diệt côn trùng, thuốc diệt nấm.*

---

*Tác giả liên hệ chính.
Email: *nguyenthimongdiep@qnu.edu.vn*

Pesticides: targets, mechanisms of action, and risk assessment

Yves Combarnous[1], Thi Mong Diep Nguyen[2,*]

[1]*INRAe, CNRS, Tours University, Unité de Physiologie de la Reproduction & des Comportements (PRC) 37380 Nouzilly, France*
[2]*Faculty of Natural Sciences, Quy Nhon University, Quy Nhon city, Binh Dinh Province, Vietnam*

ABSTRACT

Pesticides (mainly herbicides, insecticides, and fungicides) are used to chemically combat certain plants, animals, or microorganisms perceived as harmful to agriculture. Due to the fundamental similarities in all living beings, it is challenging to target unwanted species without affecting others, including humans. In this perspective, precisely identify the molecules or mechanisms targeted by pesticides is of utmost importance for assessing risk and developing efficient pesticide preparations with limited damage to crops, wildlife and humans. This review will briefly present the group of common pesticides, their mechanisms of action as well as their toxic effects on the target and possible side effects on the components of the environment such as insects and plants populations, air, water, or soil biota.

Keyword: *Biodiversity, pesticides, herbicides, insecticides, fungicides.*

1. INTRODUCTION

Originally, the term pest was limited to "*Insects or small animals which damage crops or food supplies*".[1] With this first definition, only insecticides (meaning insect killer) and rodenticides (rodent killer in general) would be called pesticides. The definition has now been extended to "*Something resembling the pest (plague) in destructiveness especially, a plant or animal detrimental to humans or human concerns, such as agriculture or livestock production*".[2] With this definition, herbicides are included among pesticides, representing about 80% of their total use. Moreover, in the scientific literature, fungicides (fungi killers) and bactericides (bacteria killers) are now taken into consideration under the general term of "pesticide" as well as many specialized products such as molluscicides (snails and slugs killers), nematicides (nematodes killer), etc.

The pesticides are intended to protect crops by acting against deleterious weeds, insects (and other invertebrates), fungi, or microorganisms. It is obvious that the mechanisms of action against such a variety of targets should be different to retain the highest possible specificity to destroy the undesired species without negatively affecting the crop to be protected as well as humans and wildlife.[3] About a thousand chemical pesticides

---

employing more than a hundred unique mechanisms have been developed. One of the challenge is to have available strains resistant to the pesticides used against the organisms harmful to the crops.[3] Thus, it is of utmost importance to have good knowledge of the pesticides targets and mechanisms of action to protect crops without affecting wildlife and human health.
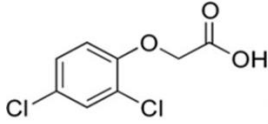
2. PESTICIDE FAMILIES (STRUCTURES AND TARGETS)

Numerous pesticides with various structures have been developed to combat different pests affecting crops (Table 1 and figure 1). In term of total quantity, around 55% are herbicides, 6% insecticides and 29% fungicides in order to control ~1800 weeds, ~10 000 insect pests, and ~80 000 fungi.
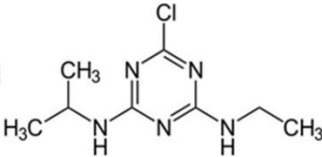
Table 1. Overview of the main classes of pesticides.

Chemical Class	Herbicides	Insecticides	Fungicides
Organochlorines	2,4-Dichlorophenoxyacetic acid (2,4-D) dichlorodiphenyltrichloroethane (DDT)	Endosulfan	Hexachlorobenzene
Organophosphates	Glyphosate	Diazinon, Omethoate, Dimethoate, Chlorpyrifos, Maldison, Methidathion	
Carbamates and thiocarbamides		Aldicarb, Carbofuran, Oxamyl, Carbaryl, Methomyl, Pirimicarb, Thiodicarb	
Metal-organic dithiocarbamates	Nabam (algicide)		Maneb, Mancozeb, Zineb
Urea derivatives	Diuron, Fenuron, Metoxuron, Miuron, Linuron, Monuron		
Heterocyclic compounds	Brassinazole	Triazines Atrazine	Strobilurins, Benzimidazole, Triazole derivatives
Phenol and nitrophenol derivatives	Dinocap	Dinoseb	Dinoseb
Fluorine-containing compounds	Phenylpyrazoles, Acetopyrazole	Fipronil	Dichlofluanid
Copper-containing compounds			Cuprous oxide, Copper sulfate, Copper octanoate. Copper hydroxide, Copper oxychloride sulfate

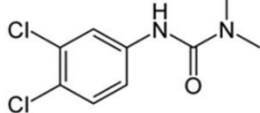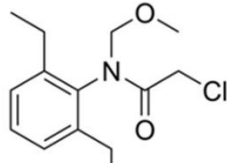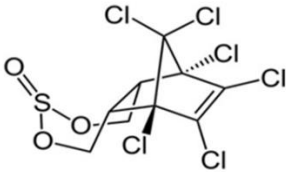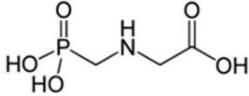|	
Synthetic pyrethroids	Allethrin, Alpha-cypermethrin, Beta-cyfluthrin, Bifenthrin Cypermethrin, Cyfluthrin, Deltamethrin, Esfenvalerate, Fluvalinate, Fenvalerate, Lambda-cyhalothrin, Pyrethrins
Neonicotinoids	Acetamiprid, Clothianidin, Imidacloprid, Thiamethoxam
Others	Spiroxamine
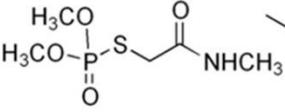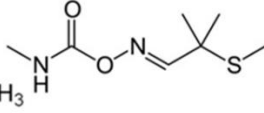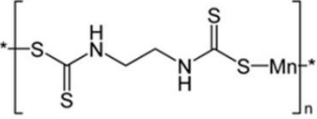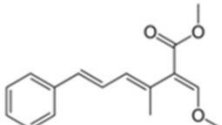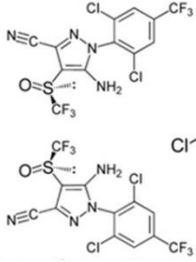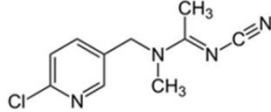
Figure 1. Chemical structure of a few pesticides.

2.1. Herbicides

Prominent herbicides belong to seven main families:

1) Photosystem II (PSII) inhibitors showing various cross-resistances among sub-families a) triazines (e.g. atrazine), pyridazinone (e.g. pyrazon), phenylcarbamate, b) anilide (e.g. propanil), ureas (e.g. diuron), c) benzothiadiazinone (e.g. bentazone), hydroxybenzonitrile (e.g. bromoxynil).

2) Superoxide promoters in chloroplasts such as paraquat and diquat.

3) Shikimimate inhibitors such as glycine derivatives (e.g. glyphosate).

4) Tubulin polymerization inhibitors such as dinitroanilines (e.g. pendimethalin).

5) Gibberillin pathway inhibitors such as chloroacetamides (e.g. acetochlor, S-metolachlor).

6) Auxin pathway disruptors such as phenoxy and benzoic acids (e.g. 2,4-dichloro-phenoxyacetic acid 2,4-D).

7) 4-hydroxyphenylpyruvate dioxygenase (HPPD) inhibitors (e.g. mesotrione).

2.2. Insecticides

Prominent chemical insecticides include organochlorines, organophosphates, carbamates, pyrethroids, and neonicoticoids.

1) Organophosphates (e.g. chlorpyriphos, acephate, dimethoate) and carbamates largely replaced organochlorines such as DDT. All operate through the inhibition of the acetylcholinesterase enzyme (AChE), causing acetylcholine to transfer nerve impulses endlessly, and then inducing weakness or paralysis. The toxicity of Organophosphates to vertebrates led to their partial replacement by the less toxic carbamates (e.g. carbofuran).

2) Pyrethroid insecticides (e.g. λ-cyhalothrin) are the synthetic counterparts of the pyrethrin pesticide, naturally found in chrysanthemums.

3) Neonicotinoids (e.g. imidacloprid) are insecticides of the neuro-active class structurally similar to nicotine[5-6] and target the nicotinic ACh receptor (nAChR).

2.3. Fungicides

Contact fungicides work by preventing fungal spores from germinating or penetrating into the plant from the leaf surface. They require care in the application as complete coverage is essential for effectiveness.

Penetrant fungicides work inside the plant and can be locally systemic or translocated throughout the plant. They can be preventative and curative.

The most common fungicides are:

1) Respiration inhibitors like succinate dehydrogenase inhibitors (SDHIs) or quinone outside inhibitors (QoIs).

2) Sterol biosynthesis inhibitors such as demethylation inhibitors DMIs which disrupt the fungi cell membrane and organelles after spore germination.

3) Fungicides are also necessary to combat fungi affecting animals, particularly humans (*Candida albicans* and others). These products for humans are pharmaceutical drugs and not « pesticides » as they are not dispersed in the environment to protect crops. Nevertheless, themselves or their metabolites can be found in the environment and exert toxic effects.

3. PESTICIDE CHEMICAL STRUCTURES AND MECHANISMS OF ACTION

Depending on their structure (Figure 1), the most commonly used pesticides can be divided into different chemical groups[7] with various usages (Table 1). The different biological targets are, of course, determined by the chemical structure of their targets. It is expected that chemical specificity would lead to biological specificity. Nevertheless, many of them exert non-specific oxidative stress.[8] A number of pesticides now consist of microorganisms or toxins from them, instead of chemicals.[9-10]

3.1. Herbicides

The main molecular targets of herbicides are the following:

1) Auxin (IAA) receptor (2,4-D, 2,4,5-T, phenoxy, and benzoic acids): The strong downstream stimulation of the auxin signaling pathway leads to uncontrolled growth of meristem cells, disorganizing the development of their vascular structures.[11] These pesticides kill most broad-leaf weeds such as plantain, common chickweed, dandelion, ground ivy, yellow wood sorrel, prostrate knotweed, or white clover.

2) Acetolactate synthase (sulfonylurea derivatives): The inhibition of this enzyme controlling the branched-chain amino acid biosynthetic pathway[12] in targeted weeds leads to their death by starvation and also breakdown, accelerated at a high light intensity, in the electron transport process.

3) D-1 plastoquinone-binding (QB) protein in photosystem II electron transport (triazines): These herbicides inhibit photosystem II by disturbing the photosynthetic electron transport through competition with the native plastoquinone for the D1 protein QB-specific site.[13-15]

4) BZR1 (Brassinazole Resistant 1) transcription factor (brassinazole triazole): Brassinazole inhibits brassinosteroid effects through binding to the BZR1 (Brassinazole Resistant 1) transcription factor in the targeted weeds.[16-18]

5) 5-enolpyruvylshikimate-3-phosphate synthase (glyphosate): Through this inhibition of 5-enolpyruvylshikimate-3-phosphate synthase, glyphosate disrupts the shikimic acid pathway, which is indispensable for the synthesis of aromatic amino acids, and thus for protein (including enzymes) expression in the targeted weeds[19] but also in a number of prokaryotes and fungi.[20-22]

3.2. Insecticides

The main targets of insecticides are the following:

1) Acetylcholinesterase (organophosphoruses, carbamates, neonicotinoids): The inhibition, by covalent binding to an active site serine residue of cholinesterase (AChE), at the cholinergic junctions of the target insect nervous system, leads to a sustained, lethal influx.[23-25] Together, the different insecticides can exert additive effects if acting the same way, or synergic effects if not.[26-27]

2) GABA-gated chloride channel (fipronil, endosulfan, lindane,): These compounds act as antagonists by stabilizing non-conducting conformations of the chloride channel and so antagonize the GABA action on insect neurons in a noncompetitive manner.[28-31]

3) Ca^{2+}, Mg^{2+} ATPase inhibitor (endosulfan): Endosulfan uncouples oxidative phosphorylation and inhibits the electron transport chain. The *in vivo* cytotoxic/insecticidal effects of endosulfan and its metabolites could be damaged mitochondrial bioenergetics.[32]

4) Cytochrome P450 monooxygenase induction (atrazine): atrazine increases cytochrome P450 monooxygenase activity by enhancing their oxidative activation to sulfoxide analogs with increased anticholinesterase activity, leading to increased toxicities of demeton-S-methyl, disulfoton, and dimethoate.[33] In contrast, atrazine may reduce omethoate toxicity by enhancing oxidative metabolic detoxification because it does not need oxidative activation.[34]

5) Antioxidant enzymes (organophosphoruses, diazinon): The inhibition of catalase (CAT), superoxide dismutase (SOD), glutathione peroxidase (GPx), glutathione S-transferase (GST), and Paraoxonases (PONs), which act as free radical scavengers, plays a complementary role in the effect of organophosphoruses, in particular for diazinon.

6) Insect midgut enzymes and transporters (*Bacilus thuringiensis* toxins): The Cry or Cyt toxins produced during the sporulation phase of the entomopathogenic bacteria *Bacilus thuringiensis (Bt)* are proteins with specific and efficient insecticidal activities.[35-36]

Different *Bt* strains do not produce the same Cry toxins, which affect insect according to their order: dipteran, coleopteran, lepidopteran, etc. In contrast the Cyt toxins show mainly dipteran specificity, being able to kill mosquitoes and black flies, and can exhibit synergy with Cry toxins in some insects.[37] Cry toxin destroys insects by interacting with key toxin receptors like aminopeptidase (APN), alkaline phosphatase (ALP), cadherin (CAD), or ATP-binding cassette transporters.[38] The genes encoding these endotoxins can be expressed by transgenic plants to be protected from insects[39-40] at least in countries not banning GMOs.[41-42]

3.3. Fungicides

The number and variety of fungi are enormous, so it isn't easy to specifically control them. Many fungicides have multisite effects to reduce the selection of resistant strains. Nevertheless, there are a few fungicides with specific targets:

1) Multisite: Amine and thiol metabolism (hexachlorobenzene): By inhibiting these pathways, this product, first introduced in 1945 and discontinued after 1972, slows fungi's growth rates and sporulation. The primary molecular sites of action of hexachlorobenzene in fungi are not well defined.

2) Cytochrome b (strobilurin): Strobilurin binds to the quinol oxidation (Q_o) site of cytochrome b to inhibit mitochondrial respiration.[43] Numerous other fungicides have been recently developed, starting from the strobilurin scaffold structure.[44]

3) Lanosterol 14-demethylase CYP51 (triazoles): The inhibitory effect of triazoles affects CYP51, a key enzyme for sterol biosynthesis in fungi[31-32] and, unfortunately, in animals.[45] There is, therefore, active research to design fungicides that do not cross-react with the host CYP51.[46]

4) Succinate dehydrogenase (pyrazole carboxamide): The inhibition of this enzyme by various pyrazole-phenyl carboxamide derivatives is particularly efficient in combating plant fungi, such as *Sclerotinia sclerotiorum*, *Rhizoctonia solani*, and *Botrytis cinerea*.[47] This new class of inhibitors allows to overcome the resistance of fungi against previously launched succinate dehydrogenase inhibitors.

4. OFF-TARGET ACTIONS OF PESTICIDES (RISK ASSESSMENT)

Life has only emerged once during earth's history, so all living organisms share common hereditary support (DNA), some genetic material, and biochemical and physiological mechanisms whose similarities are proportional to their phylogenetic closeness. Consequently, it is problematic to target weeds without affecting cultivated plants or to target herbivore insects without affecting pollinator insects. Moreover, it has been observed that numerous pesticides interact at molecular sites unrelated to their assigned targets and thus exhibit unexpected effects in unrelated species. These off-target effects are responsible for environmental and human health concerns.[48] Risk assessment is crucial to deciding about new and existing pesticides.[49]

4.1. Environmental concerns (Biodiversity)

Phenoxy herbicides impact broad-leaf weeds much more than grasses. Even when they are not targeted at all, soil microorganisms can be greatly affected by herbicides in addition to the identified target.[50-51]

Insecticides often affect non-target insects such as pollinator insects[52-55] but also soil microorganisms,[54] invertebrates other than insects (earthworms in particular[56]), and even vertebrates.[57]

From an environmental point of view, it is good that a lot of organophosphates do not persist in nature, but they also need to not disappear too quickly to be efficient, and have been modified toward this objective. The balance between environmental respect and efficacy is, of course, primordial. Many chemicals are no longer used due to their adverse impact on human health or the environment (*e.g.,* DDT, chlordane, and toxaphene).

In the late 1990s, neonicotinoids became increasingly scrutinized for their negative impact on the environment. They are highly suspected to be directly detrimental to bee colonies, and indirectly to birds due to the greatly reduced number of insects they feed on. This is why they are partially restricted in many European countries since the 2010's.

In agricultural practices, the treatment of plant seeds with pesticides and/or fungicides can cause adverse effects on soil flora through single and combined effects of them. For example, the seed dressing of winter wheat (*Triticum aestivum* L. var. Capo) by insecticides (neonicotinoid) and/ or fungicides (strobilurin and triazolinthione) significantly reduced the surface activity of earthworms.[56]

4.2. Human health concerns (Toxicology)

Research on toxicology aims at improving the knowledge of the field and developing new chemicals, assessing their efficiency and hazardousness, and regulating their usage.[4]

Hexachlorobenzene disrupts porphyrin metabolism by acting on catalytic sites through modification of sulfhydryl groups or substrate binding of the enzyme uroporphyrinogen decarboxylase. It inhibits the catalytic activity of uroporphyrinogen decarboxylase causing decarboxylation of uroporphyrinogen III to be deficient, leading to accumulation of uroporphyrin in the liver. Furthermore, cytochrome P-450 catalyzed metabolism of hexachlorobenzene produces electrochemically reactive metabolites that are covalently bound to proteins and DNA in the cells, causing irreversible damage. When the body is exposed to hexachlorobenzene, macrophages are attracted to organs such as the spleen, lungs, and skin, where they are activated by hexachlorobenzene through a chain of reactions involving innate immune cells. Evidence suggests that the importance of macrophages and granulocytes is due to gene expression profiles. Mediators secreted by these cells are directly involved in the adverse inflammatory response against hexachlorobenzene. In this way, T-cells can be activated through co-stimulatory or danger signals.

Diazinon, dieldrin, endosulfan, ivermectin, maneb, 1-methyl-4-phenyl-4-phenylpyridinium ion (MPP1), and rotenone affect Pg-P ATPase activity and modify its drug-expelling activity and, consequently, accentuate Parkinson's disease symptoms.[58] Diazinon is a prevalent compound and a food contaminant, absorbed by the gastrointestinal tract and quickly metabolized. High exposure to DZN induces the gene expression of antioxidant enzymes.

Atrazine may indirectly act as an estrogen activator and directly inhibit dopamine synthesis, and thereby reduce dopamine levels. Atrazine may also block feedback regulation, leading to increased prolactin levels and altered immune cell activation, including T-cell proliferation and antibody responses.

4.3. Risk assessment

The assessment process combines all the information from the toxicity tests (hazard) and the exposure information to evaluate the risk (risk = hazard x exposure).[59] It is a complex procedure with many actors. It is meant to ensure safety for operators, workers, bystanders, residents, consumers, non-target species as well as the environment, and to allow an efficient use of resources for risk assessment and risk management in the policy area of pesticides.[60]

There are now numerous large-scale studies for evaluating the risk assessment of pesticides in humans,[61-72] wildlife,[73-82] and ecosystems.[83-86]

Cocktail toxic effects of pollutants are well known.[72-73,87-88] How are effects of pesticide cocktails related to their mechanism of action? Intuitively, molecules with identical targets and mechanisms of action should exhibit additive effects. In contrast, molecules with an identical target but different mechanisms of action may exhibit either antagonist or synergic effects.[89-97] If toxic molecules act on different molecular targets or organs, the situation is even more complex[98-99] and difficult to anticipate.[72] Moreover, the surfactants used to help pesticide cell penetration can exert toxic effects by themselves.[100-103]

It is also essential to evaluate pesticides from an epidemiological point of view.[104] People are exposed intermittently to chemicals at different concentrations. This is why toxicology alone is insufficient to evaluate accurately the effects of pesticides on human health and must be associated with epidemiology. For example, the very wide use of glyphosate in many countries allowed the gathering of valuable epidemiological data which pointed to its responsability in some cancers. However, the large scale of these data can make them either valuable or suspicious, depending on how they are observed: while the International Agency for Research on Cancer saw a link between glyphosate and cancer, other regulatory entities considered no causal link was established.[105]

The use of pesticides is not only based on scientific authorities but has an important political dimension.[106] Industrial companies, non-governmental organizations (NGO) and national and international public agencies as well as politicians are involved in decision makings. Thus, the European Food Safety Authority (EFSA) developed a methodology by grouping pesticides to take cumulative risk assessment into consideration. However, Pesticide Action Network Europe (PAN), representing more than 600 NGOs, deemed these studies "unfit for purpose," because they did not establish that pesticides had "no impact to human health and particularly to the most vulnerable groups in the population". Complementary studies are being conducted and EFSA is currently working with the European Commission on this matter.

5. CONCLUSION

Pesticides are amidst fierce societal, economic, and political debates, which often blur scientific data. Many of them have already been banned in Vietnam and in many other parts of the world, such as in European or American countries, for being directly or indirectly harmful to the environment or human health. It mostly concerns the endocrine disruption caused by the older kinds of pesticides, such as: organochlorines, organophosphates, carbamates and Thiocarbamides. These scientific data about pesticides are not always as objective as they should be, and many are more or less oriented (not always consciously) to support the authors' convictions, whatever they are. The problem of pesticide use is so complex that absolute objectivity is almost impossible. The number of viewpoints (scientific, societal, economic, political) is too huge to provide simple conclusions that would be acceptable to everyone. In the present work, we have concentrated on scientific issues, but we are aware that it is not the whole story.

REFERENCES

1. "Pest" in Collins dictionnary, <https://www.collinsdictionary.com/dictionary/english/pest>, retrieved on 01/07/2022.

2. "Pest" in Merriam-Webster dictionary, <https://www.merriam-webster.com/dictionary/pest>, retrieved on 01/07/2022.

3. J. E. Casida. Pest toxicology: the primary mechanisms of pesticide action, *Chemical Research in Toxicology*, **2009**, *22*(4), 609-619.

4. J. E. Casida, R. J. Bryant. The ABCs of pesticide toxicology: amounts, biology, and chemistry, *Toxicology Research*, **2017**, *6*(6), 755-763.

5. Y. Zhang, D. Chen, Y. Xu, L. Ma, M. Du, P. Li, Z. Yin, H. Xu, X. Wu. Stereoselective toxicity mechanism of neonicotinoid dinotefuran in honeybees: New perspective from a spatial metabolomics study, *Science of the Total Environment*, **2022**, *809*, 151116.

6. K. Matsuda, M. Ihara, D. B. Sattelle. Neonicotinoid insecticides: Molecular targets, resistance, and toxicity, *Annual Review of Pharmacology and Toxicology*, **2020**, *60*, 241-255.

7. V. I. Lushchak, T. M. Matviishyn, V. V. Husak, J. M. Storey, K. B. Storey. Pesticide toxicity: a mechanistic approach, *EXCLI Journal*, **2018**, *17*, 1101-1136.

8. R. O. Sule, L. Condon, A. V. Gomes. A Common Feature of Pesticides: Oxidative Stress-The Role of Oxidative Stress in Pesticide-Induced Toxicity, *Oxidative Medicine and Cellular Longevity*, **2022**, *2022*, 5563759.

9. F. E. Helepciuc, A. Todor. EU microbial pest control: A revolution in waiting, *Pest Management Science*, **2022**, *78*(4), 1314-1325.

10. P. Mombert, B. Guijarro Diaz-Otero, J. L. Alonso-Prados. Study of the different evaluation areas in the pesticide risk assessment process: Focus on pesticides based on microorganisms, *EFSA Journal*, **2022**, *20*, e200412.

11. Y. Song. Insight into the mode of action of 2,4-dichlorophenoxyacetic acid (2,4-D) as an herbicide, *Journal of Integrative Plant Biology*, **2014**, *56*(2), 106-113.

12. R. A. LaRossa, J. V. Schloss. The sulfonylurea herbicide sulfometuron methyl is an extremely potent and selective inhibitor of acetolactate synthase in Salmonella typhimurium, *The Journal of Biological Chemistry*, **1984**, *259*(14), 8753-8757.

13. N. Ohad, J. Hirschberg. Mutations in the D1 subunit of photosystem II distinguish between quinone and herbicide binding sites, *Plant Cell*, **1992**, *4*(3), 273-282.

14. J. Kern, B. Loll, A. Zouni, W. Saenger, K.D. Irrgang, J. Biesiadka. Cyanobacterial photosystem II at 3.2 A resolution - the plastoquinone binding pockets, *Photosynthesis Research*, **2005**, *84*, 153-159.

15. A. Antonacci, F. L. Celso, G. Barone, P. Calandra, J. Grunenberg, M. Moccia, E. Gatto, M.T Giardi, V. Scognamiglio. Novel atrazine-binding biomimetics inspired to the D1 protein from the photosystem II of Chlamydomonas reinhardtii, *International Journal of Biological Macromolecules*, **2020**, *163*, 817-823.

16. T. Asami, Y.K. Min, N. Nagata, K. Yamagishi, S. Takatsuto, S. Fujioka, N. Murofushi, I. Yamaguchi, S. Yoshida. Characterization of brassinazole, a triazole-type brassinosteroid biosynthesis inhibitor, *Plant Physiology*, **2000**, *123*(1), 93-100.

17. C. Fan, G. Guo, H. Yan, Z. Qiu, Q. Liu, B. Zeng. Characterization of Brassinazole resistant (BZR) gene family and stress induced expression in Eucalyptus grandis, *Physiology and Molecular Biology of Plants*, **2018**, *24*(5), 821-831.

18. M. S. Kesawat, B. S. Kherawat, A. Singh, P. Dey, M. Kabi, D. Debnath, D. Saha, A. Khandual, S. Rout, Manorama, A. Ali, R. R. Palem, R. Gupta, A. A. Kadam, H. Kim, S. Chung, M. Kumar. Genome-Wide Identification and Characterization of the Brassinazole-resistant (BZR) Gene Family and Its Expression in the Various Developmental Stage and Stress Conditions in Wheat (Triticum aestivum L.), *International Journal of Molecular Sciences*, **2021**, *22*(16), 8743.

19. J. L. Rubin, C.G. Gaines, R.A. Jensen. Glyphosate inhibition of 5-enolpyruvylshikimate 3-phosphate synthase from suspension-cultured cells of nicotiana silvestris, *Plant Physiology*, **1984**, *75*(3), 839-845.

20. L. Leino, T. Tall, M. Helander, I. Saloniemi, K. Saikkonen, S. Ruuskanen, P. Puigbò. Classification of the glyphosate target enzyme (5-enolpyruvylshikimate-3-phosphate synthase) for assessing sensitivity of organisms to the herbicide, *The Journal of Hazardous Materials*, **2021**, *408*, 124556.

21. K. Haghani, A. H. Salmanian, B. Ranjbar, K. Zakikhan-Alang, K. Khajeh. Comparative studies of wild type Escherichia coli 5-enolpyruvylshikimate 3-phosphate synthase with three glyphosate-insensitive mutated forms: activity, stability and structural characterization, *Biochimica et Biophysica Acta*, **2008**, *1784*(9), 1167-1175.

22. M. J. Rainio, S. Ruuskanen, M. Helander, K. Saikkonen, I. Saloniemi, P. Puigbò. Adaptation of bacteria to glyphosate: a microevolutionary perspective of the enzyme 5-enolpyruvylshikimate-3-phosphate synthase, *Environmental Microbiology Reports*, **2021**, *13*(3), 309-316.

23. D. Vincent, R. Truhaut. Contribution to the study of the mechanism of the physiological action of the insecticide D.D.T .; D.D.T. and serum cholinesterase, *Comptes Rendus des Seances de la Societe de Biologie et de Ses Filiales*, **1947**, *141*(1-2), 65.

24. H. Futagawa, H. Takahashi, T. Nagao, S. Adachi-Akahane. A carbamate-type cholinesterase inhibitor 2-sec-butylphenyl N-methylcarbamate insecticide blocks L-type Ca2+ channel in guinea pig ventricular myocytes, *The Japanese Journal of Pharmacology*, **2002**, *90*(1), 12-20.

25. X. Shao, S. Xia, K. A. Durkin, J. E. Casida. Insect nicotinic receptor interactions in vivo with neonicotinoid, organophosphorus, and methylcarbamate insecticides and a synergist, *Proceedings of the National Academy of Sciences of the United States of America*, **2013**, *110*(43), 17273-17277.

26. L. T. Herbert, P. F. Cossi, J. C. Painefilu, G. C. Mengoni, C. M. Luquet, G. Kristoff. Acute neurotoxicity evaluation of two anticholinesterasic insecticides, independently and in mixtures, and a neonicotinoid on a freshwater gastropod, *Chemosphere*, **2021**, *265*, 129107.

27. A. Katic, V. Kasuba, N. Kopjar, B. T. Lovakovic, A. M. M. Cermak, G. Mendas, V. Micek, M. Milic, I. Pavicic, A. Pizent, S. Zunec, D. Zeljezic. Effects of low-level imidacloprid oral exposure on cholinesterase activity, oxidative stress responses, and primary DNA damage in the blood and brain of male Wistar rats, *Chemico-Biological Interactions*, **2021**, *338*, 109287.

28. J. R. Bloomquist. Chloride channels as tools for developing selective insecticides, *Archives of Insect Biochemistry and Physiology*, **2003**, *54*(4), 145-156.

29. Z. Soualah, A. Taly, L. Crespin, O. Saulais, D. Henrion, C. Legendre, H. Tricoire-Leignel, C. Legros, C. Mattei. GABAA Receptor Subunit Composition Drives Its Sensitivity to the Insecticide Fipronil, *Frontiers in Neuroscience*, **2021**, *15*, 768466.

30. Y. Ozoe. Ion channels and G protein-coupled receptors as targets for invertebrate pest control: from past challenges to practical insecticides, *Bioscience, Biotechnology, and Biochemistry*, **2021**, *85*(7), 1563-1571.

31. T. Nakao, S. Banba. Mechanisms underlying the selectivity of meta-diamides between insect resistance to dieldrin (RDL) and human gamma-aminobutyric acid (GABA) and glycine receptors, *Pest Management Science*, **2021**, *77*(8), 3744-3752.

32. R. K. Dubey, M. U. Beg, J. Singh. Effects of endosulfan and its metabolites on rat liver mitochondrial respiration and enzyme activities in vitro, *Biochemical Pharmacology*, **1984**, *33*(21), 3405-3410.

33. Y. Jin-Clark, M. J. Lydy, K.Y. Zhu. Effects of atrazine and cyanazine on chlorpyrifos toxicity in Chironomus tentans (Diptera: Chironomidae), *Environmental Toxicology and Chemistry*, **2002**, *21*(3), 598-603.

34. C. L. Sweeney, N. K. Smith, E. Sweeney, A. M. Cohen, J. S. Kim. Analysis of human serum and urine for tentative identification of potentially carcinogenic pesticide-associated N-nitroso compounds using high-resolution mass spectrometry, *Environmental Research*, **2022**, *205*, 112493.

35. J. V. Rie, S. Jansens, H. Hofte, D. Degheele, H. V. Mellaert. Specificity of Bacillus thuringiensis delta-endotoxins. Importance of specific receptors on the brush border membrane of the

mid-gut of target insects, *European Journal of Biochemistry*, **1989**, *186*(1-2), 239-247.

36. H. Hofte, H. R. Whiteley. Insecticidal crystal proteins of Bacillus thuringiensis, *Microbiology Reviews*, **1989**, *53*(2), 242-255.

37. M. Soberon, J. A. Lopez-Diaz, A. Bravo. Cyt toxins produced by Bacillus thuringiensis: a protein fold conserved in several pathogenic microorganisms, *Peptides*, **2013**, *41*, 87-93.

38. I. Alam, K. Batool, A.L. Idris, W. Tan, X. Guan, L. Zhang. Role of Lectin in the Response of Aedes aegypti Against Bt Toxin, *Frontiers in Immunology*, **2022**, *13*, 898198.

39. B. Cao, Y. Nie, Z. Guan, C. Chen, N. Wang, Z. Wang, C. Shu, J. Zhang, D. Zhang. The crystal structure of Cry78Aa from Bacillus thuringiensis provides insights into its insecticidal activity, *Communications Biology*, **2022**, *5*(1), 801.

40. D. Sun, L. Zhu, L. Guo, S. Wang, Q. Wu, N. Crickmore, X. Zhou, A. Bravo, M. Soberon, Z. Guo, Y. Zhang. A versatile contribution of both aminopeptidases N and ABC transporters to Bt Cry1Ac toxicity in the diamondback moth, *BMC Biology*, **2022**, *20*(1), 33.

41. A. E. Ricroch. What will be the benefits of biotech wheat for European agriculture?, *Methods in Molecular Biology*, **2017**, *1679*, 25-35.

42. A. E. Ricroch, J. Martin-Laffon, B. Rault, V. C. Pallares, M. Kuntz. Next biotechnological plants for addressing global challenges: The contribution of transgenesis and new breeding techniques, *New Biotechnology*, **2022**, *66*, 25-35.

43. H. Balba. Review of strobilurin fungicide chemicals, *Journal of Environmental Science and Health, Part B*, **2007**, *42*(4), 441-451.

44. L. Musso, A. Fabbrini, S. Dallavalle. Natural compound-derived cytochrome bc1 complex inhibitors as antifungal agents, *Molecules*, **2020**, *25*(19), 4582.

45. F. Wang, J. Yang, H. Wang, G. Xia. Gonadotropin-regulated expressions of lanosterol 14alpha-demethylase, sterol Delta14-reductase and C-4 sterol methyl oxidase contribute to the accumulation of meiosis-activating sterol in rabbit gonads, *Prostaglandins Other Lipid Mediat,* **2010**, *92*(1-4), 25-32.

46. N. Rani, P. Kumar, R. Singh. Molecular modeling studies of halogenated imidazoles against 14alpha- demethylase from candida albicans for treating fungal infections, *Infectious Disorders - Drug Targets*, **2020**, *20*(2), 208-222.

47. T. T. Yao, D. X. Xiao, Z. S. Li, J. L. Cheng, S. W. Fang, Y. J. Du, J. H. Zhao, X. W. Dong, G. N. Zhu. Design, synthesis, and fungicidal evaluation of novel pyrazole-furan and pyrazole-pyrrole carboxamide as succinate dehydrogenase inhibitors, *Journal of Agricultural and Food Chemistry,* **2017**, *65*(26), 5397-5403.

48. P. Nicolopoulou-Stamati, S. Maipas, C. Kotampasi, P. Stamatis, L. Hens. Chemical pesticides and human health: The urgent need for a new concept in agriculture, *Frontiers in Public Health*, **2016**, *4*, 148.

49. EPA Risk Assessment, <https://www.epa.gov/pesticide-science-and-assessing-pesticide-risks/overview-risk-assessment-pesticide-program>, retrieved on 01/07/2022.

50. L. Aristilde, M. L. Reed, R. A. Wilkes, T. Youngster, M. A. Kukurugya, V. Katz, C. R. S. Sasaki. Glyphosate-Induced specific and widespread perturbations in the metabolome of soil pseudomonas species, *Frontiers in Environmental Science*, **2017**, *5*, 34.

51. J. G. Zaller, C. A. Brühl. Editorial: Non-target Effects of pesticides on organisms inhabiting agroecosystems, *Frontiers in Environmental Science*, **2019**, *7*, 75.

52. J. E. Serrao, A. Plata-Rueda, L. C. Martinez, J. C. Zanuncio. Side-effects of pesticides on non-target insects in agriculture: a mini-review, *Naturwissenschaften*, **2022**, *109*(2), 17.

53. S. M. Williamson, G. A. Wright. Exposure to multiple cholinergic pesticides impairs olfactory learning and memory in honeybees, *Journal of Experimental Biology*, **2013**, *216*(10), 1799-1807.

54. R. A. Schmidt-Jeffris, E. H. Beers, C. Sater. Meta-analysis and review of pesticide non-target

effects on phytoseiids, key biological control agents, *Pest Management Science*, **2021**, *77*, 4848-4862.

55. M. Aoun, W. Leal Filho, A.M. Azul, L. Brandli, P.G. Özuyar, T. Wall. *Pesticides' Impact on Pollinators*, Springer International Publishing, 2019, 1-11.

56. W. V. Hoesel, A. Tiefenbacher, N. König, V. M. Dorn, J. F. Hagenguth, U. Prah, T. Widhalm, V. Wiklicky, R. Koller, M. Bonkowski, J. Lagerlöf, A. Ratzenböck, J. G. Zaller. Single and Combined effects of pesticide seed dressings and herbicides on earthworms, soil microorganisms, and litter decomposition, *Frontiers in Plant Science*, **2017**, *8,* 215.

57. S. G. English, N. I. Sandoval-Herrera, C. A. Bishop, M. Cartwright, F. Maisonneuve, J. E. Elliott, K. C. Welch Jr. Neonicotinoid pesticides exert metabolic effects on avian pollinators, *Scientific Reports*, **2021**, *11*(1), 2914.

58. S. E. Lacher, K. Skagen, J. Veit, R. Dalton, E. L. Woodahl. P-Glycoprotein transport of neurotoxic pesticides, *Journal of Pharmacology and Experimental Therapeutics*, **2015**, *355*(1), 99-107.

59. R. Stahlmann, A. Horvath. Risks, risk assessment and risk competence in toxicology, *German Medical Science*, **2015**, *13*, 09.

60. National Institute for Agricultural and Food Research and Technology (INIA); R. Molteni, J.L. Alonso-Prados. Study of the different evaluation areas in the pesticide risk assessment process, *EFSA Journal*, **2020**, *18*, e181113

61. S. N. Ali, N. Rafique, S. Akhtar, T. Taj, F. Mehboob. Analysis of multiple pesticide residues in market samples of okra and associated dietary risk assessment for consumers, *Environmental Science and Pollution Research International*, **2022**, *29*(31), 47561-47570.

62. D. B. Perkins, Z. Stone, A. Jacobson, W. Chen, A. Z. Szarka, M. White, B. Christensen, L. Ghebremichael, R. A. Brain. Development of a US national-scale, mixed-source, pesticide, rural well database for use in drinking water

risk assessment: an atrazine case study, *Environmental Monitoring and Assessment*, **2022**, *194*(8), 578.

63. K. K. Sharma, V. Tripathy, K. Sharma, R. Gupta, R. Yadav, S. Devi, S. Walia. Long-term monitoring of 155 multi-class pesticide residues in Indian vegetables and their risk assessment for consumer safety, *Food Chemistry*, **2022**, *373*, 131518.

64. Y. Yang, K. Zheng, L. P. Guo, C. X. Wang, D. B. Zhong, L. Shang, H. J Nian, X. M Cui, S. J Huang. Rapid determination and dietary intake risk assessment of 249 pesticide residues in Panax notoginseng, *Ecotoxicology and Environmental Safety*, **2022**, *233*, 113348.

65. Q. Yao, S.A. Yan, J. Li, M. Huang, Q. Lin. Health risk assessment of 42 pesticide residues in Tieguanyin tea from Fujian, China, *Drug and Chemical Toxicology*, **2022**, *45*(2)*,* 932-939.

66. Q. Zhang, C. Ma, Y. Duan, X. Wu, D. Lv, J. Luo. Determination and dietary intake risk assessment of 35 pesticide residues in cowpea (Vigna unguiculata [L.] Walp) from Hainan province, China, *Scientific Reports*, **2022**, *12*(1), 5523.

67. M. Constantinou, D. Louca-Christodoulou, A. Agapiou. Method validation for the determination of 314 pesticide residues using tandem MS systems (GC-MS/MS and LC-MS/MS) in raisins: Focus on risk exposure assessment and respective processing factors in real samples (a pilot survey), *Food Chemistry*, **2021**, *360*, 129964.

68. Y. Duan, T. Ramilan, J. Luo, N. French, N. Guan. Risk assessment approaches for evaluating cumulative exposures to multiple pesticide residues in agro-products using seasonal vegetable monitoring data from Hainan, China: a case study, *Environmental Monitoring and Assessment*, **2021**, *193*(9), 578.

69. A. Ippolito, D. Kardassi, C. Lythgo, M. Tiramani. Peer review of the pesticide risk assessment for the active substance spiroxamine in light of confirmatory data submitted, *EFSA Journal*, **2021**, *19*(2)*,* e06385.

70. Z. Li. Improving screening model of pesticide risk assessment in surface soils: Considering degradation metabolites, *Ecotoxicol Ecotoxicology and Environmental Safety*, **2021**, *222*, 112490.

71. Z. Li, S. Niu. Improving screening model of pesticide risk assessment in surface soils: Addressing regional specific human exposure risks and regulatory management, *Ecotoxicol Ecotoxicology and Environmental Safety*, **2021**, *227*, 112894.

72. O. Weisner, T. Frische, L. Liebmann, T. Reemtsma, M. Ross-Nickoll, R.B. Schafer, B. Scholz-Starke, P. Vormeier, S. Knillmann, M. Liess. Risk from pesticide mixtures - The gap between risk assessment and reality, *Science of the Total Environment*, **2021**, *796,* 149017.

73. F. Sgolastra, X. Arnan, R. Cabbri, G. Isani, P. Medrzycki, D. Teper, J. Bosch. Combined exposure to sublethal concentrations of an insecticide and a fungicide affect feeding, ovary development and longevity in a solitary bee, *Proceedings of the Royal Society B: Biological Sciences*, **2018**, *285*(1885), 20180887.

74. S. Rondeau, N. E. Raine. Fungicides and bees: a review of exposure and risk, *Environment International*, **2022**, *165*, 107311.

75. D. B. Nkontcheu Kenko, N. T. Ngameni. Assessment of ecotoxicological effects of agrochemicals on bees using the PRIMET model, in the Tiko plain (South-West Cameroon), *Heliyon*, **2022**, *8*, e09154.

76. L. Li, S. Liu, Y. Yin, G. Zheng, C. Zhao, L. Ma, Q. Shan, X. Dai, L. Wei, J. Lin, W. Xie. The toxicokinetics and risk assessment of pyrethroids pesticide in tilapia (Oreochromis mossambicus) upon short-term water exposure, *Ecotoxicol Ecotoxicology and Environmental Safety*, **2022**, *241*, 113751.

77. N. Capela, M. Xu, S. Simoes, H. Azevedo-Pereira, J. Peters, J. P. Sousa. Exposure and risk assessment of acetamiprid in honey bee colonies under a real exposure scenario in Eucalyptus sp. landscapes, *Science of the Total Environment*, **2022**, *840*, 156485.

78. L. Barascou, D. Sene, Y. Le Conte, C. Alaux. Pesticide risk assessment: honeybee workers are not all equal regarding the risk posed by exposure to pesticides, *Environmental Science and Pollution Research*, **2022**, *29*(60), 90328-90337.

79. L. Barascou, F. Requier, D. Sene, D. Crauser, Y. Le Conte, C. Alaux. Delayed effects of a single dose of a neurotoxic pesticide (sulfoxaflor) on honeybee foraging activity, *Science of the Total Environment*, **2022**, *805*, 150351.

80. P. Azevedo, N. P. Butolo, L. D. de Alencar, H. M. S. Lima, V. R. Sales, O. Malaspina, R. C. F Nocelli. Optimization of in vitro culture of honeybee nervous tissue for pesticide risk assessment, *Toxicology in Vitro*, **2022**, *84*, 105437.

81. H. M. Thompson. The use of the Hazard Quotient approach to assess the potential risk to honeybees (Apis mellifera) posed by pesticide residues detected in bee-relevant matrices is not appropriate, *Pest Management Science*, **2021**, *77*(9), 3934-3941.

82. C. Stuligross, N.M. Williams. Past insecticide exposure reduces bee reproduction and population growth rate, *Proceedings of the National Academy of Sciences of the United States of America*, **2021**, *118*(48), e2109909118.

83. M. Fatema, A. Farenhorst, C Sheedy. Using the pesticide toxicity index to show the potential ecosystem benefits of on-farm biobeds, *Journal Environmental Quality*, **2022**.

84. Y. Yang, T. Chen, X. Liu, S. Wang, K. Wang, R. Xiao, X. Chen, T. Zhang. Ecological risk assessment and environment carrying capacity of soil pesticide residues in vegetable ecosystem in the Three Gorges Reservoir Area, *Journal of Hazardous Materials*, **2022**, *435*, 128987.

85. L. Pitombeira de Figueiredo, D. B. Athayde, M. A. Daam, G. Guerra, P. J. Duarte-Neto, H. Sarmento, E. L. G. Espíndola. Integrated ecosystem models (soil-water) to analyze pesticide toxicity to aquatic organisms at two different temperature conditions, *Chemosphere*, **2021**, *270*, 129422.

86. A. R. Brown, G. Whale, M. Jackson, S. Marshall, M. Hamer, A. Solga, P. Kabouw, M. Galay-Burgos, R. Woods, S. Nadzialek, L. Maltby. Toward the definition of specific protection goals for the environmental risk assessment of chemicals: A perspective on environmental regulation in Europe, *Integrated Environmental Assessment and Management*, **2017**, *13*(1), 17-37.

87. S. Periasamy, J. F. Deng, M. Y. Liu. Who is the real killer? Chlorfenapyr or detergent micelle-chlorfenapyr complex?, *Xenobiotica*, **2017**, *47*(9), 833-835.

88. P. A. Lafon, Y. Wang, M. Arango-Lievano, J. Torrent, L. Salvador-Prince, M. Mansuy, et al. Fungicide residues exposure and beta-amyloid aggregation in a mouse model of alzheimer's disease, *Environmental Health Perspectives*, **2020**, *128*(1), 17011.

89. Y. Zhang, D. Zeng, L. Li, X. Hong, H. Li-Byarlay, S. Luo. Assessing the toxicological interaction effects of imidacloprid, thiamethoxam, and chlorpyrifos on Bombus terrestris based on the combination index, *Scientific Reports*, **2022**, *12*(1), 6301.

90. F. J. Peng, P. Palazzi, C. Viguie, B. M. R. Appenzeller. Hormonal profile changes induced by pesticide mixture exposure in female rats revealed by hair analysis, *Chemosphere*, **2022**, *303*, 135059.

91. F. Mena, A. Romero, J. Blasco, C. V. M. Araujo. Can a mixture of agrochemicals (glyphosate, chlorpyrifos and chlorothalonil) mask the perception of an individual chemical? A hidden trap underlying ecological risk, *Ecotoxicol Ecotoxicology and Environmental Safety*, **2022**, *230*, 113172.

92. P. S. Kunwar, B. Sapkota, S. Badu, K. Parajuli, A. K. Sinha, G. De Boeck, et al. Chlorpyrifos and dichlorvos in combined exposure reveals antagonistic interaction to the freshwater fish Mrigal, Cirrhinus mrigala, *Ecotoxicology*, **2022**, *31*(4), 657-666.

93. J. B. Belden. The acute toxicity of pesticide mixtures to honeybees, *Integrated Environmental Assessment and Management*, **2022**, *18*(6), 1694-1704.

94. A. Sharma, P. John, P. Bhatnagar. Fluoride and endosulfan together potentiate cytogenetic effects in Swiss albino mice bone marrow cells, *Toxicology and Industrial Health*, **2021**, *37*(2), 68-76.

95. F. F. Schmidt, D. Lichtenstein, H. Planatscher, A. Mentz, J. Kalinowski, A. E. Steinhilber, T. O. Joos, A. Braeuning, O. Pötz. Pesticide mixture effects on liver protein abundance in HepaRG cells, *Toxicology*, **2021**, *458*, 152839.

96. P. S. Kunwar, R. Basaula, A. K. Sinha, G. De Boeck, K. Sapkota. Joint toxicity assessment reveals synergistic effect of chlorpyrifos and dichlorvos to common carp (Cyprinus carpio), *Comparative Biochemistry and Physiology Part C: Toxicology and Pharmacology*, **2021**, *246*, 108975.

97. V. S. Andrade, M. F. Gutierrez, U. Reno, A. Popielarz, S. Gervasio, A. M. Gagneten. Synergy between glyphosate and cypermethrin formulations on zooplankton: evidences from a single-specie test and a community mesocosm experiment, *Environmental Science and Pollution Research,* **2021**, *28*(21)*,* 26885-26894.

98. M. J. Arlos, A. Focks, J. Hollender, C. Stamm. Improving risk assessment by predicting the survival of field gammarids exposed to dynamic pesticide mixtures, *Environmental Science and Technology*, **2020**, *54(19)*, 12383-12392.

99. T. Brock, M. Arena, N. Cedergreen, S. Charles, S. Duquesne, A. Ippolito, M. Klein, M. Reed, I. Teodorovic, P.J. Brink, A. Focks. Application of general unified threshold models of survival models for regulatory aquatic pesticide risk assessment illustrated with an example for the insecticide chlorpyrifos, *Integrated Environmental Assessment and Management*, **2021**, *17*(1), 243-258.

100. J. Dollinger, V.J. Schacht, C. Gaus, S. Grant. Effect of surfactant application practices on the vertical transport potential of hydrophobic pesticides in agrosystems, *Chemosphere*, **2018**, *209*, 78-87.

101. M. Torres-Badia, S. Solar-Malaga, R. Serrano, L. J. Garcia-Marin, M. J. Bragado. The adverse impact of herbicide Roundup Ultra Plus in human spermatozoa plasma membrane is caused by its surfactant, *Scientific Reports*, **2022**, *12*(1), 13082.

102. A. Lopes, M. Benvindo-Souza, W. F. Carvalho, H. F. Nunes, P. N. de Lima, M. S. Costa, E. J. Benetti, V. Guerra, S. M. T Saboia-Morais, C. E. Santos, K. Simões, R. P. Bastos, D. M. E Silva. Evaluation of the genotoxic, mutagenic, and histopathological hepatic effects of polyoxyethylene amine (POEA) and glyphosate on Dendropsophus minutus tadpoles, *Environmental Pollution*, **2021**, *289*, 117911.

103. J. Langrand, I. Blanc-Brisset, D. Boucaud-Maitre, E. Puskarczyk, P. Nisse, R. Garnier, C. Pulce. Increased severity associated with tallowamine in acute glyphosate poisoning, *Clinical toxicology (Philadelphia, Pa.)*, **2020**, *58*(3), 201-203.

104. J. E. Goodman, R. L. Prueitt, P. Boffetta, C. Halsall, A. Sweetman. "Good epidemiology practice" guidelines for pesticide exposure assessment, *International Journal of Environmental Research and Public Health*, **2020**, *17*(14), 5114.

105. J. N. Jouzel, <https://www.sciencespo.fr/research/cogito/home/pesticides-and-human-health-between-toxicology-and-epidemiology/?lang=en>, retrieved on 01/07/2022.

106. Z. Hu. What socio-economic and political factors lead to global pesticide dependence? A critical review from a social science perspective, *International Journal of Environonmental Research and Public Health*, **2020**, *17*(21), 8-19.

Pin nhiên liệu vi sinh sử dụng màng trao đổi Poly (vinyl alcohol) liên kết chéo ứng dụng xử lý nước thải bệnh viện

Đinh Kha Lil[1,*], Imee A. Saladag[2]

[1]*Khoa Khoa học Tự nhiên, Trường Đại học Cần Thơ, Việt Nam*
[2]*Khoa Công nghệ, Đại học bang Eastern Visayas, Phi-líp-pin*

TÓM TẮT

Bộ phận phân tách giữa cực dương và cực âm là một phần thiết yếu trong pin nhiên liệu vi sinh vật (Microbial fuel cells - MFCs) và nó ảnh hưởng đáng kể đến hiệu suất của hệ thống. Các loại màng được sử dụng hiện nay đa phần có giá thành cao là khó khăn lớn làm cho công nghệ MFC chưa được đưa vào ứng dụng thực tiễn. Trong nghiên cứu này tập trung vào việc sản xuất điện bằng cách sử dụng pin nhiên liệu vi sinh hai buồng sử dụng nước thải bệnh viện kết hợp sử dụng màng poly(vinyl alcohol) (PVA) liên kết chéo với glutaraldehyde (GA) với giá thành thấp. Mật độ công suất cao nhất 209,85 mW.m^{-2} và điện áp tối đa tạo ra là 652,75 mV khi sử dụng màng trao đổi 5% PVA. Các phát hiện chứng minh những ưu điểm của việc sử dụng thiết kế MFC dựa trên màng trao đổi thay thế Nafion chế độ tĩnh để xử lý nước thải bệnh viện là tiết kiệm chi phí vận hành, sản lượng điện cao. Các màng PVA liên kết chéo có thể là một giải pháp thay thế đầy hứa hẹn cho các vật liệu phân tách để xây dựng các hệ thống MFC thực tế.

Từ khóa: *Pin nhiên liệu vi sinh, màng polyvinyl alcohol (PVA) liên kết chéo, xử lý nước thải, nước thải bệnh viện.*

*Tác giả liên hệ chính.
Email: lildk93@gmail.com

Microbial Fuel Cells using crosslinked Poly (vinyl alcohol) membrane separator for hospital wastewater treatment

Kha Lil Dinh[1],*, Imee A. Saladag [2]

[1]College of Natural Sciences, Can Tho University, Vietnam
[2]College of Engineering, Eastern Visayas State University, Philippines

ABSTRACT

The anode and cathode separator is an essential part of microbial fuel cells (MFCs) and it significantly affects the system performance. Most of the membranes used today have a high cost, which is a big difficulty, making MFC technology not yet put into practice. The present study is focused on the production of electricity using double chambered microbial fuel cells (MFCs) to treat hospital wastewater treatment combined with poly (vinyl alcohol) (PVA) membrane cross-linked with glutaraldehyde (GA) with low cost. The highest power density of 209.85 mW.m^{-2} and the maximum voltage generated of 652.75 mV occur when using 5% PVA membrane. The findings demonstrate that the main advantages of using static mode Nafion alternative membrane based MFC configurations for hospital wastewater treatment are savings on operational cost, high power output, negligible crossover, and higher treatment efficiency. The crosslinked PVA membranes can be a promising alternative to separation materials for building practical MFC systems.

Keywords: *Microbial Fuel Cells, crosslinked polyvinyl alcohol (PVA) membrane, wastewater treatment, hospital wastewater.*

1. INTRODUCTION

Conventional wastewater treatment is an energy intensive process, with aeration accounting for 50% of the operating cost for removal of organic compounds.[1] Wastewaters are a source of large amount of potential energy in the form of pollutants.[2] Besides, anaerobic treatment of wastewater also produces biogas but the energy recovery is discouraging. With escalating energy demands, the necessity for low-energy wastewater treatment has never been greater.[3] Microbial fuel cells are an emerging, sustainable technology which enables the recovery of energy out of wastewater with the aid of bacteria, while limiting both the energy input and the excess sludge production. The most promising application is the energy-efficient treatment of wastewater.[4]

The function of the membrane is to separate the reaction between the anode and the cathode in the MFC system while allowing the selective transport of protons from the anode to the cathode and preventing oxygen transport into the anode chamber. MFC is classified as membrane or membrane-less, membrane acts as a barrier between the anode and cathode electrodes. Although membrane-less MFCs help

reduce design costs, diffusion of oxygen from the cathode to the anode side occurs, resulting in low power generation efficiency.[5] An ideal separative membrane should prevent the transfer of the substrate and oxygen between the cathode chamber and the anode chamber while allowing protons to pass.[6] Major challenges in the realization of MFC for practical applications are in terms of material costs and energy recovery efficiency. The commonly used membrane type for MFCs is Nafion. This is a persistent material due to the presence of fluorine in the structure that is harmful to the environment and also accounts for 38% of the total capital cost in investing in an MFC system.[7]

Hospitals play an important role in the human health. Their activities require large amounts of water and generate large amounts of wastewater. In general, the characteristics of hospital wastewater (HWW) are similar to those of domestic wastewater, but a part of HWW includes drugs, organic substances, toxic metals, radioactive tracer. They also carry microorganisms such as viruses, bacteria, fungi, protozoa and helminths. There is increasing evidence that HWW treatment systems contribute to the spread of antimicrobial resistant bacteria into the environment.[8]

Following our previous report on crosslinked PVA membrane with GA as separator in domestic wastewater fed MFCs which exhibited high power density and Chemical oxygen demand (COD) removal with antibacterial property, thermo-mechanical stability and negligible fuel crossover. In this study, GA-linked biodegradable PVA was used as a low-cost in a dual-chamber MFC separator fed hospital wastewater that was evaluated for practical application. The microbiota in wastewater acts as a biological catalyst while wastewater is used as a substrate.

2. MATERIALS AND METHODS

2.1. Synthesis of PVA membranes

The membranes were synthesized using solution casting and solvent evaporation. After the synthesis, all films were stored at room temperature. The synthesis of each membrane is described below:

The neat PVA (nPVA) membrane: 2 g (95 wt.%) of PVA powder was added to 100 mL of deionized water to obtain a film of about 100 μm thick. The mixture was continuously stirred at 650 rpm at 85 °C. Then, 60 mL of homogeneous PVA solution was placed on Teflon plates and airdried at room temperature. The neat sample is, here onwards, called the nPVA membrane.[9]

5% PVA membrane: The steps for preparation of the membrane are followed as reported earlier.[9] To achieve a thickness of about 100 μm, the film was synthesized using 2 g (95 wt.%) of PVA dissolved in 100 mL deionized water with continuous stirring (650 rpm) at 85 °C (the temperature at which PVA readily dissolves in water). To crosslink the polymer, 5 wt.% GA was mixed drop by drop to the PVA solution and was stirred further for 15 min. Attached to its backbone, neat PVA consists of hydroxyl groups. The addition of the crosslinker causes the acetal linkages and aldehyde side chain formations. 5 wt.% GA was selected based on the % swelling in puffiness.[9]

2.2. Reactor design, setup, and operation

2.2.1. MFC setup and operation

The shape of double chamber H-cell membrane reactor for MFCs is illustrated in Figure 1. Three identical H-cell MFC were composed of two glass chambers with a volume of 250 mL each separated by a proton exchange membrane in between the two chambers. The anode and cathode are composed of graphite felts with dimensions of 5 cm × 5 cm with nPVA and 5% PVA membranes of size 3 cm in diameter in the experimental case. Another MFCs using Nafion-117, Dupont Co., USA (with similar size) was considered as the control case.

Meanwhile, the Nafion-117 membrane were treated in 5% H_2O_2 solution at 70 °C for 1 h,

repeatedly rinsed with deionized water (DI), and then treated in 0.5 M H_2SO_4 at 90 °C for 1 h. These were rinsed repeatedly and stored in DI water for later use. Graphite felt electrodes were used as the cathode and anode. The electrodes were pretreated in 10% H_2O_2 solution for 3 h at 90 °C followed by airdrying at ambient temperature for at least two days before use.
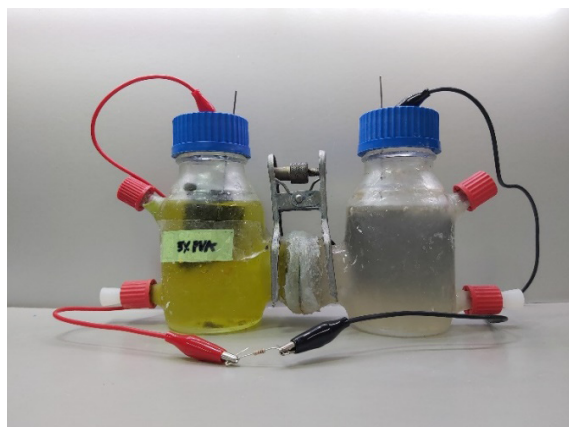

Figure 1. The schematic representation of the MFCs fed with hospital wastewater.

According to the Proton exchange membrane (PEM) applied, three MFCs were used in this study labelled as Nafion-117, nPVA and 5% PVA. All were operated batch-wise and tested at 25 °C. A steady voltage was achieved for at least three consecutive cycles before output measurements were performed.

2.2.2. Anode biofilm acclimation

A mixed culture of bacteria had the source of hospital wastewater, obtained from the National Yang Ming Chiao Tung University Hospital Xinmin Branch, Yilan City, Taiwan, used as anode inoculum. Mixture hospital wastewater containing mixed culture of bacteria and 50 mM phosphate buffer nutrient solution (1:1 ratio) as the inoculum in the anode chamber. Phosphate buffer nutrient solution (PBS) was composed of Na_2HPO_4, 9.16 g L^{-1}; $NaH_2PO_4 \cdot 2H_2O$, 5.56 g L^{-1}; NH_4Cl, 0.638 g L^{-1}; and KCl, 0.278 g L^{-1}. Sodium acetate (1 g) was added per liter of the solution as the electroactive bacteria (EAB) substrate.

During the EAB acclimation, a 1:1 solution of 100 mM $K_3[Fe(CN)_6]$ (32.924 g L^{-1}) and 100 mM PBS solution served as the catholyte. The anolyte and catholyte were replaced with new solutions when the voltage production declined to 10% of the maximum voltage produced, which indicates the end of each fed-batch cycle. A titanium wire was inserted in each electrode and then connected to a 1,000-Ω external resistance using copper wire to reduce the biofilms' acclimation time.[10] The MFCs were operated on for 3 months to obtain a robust bacterial biofilm.

2.3. Biofilm characterizations

After MFCs operations, electrode samples were microanalysis by scanning electron microscopy (SEM) (JEOL JSM-6500F, JEOL Ltd., Tokyo, Japan). To characterize the bacterial anode and structure biofilms.

2.4. Electrochemical measurements

MFCs voltage was measured every 2 h during the operations. Open circuit condition of the HMFCs was maintained for 4 h before polarization and electrochemical impedance spectroscopy (EIS) tests. Linear sweep voltammetry (LSV) was done three times at a scan rate of 10 mV s^{-1} starting from the measured open-circuit voltage (OCV) to zero. Data were acquired at 10 points per second using a multifunctional electrochemical analyzer (JIEHAN 5640, JIEHAN Technology Group, Taiwan).

The current was calculated from Ohm's Law, $I = V/R$, where I is the current (mA) and V is the output voltage (mV) through a resistance, R (Ω). Power (P, mW) was calculated from $P = V \times I$. Current density (I_D, mA.m^{-2}) and power density (P_D, mW.m^{-2}) were calculated using the total anode surface area (0.005 m^2).[11]

Electrochemical impedance spectroscopy (EIS) was carried out using HIOKY 3522-50 LCR Hi-TESTER (Japan) by applying a 10-mV AC signal within 100 kHz to 0.1 Hz frequency range. An equivalent circuit was used to fit the

EIS spectra and calculate internal resistance values in EC Lab software.[12]

3. RESULTS AND DISCUSSION

Crosslinking of PVA with GA improves the properties of the pristine PVA membrane making it suitable for real wastewater treatment which has been reported below. The continuous operation of the MFC condition with crosslinked membrane as separator is analyzed in the latter section.

3.1. Bioelectricity production in the double chambered MFC

Under the mode of fed-batch operation, the MFCs investigated took a period of 1 month to reach stable conditions. A gradual increase in voltage under an external load of 1000 Ω was observed. No significant lag in the voltage generation was observed during start-up which is indication of the microbial cell to anode adhesion efficiency. In order to inoculate the graphite electrode with mixed culture of bacteria present in HWW, three successive acclimation cycles were carried out with acetate as the carbon source.

The current and power density curves are shown in Figure 2. Among the three MFCs, the highest power density was achieved by Nafion-117 membrane MFC at 316.17 mW.m^{-2}. It also obtained the maximum voltage generated

of 736.83 mV. The 5% PVA membrane MFC followed with respective power current and maximum voltage generated: 209.85 mW.m^{-2} and 652.75 mV while nPVA membrane MFC achieved 116.46 mW.m^{-2} and 522.24 mV. The enhanced performance of the crosslinked membrane can be ascribed to the crosslinking and branching with GA as it successfully altered the undesirable properties of the nPVA membrane with enhanced stability in terms of chemical, thermal, and mechanical properties, and controlled water uptake and degree of swelling, which has been reported in the previous study by our research group.[13] It is known that the water uptake capacity with the optimum swelling ratio is desirable for the transport of protons across the polymeric membrane since it aids the proton transfer across the membrane in MFCs. However, higher water content with high swelling has a negative impact on its mechanical integrity. The nPVA being a straight-chain polymer, forms intramolecular and intermolecular hydrogen bonding with water. On crosslinking with GA, acetal ring linkage is formed with a reduction in available hydroxyl groups in PVA. The nPVA demonstrated water uptake up to 250%, which was reduced to 50% for the crosslinked membrane. Similarly, the swelling percentage reduced from 50% for the neat PVA membrane to 20% for the crosslinked membrane.[13]
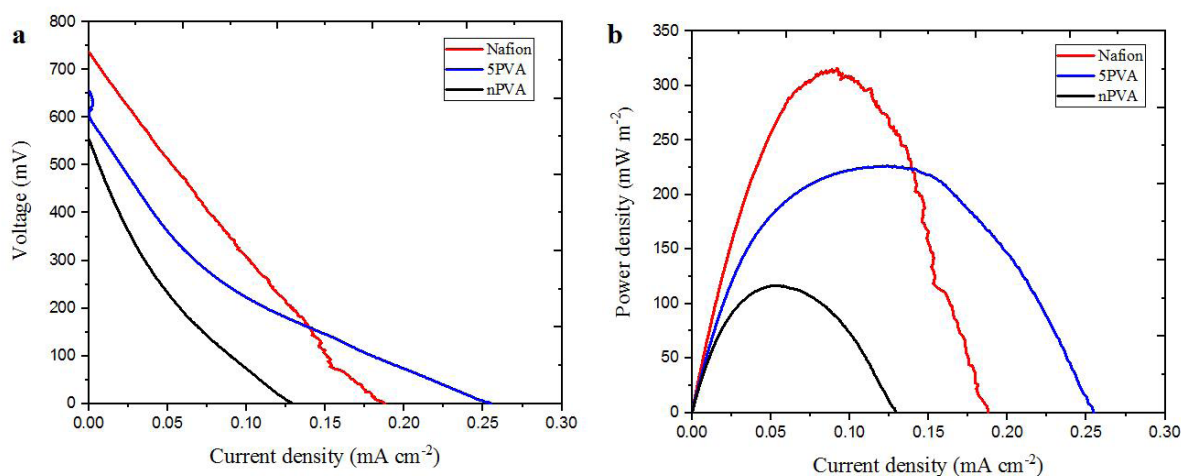

Figure 2. Polarization curves (a) and power density generated (b) by MFCs equipped with different types of membranes.

Table 1. Power density reported of different exchange membrane in MFCs.

Electrode material	Anode volume (mL)	Exchange membrane	Power density (mW m^{-2})	Ref.
Graphite granules	390	UltrexeCMI7000, Membranes International Inc., USA	8 ± 5	Rabaey et al.[14]
Graphite granules	60	UltrexeCMI7000, Membranes International Inc., USA	14 ± 1	Aelterman et al.[15]
Aluminium	2,000	Gar-salt bridge	~ 0.25	Shakunthala et al.[16]
Carbon cloth	100	Ceramic-separator	168.91 ± 3.89	Chaijak et al.[17]
Graphite felts	250	Nafion-117, Dupont Co., USA	316.17	This work
Graphite felts	250	nPVA	116.46	This work
Graphite felts	250	5%PVA	209.85	This work

Hospital wastewater is not a common source of substrate tested for electricity production by MFCs technology. The production of bioelectricity from these wastewaters depends on the type of organic compounds present in the effluent. Especially, particulate organic matters that have complex chemical structures must be converted into low molecular weight substrates, and then these substrates can then be used by microbes. Table 1 provides a series of characteristics ability to generate electricity of hospital wastewater as substrate for bioelectricity formation with MFCs in our study in comparison with other reports. MFCs is improving and power density of 209.85 mW.m^{-2} and maximum voltage generated of 652.75 mV using a crosslinked 5% PVA membrane. The results showed that hospital wastewater can be successfully employed as a cheap substrate for electricity production in MFC. However, the challenges due to the hazardous compounds in the effluents, for example, dialysis hospital wastewater has a high content of organic load and salt concentration.

3.2. Biofilm analysis

A mixed consortium is preferred for performance enhancement in MFCs fed with wastewater compared to the pure culture. The reason is it exhibits a "nutrient cycle ecosystem" in which some species degrade the organic matter, while some species act against harmful pollutants present in wastewater.[18]

The bacterial mixture in hospital wastewater has grown a biofilm on the anode, as shown in the SEM images in Figure 3. Variations on the biofilm can be observed with uniform growth and clumps as well as undeveloped areas. In previous studies, clumping growth has been associated with detrimental effects on power output as it can inhibit electron transfer.[19] As can be seen, biofilms are dominated by growth uniform growth, which is a good indication of a good bacterial colonization.[20] The combination of bacteria contributes to the diversity of biofilms. It produces a higher specific capacity than MFCs operating with monocultures in the anode compartment. The stable biofilm developed favored low resistance to the electrochemical reaction at the anode surface, as demonstrated by the low R$_1$ value in EIS analysis.
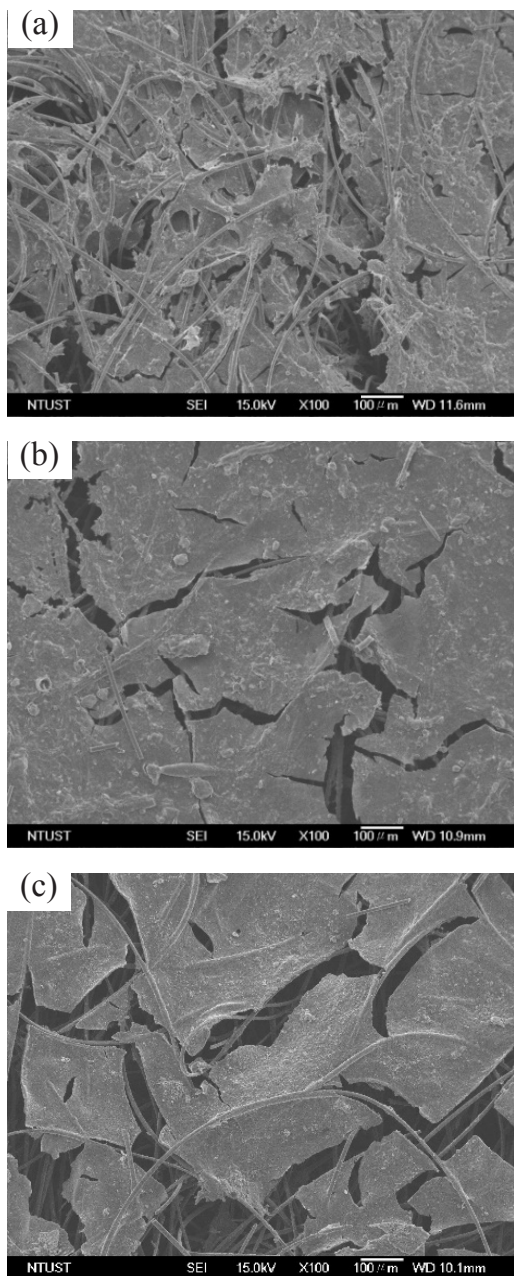
Figure 3. SEM images of anodes with electroactive bacteria biofilm were grown with: (a) Nafion membrane, (b) nPVA membrane and (c) 5% PVA membrane.

3.3. Internal resistance of the MFC with crosslinked membrane

The proton exchange membrane is one of the most critical components in the fuel cell configuration. It not only provides a separation between the two electrolytes, but also provides electroneutrality by facilitating transport of H^+ to compensate for transport of electrons. In order to assess the internal resistance of the MFCs equipped with the membranes, the EIS results were interpreted according to the Randles equivalent circuit shown in Figure 4 (a). R_1, R_2, C_2 and W_2 represent the ohmic resistance, charge transfer resistance, double layer capacitance, and Warburg impedance, respectively which are components of the internal resistances. The diameter of the semicircle in the low frequency side of the Nyquist plot as seen from Figure 4 (b) represents the charge transfer resistance while the linear portion in low frequency side represents diffusion resistance. The difference between origin to the initial start of the semicircle gives the ohmic resistance.[21] Nafion exhibited lower ohmic resistance compared to the crosslinked membrane, which is mainly due to the presence of sulphonic acid groups in its polymer chain.[22] Although PVA is an insulation material with no polar groups,[23] the charge transfer resistance was found to be lower in case of the PVA based MFCs and comparable to the charge transfer resistance observed in the Nafion based MFCs. This can be attributed to crosslinking with GA which resulted in low value of charge transfer indicating better charge transport through the crosslinked membrane due to optimum water content facilitating proton transfer through vehicular mechanism.[24]
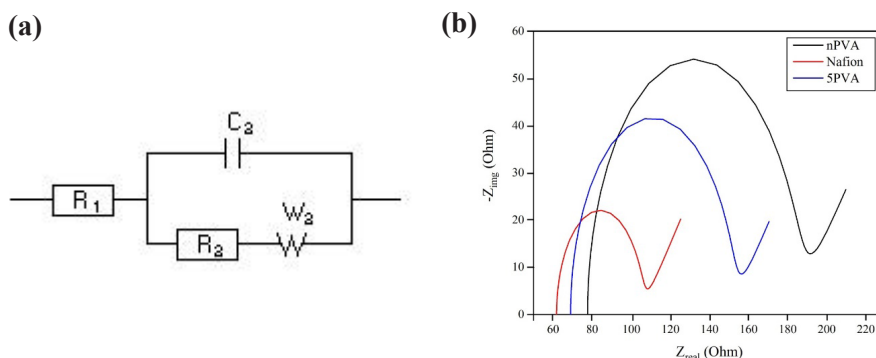

Figure 4. (a) Equivalent circuit of MFC, (b) Nyquist plot of MFC fit: Nyquist diagram from Z-fit by EC Lab software.

Table 2. Internal resistance of MFCs and other circuit parameter values.

Membrane	$R_1\ (\Omega)$	$R_2\ (\Omega)$	$C_2\ (F)$	$W_2\left(\mathrm{Ohm}\big/\sqrt{\mathrm{s}}\right)$
Nafion	62.58	41.53	43.14×10^{-6}	15.93
5%PVA	68.97	82.31	51.98×10^{-6}	15.35
nPVA	84.14	105.26	58.46×10^{-6}	15.64

The individual resistance components in the reactors used in this research are listed in Table 2. The least ohmic resistance was observed for the 5% PVA based MFC 68.97 Ω, followed by Nafion with 62.58 Ω, while nPVA showed the highest ohmic resistance 84.14 Ω. The ohmic loss in the crosslinked membrane is comparable with Nafion and relatively lesser than its neat counterpart. Nafion has sulphonic acid groups attached to its polymer chain, which explains its low resistance. nPVA is an insulation material without polar groups. However, due to crosslinking, proton transfer is facilitated, resulting in its low resistance and higher power performance.[13] Also, due to the recirculation mode, homogenous mass and ion transfer rendered by the flow straighteners contributed in reducing the ohmic and concentration losses.[25] Thus, this study has confirmed the fact that resistance in MFCs strongly influences power performance.

EIS can be used to obtain information on the electronic and ionic conductivity in the charging and discharging process. The semicircle portion of the Nyquist plot at a higher frequency corresponds to the electronic transition, which controls the electron transfer kinetics of the redox reaction at the interfacing electrode. Simultaneously, the straight line in the low-frequency region is due to the diffusion process corresponding to a diffuse resistance. The magnitude of the Nyquist arc gives the electrode's electrochemical polarization resistance quality that works in the anode configuration. At the same time, quantitative values can be obtained by mounting the equivalent circuit (EC) of the data. The MFC anode's impedance spectrum was analyzed by matching the EC, as shown in Figure 4a. The internal resistance of the HMFCs was composed of ohmic losses, charge transfer losses of cathode and anode, and concentration losses.

4. CONCLUSIONS

In this work, crosslinked PVA membrane as separators with hospital wastewater has been successfully demonstrated in MFCs. Using the low-cost membranes with hospital wastewater as a substrate not only drastically reduces its capital and operational costs but also allows to treat hospital wastewater eco-friendly, which is a competitive advantage for the practical application of MFCs in the future.

REFERENCES

1. Y. Chen, H. Zhang, Y. Yin, F. Zeng, Z. Cui. Smart energy savings for aeration control in wastewater treatment, *Energy Reports,* **2022**, *8*, 1711-1721.

2. K. M. Khalid. Correlation between air quality and Wastewater pollution, In *Environmental Sustainability-Preparing for Tomorrow*, Intech Open, 2021.

3. R. A. Rozendal, H. V. Hamelers, K. Rabaey, J. Keller, C. J. Buisman. Towards practical implementation of bioelectrochemical wastewater treatment, *Trends in Biotechnology,* **2008**, *26*(8), 450-459.

4. A. Nawaz, I. ul Haq, K. Qaisar, B. Gunes, S. I. Raja, K. Mohyuddin, H. Amin. Microbial fuel cells: Insight into simultaneous wastewater treatment and bioelectricity generation, *Process Safety and Environmental Protection,* **2022**, *161*, 357-373.

5. M. Zhou, H. Wang, D. J. Hassett, T. Gu. Recent advances in microbial fuel cells (MFCs) and microbial electrolysis cells (MECs) for wastewater treatment, bioenergy and bioproducts, *Journal of Chemical Technology & Biotechnology,* **2013**, *88*(4), 508-518.

6. D. R. Lovley. Bug juice: harvesting electricity with microorganisms, *Nature Reviews Microbiology,* **2006**, *4*(7), 497-508.

7. M. J. González-Pabón, F. Figueredo, D. C. Martínez-Casillas, E. Corton. Characterization of a new composite membrane for point of need paper-based micro-scale microbial fuel cell analytical devices, *PloS One,* **2019**, *14*(9), e0222538.

8. A. Kumari, N. S. Maurya, B. Tiwari. Hospital wastewater treatment scenario around the globe, *Current Developments in Biotechnology and Bioengineering*, **2020**, 549-570.

9. B. Das, S. S. Gaur, A. R. Katha, C.-T. Wang, V. Katiyar. Crosslinked poly (vinyl alcohol) membrane as separator for domestic wastewater fed dual chambered microbial fuel cells, *International Journal of Hydrogen Energy,* **2021**, *46*(10), 7073-7086.

10. G. Buitrón, I. López-Prieto, I. T. Zúñiga, A. Vargas. Reduction of start-up time in a microbial fuel cell through the variation of external resistance, *Energy Procedia,* **2017**, *142*, 694-699.

11. B. E. Logan, B. Hamelers, R. Rozendal, U. Schröder, J. Keller, S. Freguia, P. Aelterman, W. Verstraete, K. Rabaey. Microbial fuel cells: methodology and technology, *Environmental Science & Technology,* **2006**, *40* (17), 5181-5192.

12. A. J. Hutchinson, J. C. Tokash, B. E. Logan. Analysis of carbon fiber brush loading in anodes on startup and performance of microbial fuel cells, *Journal of Power Sources,* **2011**, *196*(22), 9213-9219.

13. B. Das, S. S. Gaur, A. R. Katha, C. T. Wang, V. Katiyar. Crosslinked poly (vinyl alcohol) membrane as separator for domestic wastewater fed dual chambered microbial fuel cells, *International Journal of Hydrogen Energy,* **2021**, *46*(10), 7073-7086.

14. K. Rabaey, P. Clauwaert, P. Aelterman, W. Verstraete. Tubular microbial fuel cells for efficient electricity generation, *Environmental Science & Technology,* **2005**, *39* (20), 8077-8082.

15. P. Aelterman, K. Rabaey, P. Clauwaert, W. Verstraete. Microbial fuel cells for wastewater treatment, *Water Science and Technology,* **2006**, *54*(8), 9-15.

16. C. Shakunthala, S. Manoj. Energy Harvesting from Dairy and Hospital Wastewater Using Microbial Fuel Cell (MFC), *International Conference on Cognitive Computing and Information Processing*, **2017**, 440-446.

17. P. Chaijak, M. Lertworapreecha, N. Changkit, P. Sola. Electricity generation from hospital wastewater in microbial fuel cell using radiation tolerant bacteria, *Biointerface Research in Applied Chemistry,* **2022**, *12*(4), 5601.

18. M. Li, M. Zhou, X. Tian, C. Tan, C. T. McDaniel, D. J. Hassett, T. Gu. Microbial fuel cell (MFC) power performance improvement through enhanced microbial electrogenicity, *Biotechnology Advances,* **2018**, *36*(4), 1316-1327.

19. X. Zhou, Y. Qu, B. H. Kim, P. Y. Choo, J. Liu, Y. Du, W. He, I. S. Chang, N. Ren, Y. Feng. Effects of azide on electron transport of exoelectrogens in air-cathode microbial fuel cells, *Bioresource Technology,* **2014**, *169*, 265-270.

20. Y. Cao, H. Mu, W. Liu, R. Zhang, J. Guo, M. Xian, H. Liu. Electricigens in the anode of microbial fuel cells: pure cultures versus mixed communities, *Microbial Cell Factories,* **2019**, *18*(1), 1-14.

21. B. Neethu, G. Bhowmick, M. Ghangrekar. A novel proton exchange membrane developed from clay and activated carbon derived from coconut shell for application in microbial fuel cell, *Biochemical Engineering Journal,* **2019**, *148*, 170-177.

22. C. Y. Wong, W. Y. Wong, K. S. Loh, R. W. Daud, K. L. Lim, M. Khalid, R. Walvekar. Development of poly (vinyl alcohol)-based polymers as proton exchange membranes and challenges in fuel cell application: A review, *Polymer Reviews,* **2020**, *60*(1), 171-202.

23. R. Rudra, V. Kumar, P. P. Kundu. Acid catalysed cross-linking of poly vinyl alcohol (PVA) by glutaraldehyde: effect of crosslink density on the characteristics of PVA membranes used in single chambered microbial fuel cells, *RSC Advances,* **2015**, *5*(101), 83436-83447.

24. S. Zinadini, A. Zinatizadeh, M. Rahimi, V. Vatanpour, Z. Rahimi. High power generation and COD removal in a microbial fuel cell operated by a novel sulfonated PES/PES blend proton exchange membrane, *Energy,* **2017**, *125*, 427-438.

25. T. Sangeetha, I.-T. Li, T.-H. Lan, C.-T. Wang, W.-M. Yan. A fluid dynamics perspective on the flow dependent performance of honey comb microbial fuel cells, *Energy,* **2021**, *214*, 118928.

Thành phần hóa học từ cành cây Máu chó đá (*Knema saxatilis*)

Lê Nguyễn Thành[1,*], Trần Hữu Giáp[1], Hà Thị Thoa[1], Vũ Thị Huế[1], Nguyễn Hoàng Nam[1], Nguyễn Quốc Vượng[1], Nguyễn Thành Công[2], Diệp Thị Lan Phương[3,*]

[1]Viện Hóa sinh biển, Viện Hàn lâm Khoa học và Công nghệ Việt Nam, Việt Nam
[2]Khoa Dược, Trường Đại học Đại Nam, Việt Nam
[3]Khoa Khoa học Tự nhiên, Trường Đại học Quy Nhơn, Việt Nam

TÓM TẮT

Nghiên cứu thành phần hóa học của cành cây Máu chó đá *Knema saxatilis* đã phân lập được 6 hợp chất. Cấu trúc hóa học của chúng được xác định dựa trên các phổ MS và NMR, đó là 8-hydroxy eriodictyol (**1**), (2S)-7-hydroxy-3′,4′-methylenedioxideflavan (**2**), sitostenone (**3**), protocatechuic acid (**4**), 4-hydroxybenzoic acid (**5**) và vanillin (**6**). Trong 6 hợp chất phân lập có **1** và **3-6** là các hợp chất lần đầu tiên được báo cáo cho chi *Knema*.

Từ khóa: *Knema saxatilis, flavonoid, phenolic acid, flavan, sterol.*

---

*Tác giả liên hệ chính.
Email: lethanh@imbc.vast.vn, diepthilanphuong@qnu.edu.vn

Chemical constituents of stems of *Knema saxatilis*

**Le Nguyen Thanh[1,*], Tran Huu Giap[1], Ha Thi Thoa[1], Vu Thi Hue[1],
Nguyen Hoang Nam[1], Nguyen Quoc Vuong[1], Nguyen Thanh Cong[2],
Diep Thi Lan Phuong[3,*]**

[1]Institute of Marine Biochemistry, Vietnam Academy of Science and Technology, Vietnam
[2]Faculty of Pharmacy, Dai Nam University, Vietnam
[3]Faculty of Natural Sciences, Quy Nhon University, Vietnam

ABSTRACT

Phytochemical study of *Knema saxatilis* stems led to the isolation of six known compounds. Their chemical structures were determined as 8-hydroxy eriodictyol (**1**), (2*S*)-7-hydroxy-3′,4′-methylenedioxideflavan (**2**), sitostenone (**3**), protocatechuic acid (**4**), 4-hydroxybenzoic acid (**5**) and vanillin (**6**) using NMR and MS spectral data. Among the isolated compounds, compounds **1** and **3-6** were reported for the first time from the genus *Knema*.

Keywords: *Knema saxatilis, flavonoid, phenolic acid, flavan, sterol.*

1. INTRODUCTION

Knema saxatilis, locally called "Mau cho da", is a native plant in Vietnam with red resins in the bark, referred to the word "mau cho" in its local name. *Knema* species have been used in the traditional medicine for the treatment of skin diseases, sore throat pains and cancers.[1] Previous chemical studies of *Knema* species led to the isolation of phenol lipid derivatives, flavonoids, lignans, terpenes and sterols.[2-7] Plants in this genus exhibited possessed a wide range of pharmacological effects such as anticancer, antidiabetic, antibacterial and anti-inflammatory activities.[2-7]

In the continuation of our study on *Knema* plants in Vietnam,[8-12] we reported herein the isolation and elucidation of six compounds including 8-hydroxy eridictyol (**1**),

(2*S*)-7-hydroxy-3′,4′-methylene- dioxideflavan (**2**), sitostenone (**3**), protocatechuic acid (**4**), 4-hydroxybenzoic acid (**5**), and vanillin (**6**). Their structures were determined by comparison of their NMR and MS spectral data with the reported literature.

2. MATERIALS AND METHODS

2.1. Plant materials

The plant stems were collected in Quangtri province, Vietnam in 2015. The plant was identified as *Knema saxatilis* de Wilde by Dr. Nguyen Quoc Binh, Vietnam Museum of Nature. A voucher specimen (VN-1672) was preserved at the Institute of Marine Biochemistry, VAST.

2.2. General experimental procedures

The ^{1}H-NMR (500 MHz) and ^{13}C-NMR (125 MHz) spectra were obtained by a Bruker AM500

FT-NMR spectrometer using TMS as an internal standard and chemical shift are expressed in ppm. The ESI-MS spectra were recorded on an Agilent 1260 LC/MS system. Column chromatography (CC) was carried out on silica gel (Merck, 230-400 mesh) or Sephadex® LH-20. Thin layer chromatography used precoated silica gel plates (Merck 60 F_{254}). Compounds were visualized by UV lamp (254 nm) or spraying with 10% sulfuric acid and heating.

2.3. Extraction and isolation

The dried, powdered plant materials of *K. saxatilis* (1.12 kg) were consecutively macerated (3L x 3 times, 1 day/time) with hexane, ethyl acetate and MeOH at room temperature. The organic extracts were combined and removed *in vacuo* to afford hexane (5 g), ethyl acetate (14.2 g) and MeOH residue (53 g), respectively.

The hexane and EtOAc residue (19 g) was subjected to a silica gel CC (4 cm size) and eluted using gradient solvents hexane/EtOAc (100:1 to 0:1, v/v) to afford 8 fractions (F1-F8). Fraction F2 (370 mg) was fractionated on silica gel CC (2 cm size), eluted with hexane/EtOAc (19:1, v/v) to afford three sub-fraction F2.1-F2.3. Sub-fraction F2.1 (80 mg) was purified by silica gel CC (1.5 cm size), eluted with hexane/CH_2Cl_2 to give **3** (7 mg). Fraction F5 (830 mg) was separated on silica gel CC (2.5 cm size) using hexane/EtOAc (19:1, v/v) as eluent to give five fractions F5.1-F.5.5. Fraction F5.1 (70 mg) was purified on silica gel CC (1.5 cm size) and eluted with CH_2Cl_2/MeOH (99/1, v/v) to yield **2** (3.5 mg). Fraction F5.2 (150 mg) was separated on silica gel CC (2 cm size), eluted with hexane/EtOAc (19:1, v/v) to afford four sub-fractions F5.2.1-F5.2.4. Sub-fraction F5.2.3 (30 mg) was further purified on silica gel CC (1 cm size) and eluted with CH_2Cl_2/MeOH (99/1, v/v) to yield **6** (4 mg). Fraction F7 (260 mg) was separated on Sephadex® LH-20 CC (2 cm size) using CH_2Cl_2/MeOH (2/8, v/v) as eluent to give four

fraction F7.1-F7.4. Fraction F7.4 (15 mg) was purified on silica gel CC (1 cm size) and eluted with CH_2Cl_2/MeOH (99/1, v/v) to yield **5** (4 mg).

The MeOH residue (53 g) was fractionated on silica gel CC (4 cm size) and eluted using gradient solvents CH_2Cl_2/MeOH (100/1 to 0/1, v/v) to afford 12 fractions M1-M12. Fraction M6 (1.7 g) was purified on Sephadex® LH-20 (2.5 cm size) eluted with CH_2Cl_2/MeOH (1/9, v/v) to afford four sub-fraction M6.1-M6.4. Fraction M6.2 (110 mg) was purified on Sephadex® LH-20 CC (1.5 cm size) using CH_2Cl_2/MeOH (2/8, v/v) to give **4** (13 mg). Fraction M6.3 (70 mg) was separated on silica gel CC (1.5 cm size), eluted with CH_2Cl_2/acetone (8/2, v/v) to yield **1** (5 mg).

8-Hydroxy eriodictyol (1) white solid, $[\alpha]_D^{25}$ −50° (*c* 0.3, MeOH); ESI-MS: *m/z* 305 $[M+H]^+$. ^{1}H-NMR (500 MHz, $CDCl_3$+ CD_3OD) δ (ppm): 6.94 (1H, d, *J* = 2.0 Hz, H-2'), 6.85 (1H, d, *J* = 8.0 Hz, H-5'), 6.81 (1H, dd, *J* = 2.0 Hz, 8.0 Hz, H-6'), 5.97 (1H, s, H-6), 5.27 (1H, dd, *J* = 12.5 Hz, 3.0 Hz, H-2), 3.06 (1H, dd, *J* = 17.0 Hz, 12.5 Hz, H-3a), 2.73 (1H, dd, *J* = 17.0 Hz, 3.0 Hz, H-3b). ^{13}C-NMR (125 MHz, $CDCl_3$+ CD_3OD) δ (ppm): 196.2 (C-4), 166.9 (C-7), 163.7 (C-9), 163.3 (C-5), 145.3 (C-4′), 144.9 (C-3′), 130.4 (C-1′), 126.0 (C-8), 118.5 (C-6′), 115.3 (C-5′), 113.5 (C-2′), 102.5 (C-10), 96.6 (C-6), 79.1 (C-2), 43.1 (C-3).

(2S)-7-hydroxy-3′,4′-methylenedioxideflavan (2) white solid, $[\alpha]^{25}_D$: -14.2 (c 0.4; $CHCl_3$). ESI-MS: *m/z* 271 $[M+H]^+$. ^{1}H-NMR (500MHz, $CDCl_3$), δ (ppm): 6.92 (1H, d, *J* = 8.0 Hz, H-5), 6.91 (1H, s, H-2′), 6.87 (1H, d, *J* = 8.5 Hz, H-6′), 6.81 (1H, d, *J* = 8.5 Hz, H-5′), 6.39 (1H, d, 8.0 Hz H-6), 6.38 (1H, s, H-8), 5.95 (1H, s, H-7′), 4.95 (1H, dd, *J* = 10 Hz, H-2), 2.88 and 2.70 (2H, m, H-4), 2.13 and 2.03 (2H, m, H-3).^{13}C-NMR (125 MHz, $CDCl_3$) δ (ppm): 155.8 (C-9), 154.9 (C-7), 147.7 (C-3′), 147.2 (C-4′), 135.6 (C-1′), 130.1 (C-5), 119.6 (C-6′), 114.1

(C-10), 108.2 (C-5′), 108.0 (C-6), 106.7 (C-2′), 103.5 (C-8), 101.1 (C-7′), 77.8 (C-2), 30.0 (C-4), 24.4 (C-3).

Sitostenone (3) white solid. ESI-MS m/z 413 [M+H]⁺. ¹H-NMR (500MHz, CDCl₃), δ (ppm): 5.72 (1H, s, H-40), 1.17 (3H, s, H-19), 0.91 (3H, d, J = 6.5 Hz, H-21), 0.84 (3H, t, J = 7.5 Hz, H-29), 0.83 (3H, d, J = 7.0 Hz, H-27), 0.81 (3H, d, J = 7.0 Hz, H-26), 0.70 (3H, s, H-18). **¹³C-NMR** (125 MHz, CDCl₃), δ (ppm): 199.6 (C-3), 171.7 (C-5), 123.7 (C-4), 56.0 (C-14), 55.9 (C-17), 53.8 (C-9), 45.9 (C-24), 42.4 (C-13), 39.6 (C-12), 38.6 (C-10), 36.1 (C-20), 35.7 (C-1), 35.6 (C-8), 34.0 (C-2), 33.9 (C-22), 33.0 (C-6), 32.1 (C-7), 29.2 (C-25), 28.2 (C-16), 26.1 (C-23), 24.2 (C-15), 23.1 (C-28), 21.0 (C-11), 19.8 (C-26), 19.0 (C-27), 18.7 (C-21), 17.4 (C-19), 12.0 (C-29), 11.9 (C-18).

Protocatechuic acid (4): brown solid. ESI-MS m/z 155 [M+H]⁺. ¹H-NMR (500MHz, CDCl₃+ CD₃OD), δ (ppm): 7.41 (1H, d, J = 1.5 Hz, H-2), 7.41 (1H, dd, J = 8.5 Hz, J =1.5 Hz, H-6), 6.76 (1H, d, J = 8.5 Hz, H-5). ¹³C-NMR (125 MHz, CDCl₃+ CD₃OD), δ (ppm): 169.4 (COOH); 149.6 (C-4); 144.0 (C-3), 123.2 (C-1), 121.6 (C-6); 116.4 (C-5); 114.5 (C-2).

4-Hydroxybenzoic acid (5): brown solid. ESI-MS m/z 139 [M+H]⁺. ¹H-NMR (500MHz, CD₃OD), δ (ppm): 7.85 (2H, d, J = 8.5 Hz, H-2, H-6), 6.76 (2H, d, J = 8.5 Hz, H-3, H-5). ¹³C-NMR (125 MHz, CD₃OD), δ (ppm): 169.9 (COOH), 163.1 (C-4), 133.0 (C-2, C-6), 122.6 (C-1), 116.0 (C-3, C-5).

Vanillin (6): pale yellow solid. ESI-MS m/z 153 [M+H]⁺. **¹H-NMR** (500 MHz, CDCl₃) δ (ppm): 9.83 (1H, s, CHO), 7.43 (2H, m, H-2, H-6), 7.04 (1H, d, J = 8.5 Hz, H-5), 6.26 (1H, OH), 3.97 (3H, s, OMe). **¹³C-NMR** (125 MHz, CDCl₃), δ (ppm): 190.8 (CHO), 151.8 (C-3),

147.2 (C-4), 129.8 (C-1), 127.4 (C-6), 114.4 (C-5), 108.8 (C-2), 56.0 (OMe).

3. RESULTS AND DISCUSSION

Compound **1** was isolated as a white solid. The ESI-MS spectrum revealed a pseudo-molecular ion peak at *m/z* 305 [M+H]⁺, suggested the molecular formula of **1** is $C_{15}H_{12}O_7$ (M= 304). The ¹H NMR spectrum showed signals of a flavanone structure with three protons of an ABX system at δ_H 6.94 (1H, d, J = 2.0 Hz, H-2'), 6.85 (1H, d, J = 8.0 Hz, H-5'), 6.81 (1H, dd, J = 2.0 Hz, 8.0 Hz, H-6'), an aromatic singlet at δ_H 5.97 (1H, s, H-6). In addition, signals of benzopyranone moiety were observed with a signal at δ_H 5.27 (1H, dd, J = 12.5 Hz, 3.0 Hz, H-2) and 2 protons at δ_H 3.06 (1H, dd, J = 17.0 Hz, 12.5 Hz, H-3a) and 2.73 (1H, dd, J = 17.0 Hz, 3.0 Hz, H-3b). The ¹³C-NMR showed 15 carbon signals of a flavanone including a carbonyl carbon at δ_C 196.2 (C-4), 12 aromatic carbons ranging from 166.9 to 96.6 ppm, an oxymethine carbon at δ_C 79.1 (C-2) and a methylene group at δ_C 43.1 (C-3). In the HMBC spectrum, the correlations of H-6 (δ_H 5.97) to C-7 (δ_C 166.9), C-5 (δ_C 163.3) and C-10 (δ_C 102.5) were observed, suggested a hydroxyl group was substituted at C-8 (Fig. 2). Based on above spectral evidences, compound **1** was identified as 8-hydroxy eriodictyol. The analytical NMR data of **1** are in accordance with those published.[13]

Compound **2** was obtained as a white solid. The ESI-MS showed a protonated molecular ion peak *m/z* 271 [M+H]⁺, corresponding to $C_{16}H_{14}O_4$ (M= 270) molecular formula. The ¹H NMR spectrum revealed signals of a flavan structure with signal of two ABX systems at δ_H 6.91 (1H, s, H-2'), 6.87 (1H, d, J = 8.5 Hz, H-6'), 6.81 (1H, d, J = 8.5 Hz, H-5') and 6.92 (1H, d, J = 8.0 Hz, H-5), 6.39 (1H, d, 8.0 Hz H-6), 6.38 (1H, s, H-8), a methylenedioxide group at δ_H 5.95 (1H, s, H-7′)
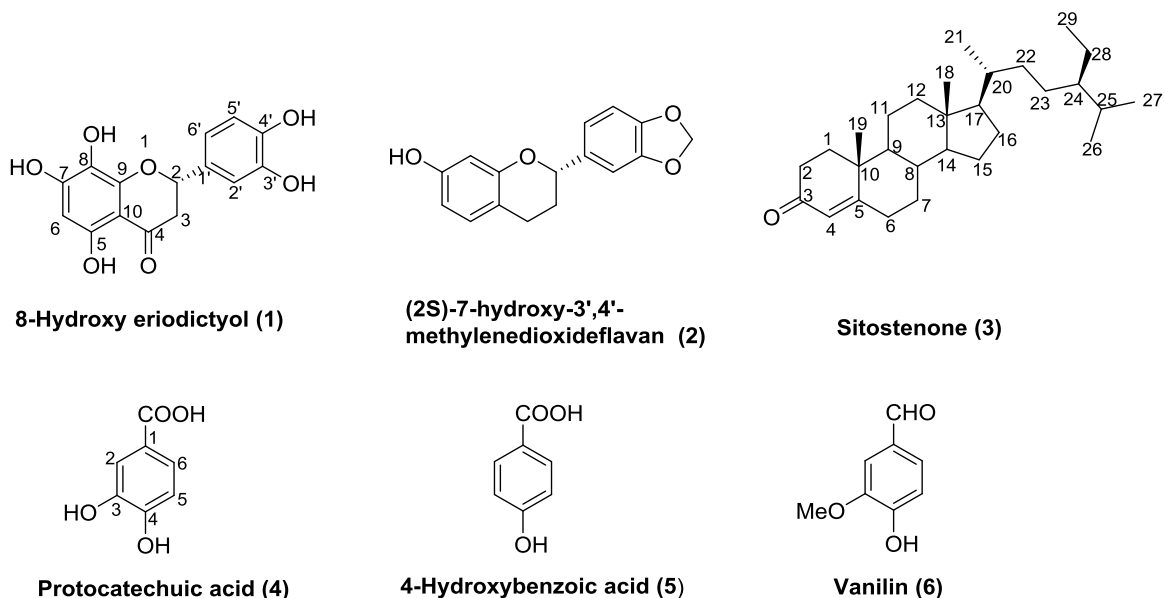
Figure 1. Chemical structures of isolated compounds **1-6** from *K. saxatilis* stems.

and signals of pyrane ring at δ_H 4.95 (1H, dd, *J* = 10 Hz, H-2), 2.88 and 2.70 (2H, m, H-4), 2.13 and 2.03 (2H, m, H-3). The ^{13}C-NMR showed 16 carbon signals of a flavan including 12 aromatic carbons ranging from 155.9 to 103.5 ppm, an methylenedioxide carbon at δ_C 101.1 (C-7′) and 3 signals at δ_C 77.8 (C-2), 30.0 (C-4) and 24.4 (C-3). In the HMBC spectrum, the correlations of H-7′ to C-3′ and C-4′; H-3, H-6, H-8 to C-10 were observed (Fig. 2). Compound **2** was determined as (2*S*)-7-hydroxy-3′,4′-methylenedioxideflavan by comparision of NMR and optical rotation data with those reported in the literature.[14-15] Compound **2** has been isolated from *K. pachycarpa* [16] and *K. laurina* stem barks.[17]
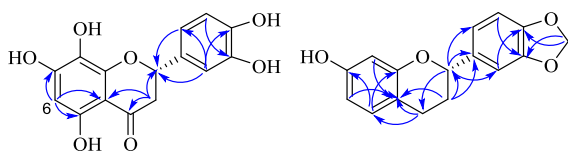

Figure 2. Key HMBC correlations of compound **1-2**.

Compound **3** was obtained as a white solid, The ESI-MS spectrum exhibited a protonated ion at *m/z* 413 [M+H]⁺, corresponding to $C_{29}H_{48}O$ (M = 412) molecular formula. The ^{1}H-NMR spectrum showed characteristic signals of a steroid with 6 methyl group including 2 singlets

at δ_H 1.17 (3H, s, H-19), 0.70 (3H, s, H-18), 3 doublets at δ_H 0.91 (3H, d, *J* = 6.5 Hz, H-21), 0.83 (3H, d, *J* = 7.0 Hz, H-27) and 0.81 (3H, d, *J* = 7.0 Hz, H-26) and a triplet at δ_H 0.84 (3H, t, *J* = 7.5 Hz, H-29), an olefinic proton at δ_H 5.71 (1H, s, H-4). The ^{13}C-NMR showed 29 carbon signals including 6 methyl groups at δ_C 19.8, 19.0, 18.7, 17.4, 12.0 , 11.9 (C-26, C-27, C-21, C-19, C-29, C-18); a carbonyl signal at δ_C 199.6 (C-3) and 2 olefinic carbons at δ_C 171.6 (C-5) and 123.7 (C-4). Compound **3** was identified as stigmast-4-en-3-one or sitostenone.[18]

Compound **4** was isolated as a brown solid. The ESI-MS spectrum exhibited a protonated molecular ion peak at *m/z* 155 [M+H]⁺ corresponding to the molecular formula of $C_7H_6O_4$ (M = 154). The ^{1}H NMR spectrum revealed signals of an ABX system with 3 protons at δ_H 7.41 (1H, d, *J* = 1.5 Hz, H-2), 7.41 (1H, dd, *J* = 1.5 Hz, *J* =8.5 Hz, H-6), 6.76 (1H, d, *J* = 8.5 Hz, H-5). The ^{13}C-NMR showed 7 carbon signals with a carboxylic signal at δ_C 169.4 (COOH) and six aromatic carbons. Comparing NMR spectral data,[19] **4** was determined as protocatechuic acid.

Compound **5** was isolated as a brown solid. The ESI-MS spectrum showed a pseudo-molecular ion peak at *m/z* 139 [M+H]⁺ suggested

the molecular formula of **1** is $C_7H_6O_3$ (M= 138). The ^{1}H NMR spectrum displayed signals of an A_2B_2 system with 4 protons at δ_H 7.85 (2H, d, J = 8.5 Hz, H-2, H-6), 6.76 (2H, d, J = 8.5 Hz, H-3, H-5). The ^{13}C-NMR also showed 7 carbon signals with a carboxylic signal at δ_C 169.9 (COOH) and six aromatic carbons. Compound **5** was assigned as 4-hydroxybenzoic acid by comparison of NMR data with those reported in the previous paper.[19]

Compound **6** was isolated as a pale yellow solid. The ESI-MS spectrum exhibited a protonated molecular ion peak at *m/z* 153 [M+H]$^+$ corresponding to the molecular formula of $C_8H_8O_3$ (M = 152). The ^{1}H NMR spectrum revealed signals of an aldehyde group at δ_H 9.83 (1H, s, CHO), 3 protons of an ABX system at δ_H 7.43 (2H, m, H-2, H-6), 7.04 (1H, d, J = 8.5 Hz, H-5), and a methoxy group at δ_H 3.97 (3H, s, OMe). The ^{13}C-NMR showed 8 carbon signals including a carbonyl carbon at δ_C 190.8 (CHO), six aromatic carbons and a methoxy group at δ_C 56.0 (OMe). Compound **6** was identified as vanillin by comparison NMR spectral data with published paper.[20]

4. CONCLUSION

Six known compounds have been isolated and elucidated as 8-hydroxy eriodictyol (**1**), (2*S*)-7-hydroxy-3′,4′-methylenedioxideflavan (**2**), sitostenone (**3**), protocatechuic acid (**4**), 4-hydroxybenzoic acid (**5**), and vanillin (**6**) from stems of *K. saxatilis* including. Compounds **1** and **3-6** were found for the first time from *Knema* genus.

Acknowledgement

REFERENCES

1. V. V. Chi. *Dictionary of Vietnamese medicinal plants*, Hanoi Medical Publisher, 2012.

2. W. M. N. H. W. Salleh, F. Ahmad. Phytochemistry and biological activities of the genus Knema (Myristicaceae), *Pharmaceutical Sciences*, **2017**, *23*, 249-255.

3. A. Zahir, A. Jossang, B. Bodo, H. A. Hadi, H. Schaller, T. Sevenet. Knerachelins A and B, antibacterial phenylacylphenols from Knema furfuracea, *Journal of Natural Products,* **1993**, *56*(9), 1634-7.

4. M. N. Akhtar, K. W. Lam, F. Abas, Maulidiani, S. Ahmad, S. A. A. Shah. New class of acetylcholinesterase inhibitors from the stem bark of Knema laurina and their structural insights, *Bioorganic & Medicinal Chemistry Letters,* **2011**, *21(*13*)*, 4097-103.

5. Y. X. Zhang, Z. Lu, W. C. Wu, Y. G. Chen, R. Zhan. Bioactive Flavonoids from Knema elegans, *Phyto Chemistry Letters*, **2021**, *42*, 121-124.

6. T. V. Pham, H. K. T. Bach, D. V. Ho, B. C. Nguyen. Chemical constituents from the Knema globularia fruits and their in vitro cytotoxicity, *Natural Product Research*, **2022**, *36*, 256-262.

7. T. K. D. Le, A. Danova, T. Aree, T. H. Duong, M. Koketsu, M. Ninomiya, Y. Samada, P. Kamsri, P. Pungpo, W. Chavasiri. α-Glucosidase inhibitors from the stems of Knema globularia, *Journal of Natural Products,* **2022**, *85*, 776-786.

8. T. H. Tung, C. T. Hue, T. H. Giap, H. T. Thoa, N. A. Dung, N. T. M. Hang, N. V. Hung, L. N. Thanh. Lignans isolated from the ethyl acetate extract of Knema pachycarpa fruit, *Vietnam Journal of Chemistry*, **2017**, *55*, 406.

9. T. H. Giap, T. T. Hoa, D. N. Thuc, N. T. M. Hang, N. V. Hung, N. Q. Chi, L. N. Thanh. Flavonoids from stems of Knema caxatilis de Wilde, *Pharmaceutical Journal*, **2018**, *58*, 62-64.

10. T. H. Giap, H. T. Thoa, V. T. K. Oanh, N. T. M. Hang, N. H. Dang, D. N. Thuc, N. V. Hung, L. N. Thanh. New acetophenone and cardanol derivatives from Knema pachycarpa, *Natural Product Communication*, **2019**, *14*, 1934578X19850046.

11. N. T. T. Oanh, P. T. T. Ha, T. H. Giap, V. T. K. Oanh, N. T. M. Hang, D. N. Thuc, D. Fedeli, S. Gabbianelli, P. T. Huong, N. V. Hung,

L. N. Thanh. Chemical constituents and biological activities of the leaves of Knema saxatilis, *Chemistry of Natural Compounds,* **2021**, *57*, 355-359.

12. T. H. Giap, P. M. Duc, N. V. The, M. Popova, V. Bankova, C. T. Hue, V. T. K. Oanh, N. T. M. Hang, N. V. Hung, T. N. Le. Chemical constituents and biological activities of the fruits of Knema pachycarpa de Wilde, *Natural Product Research,* **2021**, *35*, 455-464.

13. A. R. Bilia, L. Ciampi, J. Mendez, I. Morelli. Phytochemical investigations of Licania genus. Flavonoids from Licania pyrifolia, *Pharmaceutica Acta Helvetiae*, **1996**, *71*, 199-204.

14. S. Ghosal, S. K. Singh, R. S. Srivastava. Flavans from Zephyranthes flava, *Phytochemistry,* **1985**, *24*, 151-153.

15. O. O. Oluyemisi, A. E. Oriabure, A. J. Adekunle, K. S. T. Ramsay, S. Shyyaula, M. I. Choudhary. Bioassay-guided isolation of Poliovirus-inhibiting constituents from Zephyranthes candida, *Pharmaceutical Biology*, **2015**, *53*(6), 882-887.

16. T. H. Giap, H. T. Thoa, C. T. Hue, N. T. T. Oanh, V. T. K. Oanh, N. T. M. Hang, N. V. Hung, N. S. Mishchenko, S. A. Fedoreev, L. N. Thanh. Flavanes and fatty acids from bark of Knema pachycarpa de Wilde, *Pharmaceutical Journal*, **2017**, *57*, 33-36.

17. M. J. G. Gonzalez, C. J. DeOliveira, J. Fernandes, A. Kijjoa, W. Herz. Further alkyl and alkenylphenols of Knema laurina and Knema austrosiamensis: location of the double bond in the alkenyl side chains, *Phytochemistry*, **1996**, *43*, 1333-1337.

18. Q. Y. Wang, G. X. Cui, J. C. Wu, Y. G. Chen. Steroid from Trigonostemon heterophyllus, *Chemistry of Natural Compounds,* **2015**, *51*, 1196-1198.

19. D. L. Vu, G. L. Pham, V. H. Hoang, T. P. Nguyen, Isolated compounds from leaves of *Leea rubra Blume* ex Spreng, *VNU Journal of Science: Medical and Pharmaceutical Sciences*, **2016**, *32*, 12-17.

20. N. P. Hung, D. T. Thuy, D. N. Quang, N. A. Tuan, T. N. T. Vy, N. T. N. Yen, G. T. K. Lien. PTP1B inhibitory constituents from Gymnosporia Stylosa Pierre, *The University of Danang Journal of Science and Technology*, **2021**, 33-36.

Giới hạn thủy động lực học của động lực Kawasaki với trường hỗn độn không bị chặn

Nguyễn Đặng Thiên Thư*

Khoa Toán và Thống kê, Trường Đại học Quy Nhơn, Việt Nam

TÓM TẮT

Vào năm 2003, Faggionato A. và Martinelli F. đã chứng minh được rằng giới hạn thủy động lực học của một quá trình loại trừ đơn giản dưới tác động của một trường hỗn độn bị chặn có thể được mô tả bởi một bài toán Cauchy. Trong bài báo này, ta chỉ ra rằng một kết luận tương tự cũng đúng nếu trường hỗn độn không bị chặn và phân phối của nó thoả mãn một điều kiện nào đó.

Từ khóa: *Giới hạn thủy động lực học, hệ hỗn độn, quá trình loại trừ.*

---

*Tác giả liên hệ chính.
Email: nguyendangthienthu@qnu.edu.vn

Hydrodynamic limit of the Kawasaki dynamics with unbounded disorder

Nguyen Dang Thien Thu*

Department of Mathematics and Statistics, Quy Nhon University, Vietnam

ABSTRACT

In 2003, Faggionato A. and Martinelli F. proved that the hydrodynamic behavior of a simple exclusion process under the influence of a bounded disorder field can be described by a Cauchy problem. In this paper, we show that a similar conclusion also holds true if the disorder field is unbounded and satisfies a certain condition on its distribution.

Keywords: *Hydrodynamic limits, disordered systems, exclusion processes.*

1. INTRODUCTION AND MAIN RESULT

A lot of techniques have been developed so far in order to investigate the hydrodynamic limit of an interacting particle system in which each particle moves on an integer lattice. An interacting particle system is said to have a hydrodynamic limit if for which there exists a time and space rescaling in which the conserved quantities evolve according to a certain partial differential equation. This partial differential equation is called the hydrodynamic equation corresponding with the system. The simplest and most widely studied interacting particle system is the simple exclusion process, where a particle sitting on a site x of the d-dimensional torus $\mathbf{T}^d = \mathbb{R}^d/\mathbb{Z}^d$ with unit volume, waits an exponential time and attempts to jump to the nearest neighbor site y together with the exclusion rule that forbids the jumps to occupied sites. Furthermore, it is assumed that the total number of particles is the unique quantity conserved by the time evolution. We denote by $\mathbf{T}_N^d = \mathbb{Z}^d/N\mathbb{Z}^d$ the corresponding microscopic space and by π_t^N the empirical measure on $\mathbf{T}^d$ obtained by assigning to each particle a mass N^{-d},

$$\pi_t^N(d\theta) = \pi_t^N(\eta, d\theta) = \underset{x \in \mathbf{T}_N^d}{Av}\, \eta_x(tN^2)\delta_{x/N}(d\theta)$$

where $\underset{x \in \mathbf{T}_N^d}{Av}$ stands for the spatial average and η_x is the number of particles at site x. Then the dynamics is determined by the diffusively rescaled Markov generator $N^2\mathcal{L}_N$,

$$\mathcal{L}_N f(\eta) = \sum_{e \in \mathcal{E}} \sum_{x \in \mathbf{T}_N^d} c_{x,x+e}(\eta)[f(\eta^{x,x+e}) - f(\eta)],$$

where $\mathcal{E}$ is the canonical basis of the d-dimensional lattice $\mathbb{Z}^d$.

In the above expression, the configuration $\eta^{x,y}$ is obtained from η by exchanging the values η_x and η_y, the positive and bounded transition rate $c_{x,y}(\eta)$ is not only translation invariant

---

Corresponding author.
Email: nguyendangthienthu@qnu.edu.vn

in the sense that $c_{x+z,y+z}(\eta) = c_{x,y}(\tau_z\eta)$, where $\tau_z\eta$ is the particle configuration translated by z, but also satisfies the identity $c_{x,y}(\eta) = c_{y,x}(\eta)$.

Given a symmetric, finite range and translation invariant transition probability $p(x,y)$ on $\mathbb{Z}^d$, i.e. $p(x,y) = p(0, y-x) =: p(y-x)$, the set $\{x : p(x) > 0\}$ is finite and $p(x) = p(-x)$. If $c_{x,x+e}(\eta) := \sum_{y\in\mathbb{Z}^d} p(e + yN), \forall x \in \mathbf{T}_N^d, \forall e \in \mathcal{E}$ then such a system is called a symmetric simple exclusion process. We denote by $\mathcal{M}_2$ the set of probability measures on $\mathbf{T}^d$, which are absolutely continuous with respect to Lebesgue measure with density bounded by 1. Now, let a sequence of probability measures $\{\mu^N\}_{N\geq 1}$ on $\Omega_N = \{0,1\}^{\mathbf{T}_N^d}$ be associated to a function ρ_0 on $\mathbf{T}^d$ in the sense that under μ^N, the sequence of empirical measures π_0^N on $\mathbf{T}^d$ converges in probability to $\rho_0(\theta)d\theta \in \mathcal{M}_2$. Then, it is shown that after a suitable space and time rescaling, the corresponding sequence $\{\mathbb{P}_t^{\mu^N}\}_{N\geq 1}$ of the distributions at time t of a symmetric simple exclusion process with the initial measures μ^N, is associated to the density of particles $\rho(t,\cdot)$ which is the unique weak solution of the heat equation

$$\partial_t\rho(t,\theta) = \frac{1}{2}\Delta\rho(t,\theta), \ \ \rho(0,\theta) = \rho_0(\theta). \quad (1)$$

More generally, the hydrodynamic behavior of the gradient exclusion process and the nongradient exclusion process are also obtained. For a more comprehensive view, we recommend[2] Section 7.

In[1], Faggionato A. and Martinelli F. study the hydrodynamic behavior of a simple exclusion process under the influence of an external random field. The disorder field α is given by independent identically distributed random variables with $|\alpha_x| \leq B, \forall x \in \mathbb{Z}^d$. Let us describe the dynamics. Given a disorder configuration α and a subset Λ of $\mathbb{Z}^d$, they define the grand canonical Gibbs measure $\mu_\Lambda^{\alpha,\lambda}$ on $\{0,1\}^\Lambda$ associated to the chemical potential $\lambda \in \mathbb{R}$ as the product measure

$$\mu_\Lambda^{\alpha,\lambda}(\eta) = \prod_{x\in\Lambda} \frac{e^{(\alpha_x+\lambda)\eta_x}}{1 + e^{\alpha_x+\lambda}}$$

and the corresponding canonical measure $\nu_{\Lambda,\rho}^\alpha$ with density ρ as

$$\nu_{\Lambda,\rho}^\alpha(\cdot) = \mu_\Lambda^{\alpha,\lambda}(\cdot\,|m_\Lambda = \rho),$$

where the particle density is $m_\Lambda = \dfrac{1}{|\Lambda|}\sum_{x\in\Lambda}\eta_x$.

The positive and bounded transition rate $c_{x,y}^\alpha(\eta)$ depending on the disorder configuration (α_x, α_y) is not only translation invariant, i.e.

$$c_{x,y}^{\tau_z\alpha}(\tau_z\eta) = c_{x+z,y+z}^\alpha(\eta), \forall z \in \mathbb{Z}^d,$$

where $\tau_z\alpha, \tau_z\eta$ is the disorder and particle configuration translated by z, but also satisfies the identity $c_{x,y}^\alpha(\eta) = c_{y,x}^\alpha(\eta)$. Moreover, it satisfies the detailed balance condition with respect to the Gibbs measure $\mu_\Lambda^{\alpha,\lambda}$, i.e.

$$c_{x,y}^\alpha(\eta) = c_{x,y}^\alpha(\eta^{x,y})e^{-(\alpha_x-\alpha_y)(\eta_x-\eta_y)}.$$

Then, the lattice gas with Kawasaki dynamics is a continuous time Markov chain determined by the diffusively rescaled Markov generator $N^2\mathcal{L}_N^\alpha$, where $\mathcal{L}_N^\alpha := \mathcal{L}_{\mathbf{T}_N^d}^\alpha$ and for all $\Lambda \subset \mathbb{Z}^d$,

$$\mathcal{L}_\Lambda^\alpha f(\eta) = \sum_{e\in\mathcal{E}}\sum_{x\in\Lambda} c_{x,x+e}^\alpha(\eta)[f(\eta^{x,x+e}) - f(\eta)].$$

Since the present system does not satisfy the gradient condition, except the trivial case when the disorder field is constant, they apply the classical approach, i.e. looking for a generalized Fick's law to establish the hydrodynamic limit of a disordered nongradient system but with a slight modification. Namely, they are interested in the limit

$$\lim_{l\uparrow\infty}(2l)^{-d}\mathbb{E}[\mu^{\alpha,\lambda_0(\rho)}$$
$$\left(\sum_{|x|\leq l-\sqrt{l}}\tau_x f, (-\mathcal{L}_{\Lambda_l}^\alpha)^{-1}\sum_{|x|\leq l-\sqrt{l}}\tau_x g\right)],$$

where $\mathbb{E}$ stands for the corresponding expectation with respect to the product measure defined on the disorder configuration space and $\lambda_0(\rho)$ is the annealed chemical potential such that $\mathbb{E}[\mu^{\alpha,\lambda_0(\rho)}(\eta_0)] = \rho$.

By the theory of closed and exact forms generalized from the ones for the nondisordered and nongradient system, it can be proved that the above limit exists and defines the semi-inner product $V_\rho(f, g)$. On the other hand, the subspace $\{\sum_{e \in \mathcal{E}} a_e j^\alpha_{0,e} + \mathcal{L}^\alpha_{\mathbb{Z}^d} g : a \in \mathbb{R}^d, g \in \mathbb{G}\}$ is dense in $\mathcal{G}$ endowed with the semi-inner product V_ρ, c.f.[1] Section 7.1, where the instantaneous current $j^\alpha_{x,y}(\eta) = c^\alpha_{x,y}(\eta)(\eta_x - \eta_y)$ defined as the difference between the rate at which a particle jumps from x to y and the rate at which a particle jumps from y to x, $\mathbb{G}$ stands for the space of local and bounded functions on $[-B, B]^{\mathbb{Z}^d} \times \{0, 1\}^{\mathbb{Z}^d}$, and $\mathcal{G}$ is the space of mean-zero functions $g \in \mathbb{G}$ with respect to all canonical measures on some cube. Nevertheless, $\eta_e - \eta_0 \notin \mathcal{G}$ because of the disorder field, hence $\{\eta_e - \eta_0\}_{e \in \mathcal{E}}$ no longer forms a basis of $\mathcal{L}^\alpha \mathbb{G}^\perp$. Therefore, they try to consider the difference

$$\eta_e - \eta_0 - \nu^\alpha_{\Lambda_n, m_n(\eta)}(\eta_e - \eta_0).$$

Similar to the one considered in[4], it can be proved that for each $e \in \mathcal{E}$, the sequence of these differences is Cauchy in $\overline{\mathcal{G}}$ with the semi-norm $V_\rho^{1/2}$ and that the limit points of these sequences with e varying in $\mathcal{E}$ form a basis of $\mathcal{L}^\alpha \mathbb{G}^\perp$. Then the current $j^\alpha_{x,x+e}$ can be written as the sum of some negligible fluctuation $\tau_x \mathcal{L}^\alpha g$ and

$$-\sum_{e' \in \mathcal{E}} D_{e,e'}(\rho) \tau_x (\eta_{e'} - \eta_0 - \nu^\alpha_{\Lambda_n, m_n(\eta)}(\eta_{e'} - \eta_0))$$

for some $d \times d$ matrix $D(\rho)$.

In order to get a generalized Fick's law, it remains to show the negligibility of the term $\tau_x(\nu^\alpha_{\Lambda_n, m_n(\eta)}(\eta_e - \eta_0)), \forall x \in \mathbf{T}^d_N$. Unfortunately, in the presence of the disorder field, $\|\nu^\alpha_{\Lambda_n, m_n(\eta)}(\eta_e - \eta_0)\|_\infty = O(1), \forall n$. Therefore, Faggionato and Martinelli considered the gradient of the density in two large adjacent cubes in the hope that the fluctuations are small. This problem has already solved by Faggionato and Martinelli as long as $d \geq 3$ in[1].

They finally arrive at the main conclusion on the hydrodynamic limit of a system with the bounded disorder. Namely, in dimension larger

than 2, for almost every disorder configuration, by rescaling space and time diffusively, the hydrodynamic equation is the nonlinear parabolic equation

$$\partial_t \rho(t, \theta) = \nabla(D(\rho(t, \theta)) \nabla \rho(t, \theta)),$$

$$\rho(0, \theta) = \rho_0(\theta),$$

where the deterministic diffusion matrix D can be described by the following variational characterization, for any $a \in \mathbb{R}^d$,

$$(a, D(\rho)a) = \frac{1}{2\chi(\rho)} \inf_{g \in \mathbb{G}} \sum_{e \in \mathcal{E}} \mathbb{E}\Big[\mu^{\alpha, \lambda_0(\rho)}$$

$$\Big(c^\alpha_{0,e}\Big(a_e(\eta_e - \eta_0) + \nabla_{0,e}\Big(\sum_{x \in \mathbb{Z}^d} \tau_x g\Big)\Big)^2\Big)\Big]$$

where $\chi(\rho) = \mathbb{E}[\mu^{\alpha, \lambda_0(\rho)}(\eta_0) - \mu^{\alpha, \lambda_0(\rho)}(\eta_0)^2]$ and $\nabla_{x,y} g(\alpha, \eta) = g(\alpha, \eta^{x,y}) - g(\alpha, \eta)$. Furthermore, Faggionato and Martinelli also prove that $D(\cdot)$ is positive, bounded and continuous in $(0, 1)$. That hydrodynamic equation is obtained under the assumption that $D(\cdot)$ has a continuous extension in the closed interval $[0, 1]$. A few years later on, in[3], Quastel proved that this diffusion matrix D is actually continuous in the closed interval $[0, 1]$.

The above conclusion on the hydrodynamic behavior of a disordered system has been obtained as long as the disorder field is bounded. A natural question posed here is that whether that conclusion holds true if the random field is unbounded. In this paper, we will indicate that a similar conclusion also holds true if the disorder field is unbounded and satisfies a certain condition on its distribution. Let us consider the disorder field given by independent identically distributed random variables satisfying the technical condition that there exists some $u > 0$ such that for all $x \in \mathbb{Z}^d, \mathbb{E}[e^{u|\alpha_x|}] < +\infty$. Then, under the assumption that the diffusion matrix D has a continuous extension in the closed interval $[0, 1]$, in dimension larger than 2, for almost every disorder configuration, by rescaling space and time diffusively, the macroscopic evolution of the system with this new disorder field is described by the nonlinear parabolic equation as above.

More precisely, let us present the main result as follows.

Theorem 1.1. *Let $d \geq 3, T > 0$. Let the disorder field be given by iid random variables satisfying the technical condition*

$$\exists u > 0 \text{ such that } \forall x \in \mathbb{Z}^d, \mathbb{E}[e^{u|\alpha_x|}] < +\infty. \quad (2)$$

Assume that the diffusion matrix D defined as in[1] Theorem 2.1 for $\rho \in (0,1)$ has a continuous extension in the closed interval $[0,1]$. Consider a sequence of probability measures $\{\mu^N\}_{N \geq 1}$ on Ω_N associated to the macroscopic profile $\rho_0(\theta)d\theta \in \mathcal{M}_2$. Then for almost every disorder configuration α, any $t \in [0,T]$, the sequence of probability measures $\{\mathbb{P}_t^{\alpha, \mu^N}\}_{N \geq 1}$ is associated to the macroscopic profile $\rho(t, \theta)d\theta \in \mathcal{M}_2$ whose density is the unique weak solution $\rho \in C([0,T], \mathcal{M}_2)$ of the Cauchy problem

$$\begin{cases} \partial_t \rho(t, \theta) & = \nabla(D(\rho(t, \theta))\nabla\rho(t, \theta)) \\ \rho(0, \theta) & = \rho_0(\theta). \end{cases} \quad (3)$$

and satisfying the energy estimate

$$\int_0^T \int_{\mathbf{T}^d} |\nabla\rho(t, \theta)|^2 d\theta dt < \infty.$$

This result follows from repeating the proof for the case of bounded random field and replacing the arguments where the boundedness is used by the different ones.

For this purpose, it is enough to deal with all the estimates involved in the boundedness of the random field we have considered above. Namely, they are the estimate on the entropy $H(\mathbb{P}^{\mu^N} | \mathbb{P}^{\mu_N})$, the equilibrium bounds and the results applying them as well as the description of $(a, D(0)a), (a, D(1)a)$ as the limit of $(a, D(\rho)a)$ when $\rho \downarrow 0$ and $\rho \uparrow 1$, respectively. We will carry them out with more details in the following three sections.

2. ESTIMATE ON THE ENTROPY

As mentioned in[1] Section 4, if $|\alpha_x| \leq B, \forall x \in \mathbb{Z}^d$ then there exists some constant $C(B) > 0$ such

that for every disorder configuration α and any $N \geq 1$,

$$\mu_N(\eta) = \prod_{x \in \mathbf{T}_N^d} \frac{e^{\alpha_x \eta_x}}{1 + e^{\alpha_x}} \geqslant e^{-C(B)N^d}, \ \forall \eta \in \Omega_N$$

and the estimate on the entropy $H(\mathbb{P}^{\mu^N} | \mathbb{P}^{\mu_N})$ will thus follow, i.e. $\exists C > 0$ such that $H(\mathbb{P}^{\mu^N} | \mathbb{P}^{\mu_N}) \leq CN^d$.

Let us now show that for the present model, i.e. the system with unbounded random field satisfying the technical condition (2), we also obtain the above bound on $\mu_N(\eta)$ for almost any disorder configuration and any N large enough.

Lemma 2.1. *There exists a constant $C > 0$ such that for almost any disorder configuration α and any N large enough,*

$$\mu_N(\eta) = \prod_{x \in \mathbf{T}_N^d} \frac{e^{\alpha_x \eta_x}}{1 + e^{\alpha_x}} \geq e^{-CN^d}, \quad \forall \eta \in \Omega_N. \quad (4)$$

Proof. By the technical condition (2), there exists $u_0 > 0$ such that $\mathbb{E}[e^{u_0|\alpha_x|}] \leq C'$. We set

$$\mathcal{Q}_N := \left\{ \alpha : \prod_{x \in \mathbf{T}_N^d} \frac{e^{-|\alpha_x|}}{1 + e^{\alpha_x}} \geq e^{-CN^d} \right\}$$

where $C := K + \ln 2$ for some $K > \dfrac{2 \ln C'}{u_0}$. Then, we have

$$\mathbb{P}(\mathcal{Q}_N) \leq \mathbb{P}\left(\prod_{x \in \mathbf{T}_N^d} \frac{1}{2e^{2|\alpha_x|}} \geq e^{-CN^d} \right)$$

$$\leq \mathbb{P}\left(\prod_{x \in \mathbf{T}_N^d} e^{2|\alpha_x|} \geq e^{KN^d} \right)$$

$$\leq \inf_{u \geq 0} e^{-\frac{u}{2}KN^d} \mathbb{E}\left[\left(\prod_{x \in \mathbf{T}_N^d} e^{2|\alpha_x|} \right)^{\frac{u}{2}} \right]$$

$$= \inf_{u \geq 0} \left(e^{-\frac{u}{2}K} \mathbb{E}[e^{u|\alpha_x|}] \right)^{N^d}$$

$$\leq \left(e^{-\frac{u_0}{2}K} \mathbb{E}[e^{u_0|\alpha_x|}] \right)^{N^d}$$

$$\leq e^{(\ln C' - \frac{u_0}{2}K)N^d}.$$

Hence,

$$\sum_{N \geq 1} \mathbb{P}(\mathcal{Q}_N) \leq \sum_{N \geq 1} e^{(\ln C' - \frac{u_0}{2}K)N^d} < +\infty.$$

Then by Borel-Cantelli lemma, for almost every disorder configuration α, for all $N \geq N_0(\alpha), \alpha \notin \mathcal{Q}_N$. Moreover, due to the fact that $-|\alpha_x| \leq \alpha_x \eta_x, \forall \eta \in \Omega_N$, the assertion of the lemma follows. □

3. GENERALIZED EQUILIBRIUM BOUNDS

In the proof of[1] Lemma A.2, all the estimates originate from bounding $\mu^\lambda(\eta_x)$ at a single point x, i.e.

$$\frac{e^{-2B}e^\lambda}{1+e^\lambda} \leq \mu^\lambda(\eta_x) = \frac{e^{\alpha_x+\lambda}}{1+e^{\alpha_x+\lambda}} \leq \frac{e^{2B}e^\lambda}{1+e^\lambda} \quad (5)$$

if $|\alpha_x| \leq B, \forall x \in \mathbb{Z}^d$. It thus implies the estimate

$$C^{-1}\mu^\lambda(m_\Lambda) \leq \mu^\lambda(m_\Delta) \leq C\mu^\lambda(m_\Lambda) \quad (6)$$

for all $\Delta \subset \Lambda$ and every disorder configuration.

Now, if the disorder field is unbounded then we no longer obtain an estimate as (5). However, the bound (6) still holds true but for almost all disorder configurations and all finite subsets $\Lambda \subset \mathbb{Z}^d$ large enough by applying the Large deviation estimate ([1] Lemma A.1). More precisely,[1] Lemma A.2 is substituted by a more generalized one as follows.

Lemma 3.1. *Given a nonempty finite subset $\Lambda \subset \mathbb{Z}^d$ of cardinality L and $\lambda \in \mathbb{R}$. We set $A := \mathbb{E}\left(\frac{e^{\alpha_0+\lambda}}{1+e^{\alpha_0+\lambda}}\right), \rho := \mu^\lambda(m_\Lambda)$ and $a_\rho := \min(\rho, 1-\rho)$. Then, there exists a constant $C > 0$ such that for almost any disorder configuration α, any L large enough, any subset $\Delta \subset \Lambda$ satisfying $KL \leq |\Delta| \leq L$, where $\frac{16\ln 2}{(C-2)^2 A^2} < K < \frac{1}{2}$,*

a) $C^{-1}|\Delta|\rho \leq \mu^\lambda(N_\Delta) \leq C|\Delta|\rho$,

b) $C^{-1}|\Delta|(1-\rho) \leq \mu^\lambda(|\Delta|-N_\Delta) \leq C|\Delta|(1-\rho)$,

c) $C^{-1}|\Delta|a_\rho \leq \mu^\lambda(N_\Delta; N_\Delta) \leq C|\Delta|a_\rho$,

d) $|\mu^\lambda(f; N_{\Delta_f})|$
$\leq C\|f\|_\infty \min(|\Delta_f|a_{\overline{\rho}}, \sqrt{|\Delta_f|a_{\overline{\rho}}})$,
for any function f with Δ_f large enough, where $\overline{\rho} := \mu^\lambda(m_{\Delta_f})$.

Proof. Due to[1] Lemma A.1 applied to $f(\alpha) = \frac{e^{\alpha_0+\lambda}}{1+e^{\alpha_0+\lambda}} - A$, for any $\delta > 0$ and any nonempty finite subset $\Lambda \subset \mathbb{Z}^d$, we obtain

$$\mathbb{P}(|\mu^\lambda(m_\Lambda) - A| \geq \delta) \leq 2e^{-\frac{1}{4}\delta^2|\Lambda|}. \quad (7)$$

We set

$$\mathcal{S} := \{\Delta : \Delta \subset \Lambda \text{ with } KL \leq |\Delta| \leq L\},$$

$$\mathcal{Q}_L := \{\exists\Delta \in \mathcal{S} : \mu^\lambda(m_\Delta) > C\mu^\lambda(m_\Lambda)\},$$

for a constant $C > 2 + \frac{4\sqrt{2\ln 2}}{A}$ and any $\frac{16\ln 2}{(C-2)^2 A^2} < K < \frac{1}{2}$. Therefore, by (7), we get

$$\sum_{L \geq 0} \mathbb{P}(\mathcal{Q}_L) \leq \sum_{L \geq 0} \sum_{\Delta \in \mathcal{S}} \mathbb{P}(\mu^\lambda(m_\Delta) > C\mu^\lambda(m_\Lambda))$$

$$\leq \sum_{L \geq 0} 2^L[\mathbb{P}(\mu^\lambda(m_\Delta) \geq \frac{C}{2}A) + \mathbb{P}(\mu^\lambda(m_\Lambda) \leq \frac{A}{2})]$$

$$\leq \sum_{L \geq 0} 2^L[\mathbb{P}(\mu^\lambda(m_\Delta) - A \geq (\frac{C}{2}-1)A)$$

$$+ \mathbb{P}(\mu^\lambda(m_\Lambda) - A \leq -\frac{A}{2})]$$

$$\leq \sum_{L \geq 0} 2^L(e^{-\frac{1}{16}(C-a)^2 A^2 KL} + e^{-\frac{1}{16}A^2 L}) < +\infty.$$

Then, by Borel-Cantelli lemma, for almost all disorder configurations α, there exists $L_0(\alpha)$ such that for all $L \geq L_0(\alpha), \alpha \notin \mathcal{Q}_L$. It implies the upper bound of a). For the lower bound of a), we do the same argument. Then, the estimate b) easily follows from a).

Let us now verify the estimate c). We obtain the upper bound from using the fact that $\mu^\lambda(N_\Delta; N_\Delta) \leq \mu^\lambda(N_\Delta)$ and applying a). For the lower bound, we assume $\rho \in [0, \frac{1}{2}]$ and consider the set $W := \{x \in \Lambda : \mu^\lambda(\eta_x) \leq \frac{1}{2}\}$.

⋆ If $|W| \geq \frac{1}{2}|\Lambda|$ then $W \in \mathcal{S}$. Hence, we have

$$\mu^\lambda(N_\Lambda; N_\Lambda) = \sum_{x \in \Lambda} \mu^\lambda(\eta_x; \eta_x) \geq \sum_{x \in W} \mu^\lambda(\eta_x; \eta_x)$$

$$= \sum_{x \in W} \mu^\lambda(\eta_x)(1 - \mu^\lambda(\eta_x))$$

$$\geq \frac{1}{2} \sum_{x \in W} \mu^\lambda(\eta_x) = \frac{1}{2}\mu^\lambda(N_W)$$

$$\geq \frac{1}{2}C^{-1}|W|\rho \geq C^{-1}|\Lambda|\rho.$$

⋆ If $|W| < \frac{1}{2}|\Lambda|$ then $|W^c| \geq \frac{1}{2}|\Lambda|$, i.e. $W^c \in \mathcal{S}$. Hence, we have

$$\mu^\lambda(N_\Lambda; N_\Lambda) = \sum_{x \in \Lambda} \mu^\lambda(\eta_x; \eta_x) \geq \sum_{x \in W^c} \mu^\lambda(\eta_x; \eta_x)$$

$$= \sum_{x \in W^c} \mu^\lambda(\eta_x)(1 - \mu^\lambda(\eta_x))$$

$$\geq \frac{1}{2} \sum_{x \in W^c} \mu^\lambda(1 - \eta_x)$$

$$= \frac{1}{2}\mu^\lambda(|W^c| - N_{W^c})$$

$$\geq \frac{1}{2}C^{-1}|W^c|(1 - \rho) \geq C^{-1}|\Lambda|\rho.$$

From two cases above, we get

$$\mu^\lambda(N_\Lambda; N_\Lambda) \geq C^{-1}|\Lambda|a_\rho. \qquad (8)$$

Now, given $\Delta \in \mathcal{S}$, applying (8) gives us $\mu^\lambda(N_\Delta; N_\Delta) \geq C^{-1}|\Delta|\min(\rho', 1 - \rho')$, where $\rho' := \mu^\lambda(m_\Delta)$. This estimate together with a), b) then imply the lower bound of c).

The estimate d) then follows from a) and c) similar to the one as presented in[1] Lemma A.2. □

Lemma 3.2. *There exists a constant $C > 0$ such that for almost any disorder configuration α, any function f with support Δ_f large enough and any subset $\Lambda \subset \mathbb{Z}^d$ large enough, for all $\lambda, \lambda' \in \mathbb{R}$,*

$$|\mu^{\lambda'}(f) - \mu^\lambda(f)|$$
$$\leq C\|f\|_\infty|\Delta_f||\mu^{\lambda'}(m_{\Delta_f}) - \mu^\lambda(m_{\Delta_f})|, \quad (9)$$

$$|\mu^{\lambda'}(m_\Lambda; N_\Lambda) - \mu^\lambda(m_\Lambda; N_\Lambda)|$$
$$\leq \frac{2|\Lambda'|}{|\Lambda|}|\mu^{\lambda'}(m_{\Lambda'}) - \mu^\lambda(m_{\Lambda'})|, \forall \Lambda' \subset \Lambda. \quad (10)$$

For any $\rho, \rho' \in (0, 1)$,

$$|\mu^{\lambda_0(\rho')}(\eta_0) - \mu^{\lambda_0(\rho)}(\eta_0)| \leq C|\rho' - \rho|, \tag{11}$$

$$|\mu^{\lambda_0(\rho')}(\eta_0; \eta_0) - \mu^{\lambda_0(\rho)}(\eta_0; \eta_0)| \leq C|\rho' - \rho|, \tag{12}$$

$$|\lambda_\Lambda(\rho) - \lambda_0(\rho)| \leq \frac{C}{\rho(1 - \rho)}|\rho - \mu^{\lambda_0(\rho)}(m_\Lambda)|. \tag{13}$$

Proof. Let us first prove (9). By setting $\rho := \mu^\lambda(m_{\Delta_f}), \rho' := \mu^{\lambda'}(m_{\Delta_f})$, we can write

$$|\mu^{\lambda'}(f) - \mu^\lambda(f)| = \left|\int_\rho^{\rho'} \frac{d}{ds}\mu^{\lambda_{\Delta_f}(s)}(f)ds\right|$$

$$\leq \int_\rho^{\rho'} |\mu^{\lambda_{\Delta_f}(s)}(f; N_{\Delta_f})\lambda'_{\Delta_f}(s)|ds. \quad (14)$$

By Lemma 3.1, for any function f with support large enough,

$$|\mu^{\lambda_{\Delta_f}(s)}(f; N_{\Delta_f})|$$
$$\leq C\|f\|_\infty|\Delta_f|$$
$$\times \min(\mu^{\lambda_{\Delta_f}(s)}(m_{\Delta_f}), 1 - \mu^{\lambda_{\Delta_f}(s)}(m_{\Delta_f}))$$
$$= C\|f\|_\infty|\Delta_f|\min(s, 1 - s).$$

Moreover,

$$\lambda'_{\Delta_f}(s) = \frac{1}{\mu^{\lambda_{\Delta_f}(s)}(m_{\Delta_f}; N_{\Delta_f})}$$

$$\leq \frac{C}{\min(\mu^{\lambda_{\Delta_f}(s)}(m_{\Delta_f}), 1 - \mu^{\lambda_{\Delta_f}(s)}(m_{\Delta_f}))}$$

$$= \frac{C}{\min(s, 1 - s)}.$$

Therefore, for any function f with support large enough,

$$|\mu^{\lambda_{\Delta_f}(s)}(f; N_{\Delta_f})\lambda'_{\Delta_f}(s)| \leq C\|f\|_\infty|\Delta_f|.$$

Hence, we obtain (9).

Now we verify (10). Let us observe that

$$|\mu(N_\Lambda; N_\Lambda; N_\Lambda)| \leq 2\sum_{x\in\Lambda}|\mu(\eta_x; \eta_x; \eta_x)|$$

$$\leq 2\sum_{x\in\Lambda}\mu(\eta_x)(1 - \mu(\eta_x))|2\mu(\eta_x) - 1|$$

$$\leq 2\sum_{x\in\Lambda}\mu(\eta_x)(1 - \mu(\eta_x))$$

$$= 2\sum_{x\in\Lambda}\mu(\eta_x; \eta_x) = 2\mu(N_\Lambda; N_\Lambda). \qquad (15)$$

We set $\tilde\rho := \mu^\lambda(m_{\Lambda'}), \tilde\rho' := \mu^{\lambda'}(m_{\Lambda'})$. By this setting, we have $\lambda_{\Lambda'}(\tilde\rho) = \lambda, \lambda_{\Lambda'}(\tilde\rho') = \lambda'$ and we can write

$$|\mu^{\lambda'}(m_\Lambda; N_\Lambda) - \mu^\lambda(m_\Lambda; N_\Lambda)|$$

$$= \left|\int_{\tilde\rho}^{\tilde\rho'}\frac{d}{ds}\mu^{\lambda_{\Lambda'}(s)}(m_\Lambda; N_\Lambda)ds\right|$$

$$\leq \int_{\tilde\rho}^{\tilde\rho'}|\mu^{\lambda_{\Lambda'}(s)}(m_\Lambda; N_\Lambda; N_\Lambda)\lambda_{\Lambda'}(s)|ds$$

$$\leq \int_{\tilde\rho}^{\tilde\rho'}\frac{2}{|\Lambda|}\mu^{\lambda_{\Lambda'}(s)}(N_\Lambda; N_\Lambda)\lambda_{\Lambda'}(s)ds$$

$$\leq \int_{\tilde\rho}^{\tilde\rho'}\frac{2}{|\Lambda|}\frac{\mu^{\lambda_{\Lambda'}(s)}(N_{\Lambda'}; N_{\Lambda'})}{\mu^{\lambda_{\Lambda'}(s)}(m_{\Lambda'}; m_{\Lambda'})}ds$$

$$\leq \frac{2|\Lambda'|}{|\Lambda|}|\tilde\rho' - \tilde\rho|.$$

and we arrive at (10).

Let us next consider the estimate (11). With no restriction, we assume that $0 < \rho < \rho' < 1$. Since $\lim_{\tilde B\uparrow\infty}\mathbb{P}(|\alpha_0| \leq \tilde B) = 1$, there exists some constant $\tilde B > 0$ such that $\mathbb{P}(|\alpha_0| \leq \tilde B) \geq \frac{1}{2}$ and we have

$$\chi(\rho) = \mathbb{E}\left[\mu^{\lambda_0(\rho)}(\eta_0; \eta_0)\right]$$

$$= \mathbb{E}\left[\frac{e^{\alpha_0+\lambda_0(\rho)}}{\left(1 + e^{\alpha_0+\lambda_0(\rho)}\right)^2}\right]$$

$$= \mathbb{E}\left[\mathbb{I}_{\{|\alpha_0|\leqslant\tilde B\}}\frac{e^{\alpha_0+\lambda_0(\rho)}}{\left(1 + e^{\alpha_0+\lambda_0(\rho)}\right)^2}\right]$$

$$+ \mathbb{E}\left[\mathbb{I}_{\{|\alpha_0|>\tilde B\}}\frac{e^{\alpha_0+\lambda_0(\rho)}}{\left(1 + e^{\alpha_0+\lambda_0(\rho)}\right)^2}\right]$$

$$\geq \mathbb{P}(|\alpha_0| \leq \widetilde B)\min\left(h(-\widetilde B), h(\widetilde B)\right),$$

where $h(\beta) = \frac{e^{\beta+\lambda_0(\rho)}}{\left(1+e^{\beta+\lambda_0(\rho)}\right)^2}$. Therefore,

$$|\mu^{\lambda_0(\rho')}(\eta_0) - \mu^{\lambda_0(\rho)}(\eta_0)|$$

$$= \left|\int_\rho^{\rho'}\frac{d}{ds}\mu^{\lambda_0(s)}(\eta_0)ds\right| \leq \int_\rho^{\rho'}\frac{\mu^{\lambda_0(s)}(\eta_0)}{\chi(s)}ds$$

$$\leq C(\rho' - \rho),$$

and this implies (11).

On the other hand, (12) is a simple consequence of (11). In fact, we have

$$|\mu^{\lambda_0(\rho')}(\eta_0; \eta_0) - \mu^{\lambda_0(\rho)}(\eta_0; \eta_0)|$$

$$\leq |\mu^{\lambda_0(\rho')}(\eta_0) - \mu^{\lambda_0(\rho)}(\eta_0)|$$

$$+ |\mu^{\lambda_0(\rho')}(\eta_0)^2 - \mu^{\lambda_0(\rho)}(\eta_0)^2|$$

$$\leq C|\mu^{\lambda_0(\rho')}(\eta_0) - \mu^{\lambda_0(\rho)}(\eta_0)|$$

$$\leq C|\rho' - \rho|.$$

$\square$

4. ON THE CONTINUITY OF THE DIFFUSION MATRIX AT THE END POINTS 0 AND 1

As we can see in the proof of[3] Theorem 5, Section 11, the assumption on the boundedness of the disorder field is essential to describe $(a, D(0)a)$ and $(a, D(1)a)$ as the limit of $(a, D(\rho)a)$ when $\rho \downarrow 0$ and $\rho \uparrow 0$, respectively.

More concretely, let us go through that proof. By the boundedness of the random field, there exists some constant $C_3 > 0$ such that

$$p_x := \frac{e^{\alpha_x + \lambda_0(\rho)}}{1 + e^{\alpha_x + \lambda_0(\rho)}} \geq C_3 \rho. \qquad (16)$$

This assertion helps the author to verify the following inequality

$$\Psi(\rho) \geq C_1 \rho^2 \mathbb{E}[\hat{g}_{0,e}^2].$$

Unfortunately, when the random field is unbounded, that assertion does not hold true. Indeed, if there were some constant $C_3 > 0$ such that we have the estimate (16), then by taking the limit $\alpha_x \downarrow -\infty$ in both sides of (16), we would get a wrong bound $C_3 \leq 0$.

Moreover, as we keep looking at that proof, we can see that the assumption on the boundedness of the disorder field is also used to prove the equality (11.35) as follows

$$\lim_{\rho \downarrow 0} \lambda_0'(\rho) \inf_{U(\alpha)} \mathbb{E}\Big[\sum_{e \in \mathcal{E}} (\mu^{\lambda_0(\rho)}(\eta_e - \eta_0)^2 + C\rho^2)$$
$$\times (\beta_e + \tau_{-e}U - U)^2\Big]$$
$$= \frac{\inf_{U(\alpha)} \mathbb{E}\Big[\sum_{e \in \mathcal{E}}(e^{\alpha_0} + e^{\alpha_e})(\beta_e + \tau_{-e}U - U)^2\Big]}{\mathbb{E}[e^{\alpha_0}]}.$$

Namely, one has

$$\lambda_0'(\rho) = \frac{1}{\chi(\rho)} = \frac{1}{\mathbb{E}\Big[\dfrac{e^{\alpha_0 + \lambda_0(\rho)}}{(1 + e^{\alpha_0 + \lambda_0(\rho)})^2}\Big]},$$

and

$$\mu^{\lambda_0(\rho)}(\eta_e - \eta_0)^2 = \frac{e^{\lambda_0(\rho)}(e^{\alpha_0} + e^{\alpha_e})}{(1 + e^{\alpha_0 + \lambda_0(\rho)})(1 + e^{\alpha_e + \lambda_0(\rho)})}.$$

If $-B \leq \alpha_x \leq B$ then

$$\frac{e^{\lambda_0(\rho)}(e^{\alpha_0} + e^{\alpha_e})}{(1 + e^{B + \lambda_0(\rho)})^2} \leq \mu^{\lambda_0(\rho)}(\eta_e - \eta_0)^2$$
$$\leq \frac{e^{\lambda_0(\rho)}(e^{\alpha_0} + e^{\alpha_e})}{(1 + e^{-B + \lambda_0(\rho)})^2}.$$

Hence, the equality (11.35) follows from checking that as $\rho \to 0$, $\lambda_0(\rho) \sim \ln \rho - \ln z$ and $\lambda_0'(\rho) \sim \rho$.

We now claim that it is not necessary to require the boundedness of the disorder field in order to obtain the equality (11.35). In fact, due to the Monotone Convergence Theorem, we have the following two estimates

$$\lim_{\lambda \downarrow -\infty} \frac{1}{\mathbb{E}\Big[\dfrac{e^{\alpha_0}}{(1 + e^{\alpha_0 + \lambda})^2}\Big]} = \frac{1}{\mathbb{E}[e^{\alpha_0}]},$$

$$\lim_{\lambda \downarrow -\infty} \mathbb{E}\Big[\frac{(e^{\alpha_0} + e^{\alpha_e})(\beta_e + \tau_{-e}U - U)^2}{(1 + e^{\alpha_0 + \lambda})(1 + e^{\alpha_e + \lambda})}\Big]$$
$$= \mathbb{E}[(e^{\alpha_0} + e^{\alpha_e})(\beta_e + \tau_{-e}U - U)^2].$$

They immediately imply the equality (11.35).

Therefore, based on the previous observations, in order to get the hydrodynamic behavior of our system with unbounded disorder as the Cauchy problem (3), we just add another assumption that the diffusion matrix $D(\rho)$ has a continuous extension in the closed interval $[0, 1]$, i.e. we arrive at the assertion of Theorem 1.1.

Acknowledgment

REFERENCES

1. A. Faggionato, F. Martinelli. Hydrodynamic limit of a disordered lattice gas, *Probability Theory and Related Fields*, **2003**, *127*, 535–608.

2. C. Kipnis, C. Landim. *Scaling limits of interacting particle systems, Grundlehren der mathematischen Wissenschaften 320*, Springer Verlag, 1999.

3. J. Quastel, H.T. Yau. Bulk diffusion in a system with site disorder, *Annals of Probability*, **2006**, *34*(5), 1990–2036.

4. S. R. S. Varadhan, H. T. Yau. Diffusive limit of lattice gas with mixing conditions, *Asian Journal of Mathematics*, **1997**, *1*(4), 623–678.

Sử dụng điện cực platin nano hình hoa biến tính trên bề mặt điện cực glassy cacbon để xác định Chì bằng phương pháp Von - Ampe hòa tan anot

Nguyễn Thị Liễu*

Khoa Khoa học Tự nhiên, Trường Đại học Quy Nhơn, Việt Nam

TÓM TẮT

Chì (II) được xác định bằng phương pháp Von – Ampe hòa tan anot sử dụng điện cực platin nano hình hoa biến tính trên bề mặt điện cực glassy cacbon (PtNFs/GCE). Các điều kiện thí nghiệm tối ưu là dung dịch đệm axetat 0,1 mol.L^{-1} (pH = 4,5), thế điện phân làm giàu -1,1 V, thời gian điện phân làm giàu 120 s, biên độ xung 60 mV và tốc độ quét 0,23 V.s^{-1}. Khoảng nồng độ tuyến tính là 1-100 μg.L^{-1} với R = 0,9981. Giới hạn phát hiện và giới hạn định lượng của phương pháp phân tích được xác định lần lượt là 0,398 μg.L^{-1} và 1,272 μg.L^{-1}. Ảnh hưởng của một số ion kim loại như Zn, Cd, Cu đã được nghiên cứu. Điện cực đã được áp dụng để xác định chì (II) trong một số mẫu nước sông, nước hồ với kết quả hoàn toàn phù hợp về mặt thống kê với phương pháp quang phổ hấp phụ nguyên tử lò graphite (GFAAS).

Từ khóa: *Phương pháp điện hóa, chì, platinum nanoflowers, biến tính điện cực, glassy cacbon.*

*Tác giả liên hệ chính.
Email: nguyenthilieu@qnu.edu.vn

Using platinum nanoflowers modified glassy carbon electrode for determination of Lead by anodic stripping voltammetric method

Nguyen Thi Lieu*

Faculty of Natural Sciences, Quy Nhon University, Vietnam

ABSTRACT

Lead (II) was determined by anodic stripping voltammetric method using platinum nanoflowers modified glassy carbon electrode (PtNFs/GCE). Optimal experimental conditions were found acetate buffer solution 0.1 mol.L^{-1} (pH = 4.5), an preconcentration potential of -1.1 V, preconcentration time of 120 s, pulse amplitude of 60 mV and scan rate of 0.23 V.s^{-1}. The peak current response increased linearly with the metal concentration in a range of 1-100 µg.L^{-1} with R = 0.9981. The limit of detection and limit of quantity were 0.398 µg.L^{-1} and 1.272 µg.L^{-1}, respectively. The interference effects of some metal ions such as Zn, Cd, and Cu were studied. The PtNFs/GCE was applied to analysis of lead (II) in some river water, and lake water samples with results in satisfactory statistical agreement with graphite furnace atomic absorption spectroscopy (GFAAS).

Keywords: *Lead, electrochemical method, platinum nanoflowers, modified electrode, glassy carbon electrode.*

1. INTRODUCTION

Pollution caused by heavy metals poses a serious menace to human health and ecological systems.[1] Among heavy metals, lead is especially pointed out for its toxicity and negative effects on human beings and living organisms, including carcinogenic and mutagenic effects.[2,3]

Accordingly, it is highly desirable to develop highly sensitive methods for the determination of trace amounts of lead. A wide range of analytical methods are normally exploited for the quantification of lead that includes atomic absorption spectrometry,[4] inductively coupled plasma mass spectrometry,[5] atomic fluorescence spectrometry.[6] However, they still have some drawbacks such as the expensive and sophisticated equipment, complex operation, impossibility for on-site measurement, highly qualified operator demand. Recently, electrochemical methods[7,8] are promising techniques for the determination of lead ions due to their low cost, high sensitivity, easy operation, and ability to analyze element speciation.

In recent years, modified electrodes have attracted much interest. Modified electrodes can be prepared by deposition of various compounds such as conducting polymers, metal complexes, transition metals and metal oxides on various electrodes.[9,10] Metal nanoparticles have drawn renewed attention in recent years due to their wide range of applications in nanosensor, biosensors and many other fields.[11] They have special properties such as large surface area, catalyst, mechanical and electronics. Previous studies indicated that Pt nanoparticles could

*Corresponding author.

Email: nguyenthilieu@qnu.edu.vn

increase the surface area and conducive to electron transfer with strong catalytic properties, and have attracted more and more interests as electrode modified materials.[12,13]

In this work, the electrochemical behavior of lead has been investigated with sensitive, fast and simple different pulse anodic stripping voltammetry (DPASV) method. This preliminary work is an initial step toward the fabricating one type of electrochemical sensors used for sensitive determination of Pb (II) at trace concentration.

2. MATERIALS AND METHODS

2.1. Reagents and apparatus

Reagents: Hexachloroplatinic (IV) acid hexahydrate ($H_2PtCl_6.6H_2O$) was used for the PtNFs modified GCE. It was purchased from Merck (KGaA, 64271 Darmstadt Germany). The electrolyte solution is made up of 1 mM H_2PtCl_6 and 0.1 M H_2SO_4 solution and a $[Fe(CN)_6]^{3-}$ redox system in 0.2 M phosphate buffer solution pH = 7 was used for the study of electrochemical properties. CH_3COOH, $CH_3COONa.2H_2O$, NaOH, K_2HPO_4, KH_2PO_4, H_3PO_4, H_3BO_3, KCl, HCl were purchased from Merck (KGaA, 64271 Darmstadt Germany). Lead stock solution (1000 ppm) purchased from Merck (KGaA, 64271 Darmstadt Germany) was used for dilution. All of the solutions were prepared by using distilled water.

2.2. Preparation of modified electrode

The electrodeposition of platinum nanoparticles on the bare glassy carbon electrode (GCE) was carried out in H_2SO_4 0.1 M solution containing 1.0 mM H_2PtCl_6 at a constant potential of -0.2 V and deposition time of 150 s. Following that, the Pt/GCE was gently cleaned with distilled water before use.

2.3. Electrochemical measurements

Electrochemical measurements were performed using an Autolab Electrochemical (CPA-HH5). Electrochemical measurements were performed by a custom-made multi-functional potentiostat/galvanostat manufactured at Vietnam Academy of Science and Technology, Hanoi, Vietnam. The formation of PtNFs/GCE and their properties were investigated by cyclic voltammetric method (CV). Measurements performed in 5 mM $[Fe(CN)_6]^{3-}$ from -0.3 V to 0.8 V at a scan rate of 0.1 V.s^{-1} was used to predict electrochemical features of electrodes and compare their electrochemically active surface areas. Detection of Pb(II) was performed by different pulse voltammetry (DPV) in an acetate buffer solution, pH of 4.5; the accumulation of Pb was carried out at a constant potential of -1.1 V for 120s; the potential was scanned from -1.2 V to +0.2 V with pulse amplitude 0.060 V; pulse time 0.050 s; step potential 0.007 V; step time 0.03s; sweep rate 0.23 V.s^{-1}. All experiments described in this section were performed at room temperature (25 ± 1 ^{0}C).

3. RESULTS AND DISCUSSION

3.1. Optimization of experimental parameters

3.1.1. Effect of electrochemical technologies

Electrochemical technologies such as differential pulse voltammetry (DPV), square wave voltammetry (SWV), and normal pulse voltammetry (NPV) are studied. These electrochemical techniques are comparatively used in the detection of Pb(II) on the PtNFs/GCE as shown in Figure 1. The result shows that the electrochemical signal of DPV is larger than that of SWV, and NPV. Therefore, the DPV technique is used in the following electrochemical experiments.
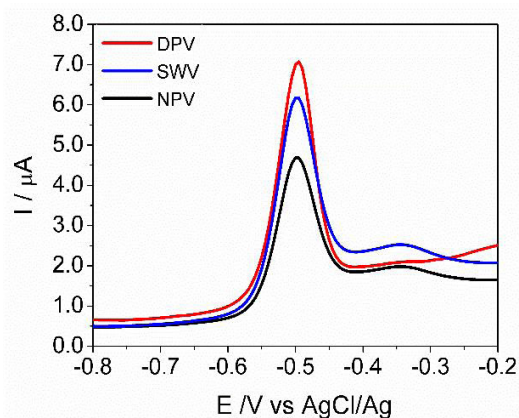

Figure 1. Different electrochemical techniques for the detection of Pb(II) in 0.1 mol.L^{-1} acetate buffer (pH 4.5) solution containing 10 µg.L^{-1} Pb(II).

3.1.2. Effect of electrolytic solution

The effect of the various electrolytic solution including acetate buffer solution (ABS), Britton - Robinson buffer solution (BRBS), phosphate buffer solution (PBS), KCl/HCl on the stripping peak currents of Pb(II) is studied (Figure 2). The concentration of Pb(II) was 10 μg.L^{-1}. The best electrolytic solution is received in acetate buffer solution. Thus, 0.1 mol.L^{-1} acetate buffer solution is chosen as the electrolytic solution in the subsequent experiments.
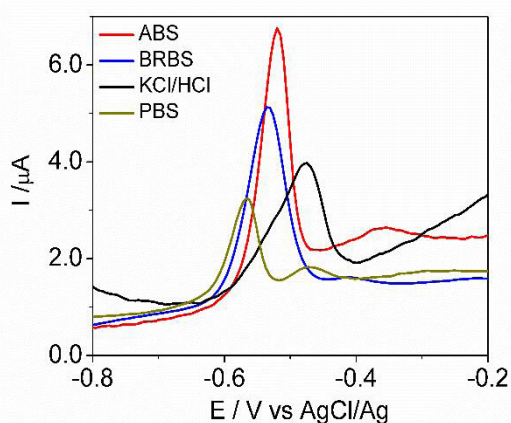

Figure 2. Effect of electrolytic solution on the peak current of 10 μg.L^{-1} Pb(II).

3.1.3. Effect of solution pH

The effect of pH on the stripping peak current was studied in 0.1 M acetate buffer solution, with pH values ranging from 2.0 to 6.0 (Figure 3). With increasing pH, the stripping peak increased initially and then decreased at higher pH. Possibly because in the low pH, metal exists as a weak link (labile form), so it can be reduced and accumulated easily on the electrode surface. In the high pH, metal can be in the form of strong bonds (bound form), so it is difficult to be eliminated. As a result, less efficient enrichment happens, leading to the lower stripping peak current. Particularly, the peak current reaches a maximum value at pH 4.5. The continuous increase in pH values results in a decrease in peak current. In order to obtain good sensitivity, we chose pH 4.5 as the optimal pH value for subsequent experiments.
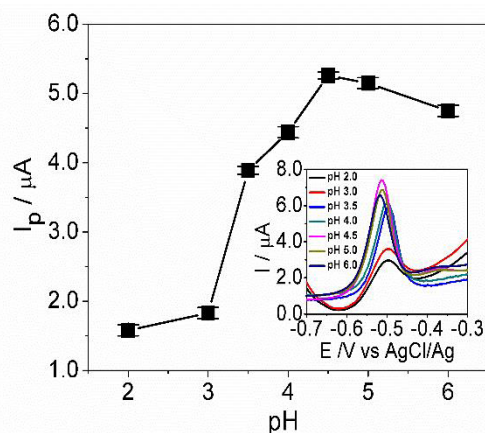

Figure 3. Effects of pH value on the peak current of 10 μg.L^{-1} Pb(II) in an acetate buffer solution.

3.1.4. Effect of Pb preconcentration time and potential on its signal

The preconcentration time and potential (accumulation time/ potential) are the time/ potential to accumulate the analyte onto the electrode surface. The influences of accumulation time and potential on Pb stripping signal were studied in the ranges from 60 s to 300 s and from -0.8 V to − 1.4 V, respectively that have been shown in our previous publication.[14] According to the results, an accumulation time of 120s was chosen as the optimal value since it provided high peak current. In addition, under this optimized condition, the time of analysis performance could be economized and the wide range of calibration curve could be acquired. Besides, -1.1 V was chosen as the preconcentration potential for the subsequent experiments because of the highest Pb signal and the lowest relative standard deviation obtained at this value.

3.1.5. Optimization of DPV parameters

The pulse voltammetric response depends considerably on instrumental conditions. To obtain a much more sensitive peak current, the optimum instrumental conditions, for example, amplitude and step potential, were studied for 10 μg.L^{-1} Pb(II) solution. The effect of pulse amplitude and step potential were studied. The result is the best peak definition was recorded

when using 60 mV pulse amplitude, and 7 mV step potential.

3.2. Calibration data and detection limit

The linear range and detection limit were evaluated under the optimized conditions. The analytical calibration curve was obtained by varying the concentration of Pb(II) in the accumulating medium, in the range from 1 µg.L^{-1} to 100 µg.L^{-1}. Figure 4 shows the DPASV responses for the determination of Pb(II) at the PtNFs/GCE in 0.1 M acetate buffer solution (pH 4.5). The different pulse peak current showed a linear range of Pb(II) concentration: 1 µg.L^{-1} - 100 µg.L^{-1} with correlation coefficients of 0.9981. The corresponding calibration plot is y = 0.371x + 1.603 (x: concentration (µg/L), y: current (µA)). The limit of determination (LOD) calculated using the definition $3S_B/b$ (where S_B is the standard deviation of 10 measurements of the blank and b is the slope of the calibration line), was calculated to be 0.398 µg.L^{-1}. The comparison results of the proposed sensor with some reported sensors for the determination of Pb(II) are given in Table 1. It can be seen that the PtNFs/GCE offered a wider linear range than the one in many previous reports.[15,16] The limit of detection (LOD) of this our electrode is higher than that of some sensors reported in Table.[15,16] It can be attributed to the longer Pb deposition period (300 s) and more negative accumulation potential (-1.4 V),[17] while, in reference,[15] the authors used different analysis method–adsorptive stripping voltammetry method that spend much more time on Pb adsorption onto electrode surface (40 min) for preconcentration. Thus, the analysis procedure in this study waste less time. Furthermore, the LOD is much lower than recent publication with LOD of 1.12 µg·L^{-1}.[18] In addition, this electrode is prepared more simply than the ones in[16]. Meanwhile, the LOD obtained by using this electrode is far below the acceptable limit by World Health Organisation.
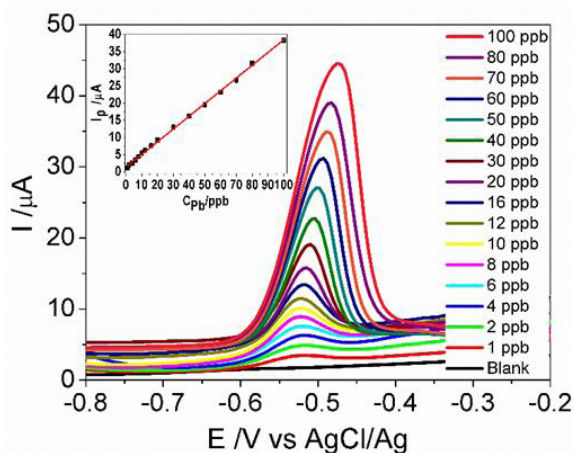
Figure 4. DPASVs of Pb(II) samples ranging in concentration from 1 to 100 µg.L^{-1} and relationship between Pb(II) concentrations with corresponding peak current (inset).

Table 1. A comparison of the different methods reported for the detection of Pb(II).

Electrode	Modifier	Method	LOD (µg.L^{-1})	Linear range (µg.L^{-1})	Ref
GCE	ETO	AdSV	0.035	0.104-2.07	[15]
GCE	PANI/MMT	DPASV	0.207	0.828-20.7	[16]
GCE	EG/Bi	DPASV	0.11	1-100	[17]
GCE	ZnFe$_2$O$_4$	DPASV	1.12	10-130	[18]
GCE	PtNFs	DPASV	0.398	1 – 100	This work

GCE: glassy carbon electrode; EG/Bi: electrochemically deposited graphene/bismuth; AdSV: adsorptive stripping voltammetry; ETO: etodolac; PANI/MMT: polyaniline/montmorillonite; ZnFe$_2$O$_4$: Nano sized zinc ferrite; SWASV: square wave anodic stripping voltammetry.

3.3. Repeatability of PtNFs/GCE

A series of repetitive DPASV response measurements for 10 µg.L⁻¹ Pb(II) in 0.1 M acetate buffer solution was performed to further evaluate the stability of the PtNFs/GCE. As shown in Figure 5, the relative standard deviation (RSD) values were calculated to investigate repeatability of the PtNFs/GCE is 1.51%. Therefore, the PtNFs/GCE has an excellent stability for repetitive DPASV measurements.
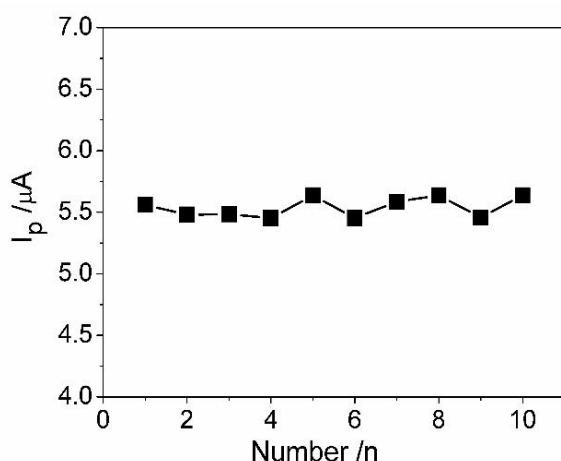

Figure 5. The stability of 10 repetitive measurements of 10 µg.L⁻¹ Pb(II) on the PtNFs/GCE in solution.

3.4. Interference study

Analytical selectivity is one of the important parameters that affect the accuracy of the analysis. In order to evaluate the selectivity of the proposed method for the determination of lead, the influence of some metal ions such as zinc, cadmium, and copper on the stripping voltammetric measurements were examined in 0.1 M acetate buffer containing lead (20 µg.L⁻¹) under the optimized working conditions (Figure 6). The results showed that the effect of zinc, cadmium ions on the Pb signal is insignificant in the large concentration. When 1500 µg.L⁻¹ of cadmium ions, 1600 µg.L⁻¹ of zinc were added, stripping response of lead decreased by

15.56%, 14.45%, respectively. Cu (II) affected lead stripping response at the concentration ratio (ppb/ppb) of $Cu^{II}/Pb^{II} > 10$. Furthermore, there is a small peak observed at about -0.4 V when the concentrations of Cu(II) increased to 200 µg.L⁻¹. This peak may be attributed to the formation of a Pb-Cu alloy.[19] However, the addition of ferrocyanide ions can overcome the effect of Cu (II) because it forms a stable complex with Cu(II), as suggested previously.[19]
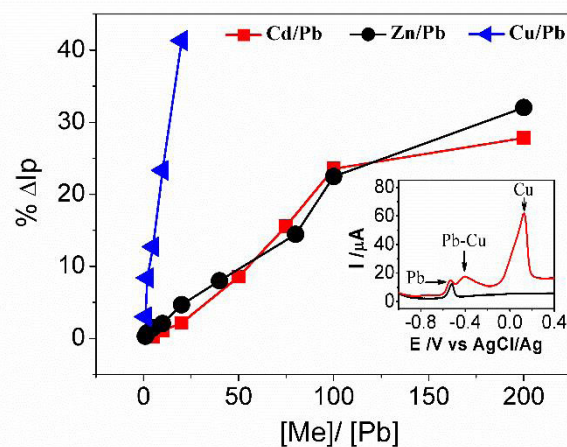
Figure 6. Influence of zinc, cadmium, and copper on the anodic stripping peak current of 20 µg.L⁻¹ Pb(II) on PtNFs/GCE under the optimized working conditions.

3.5. Analysis of real samples

The PtNFs/GCE was employed for the determination of Pb(II) in the local environment by using standard addition method. All water samples were added to 0.1 mol.L⁻¹ acetate buffer (pH = 4.5) and determined under the optimal conditions. The experimental values were shown in Table 2. The comparative results as shown in Table 2 suggest that the concentrations of lead ions were in good agreement with the results found in the graphite furnace atomic absorption spectrometry (GFAAS) measurement. Therefore, the PtNFs/GC electrode is potentially useful for the analysis of trace heavy metals in real samples.

Table 2. Analytical results for the determination of lead (n=3) in real water samples.

Sample	Pb(II) (μg.L^{-1})			
	Sample location	DPASV[a]	GFAAS[b]	Error (%)
Phu Hoa Lake's water	13°46'18.6"N 109°11'23.9"E	12.04±0.34	12.83±ND	6.16
Ha Thanh River's water	13°47'21.9"N 109°13'15.9"E	11.62±0.26	12.30±ND	5.52
Thi Nai Lake's water	13°47'00.7"N 109°13'53.2"E	9.38±0.20	10.30±ND	8.93
Nui Mot Lake's water	13°47'34.5"N 108°58'50.8"E	9.44±0.41	8.70±ND	8.50
Tra O Lake's water	14°18'15.4"N 109°07'28.4"E	7.41±0.18	7.80±ND	5.01

DPASV: different pulse anodic stripping voltammetry; GFAAS: graphite furnace atomic absorption spectrometry
[a]Mean of three repetitive measurements at a 95% confidence level; [b]n=1, ISO/IEC17025:2005
ND: Not determined

4. CONCLUSIONS

This work is useful for producing the electrochemical sensor for determination of Pb(II) at trace concentration. A simple, sensitive, and inexpensive method for determination of lead is proposed. The PtNFs/GCE demonstrated better detection sensitivity and higher DPASV signals than the bare GCE, with the limit of detection of about 0.398 μg.L^{-1}. Further studies will be focused on detection of other metals (cadmium, zinc, cobalt, mercury, etc.) by combining with different electrochemical technique.

REFERENCES

1. L. Fu, X. Li, J. Yu, and J. Ye. Facile and simultaneous stripping determination of zinc, cadmium and lead on disposable multiwalled carbon nanotubes modified screen-printed electrode, *Electroanalysis*, **2013**, *25*(2), 567-572.

2. P. Elliott, R. Arnold, D. Barltrop, I. Thornton, I. M. House, and J. A. Henry. Clinical lead poisoning in England: An analysis of routine sources of data, *Occupational and Environmental*, **1999**, *56*(12), 820-824.

3. I. Gęca and M. Korolczuk. Anodic stripping voltammetry following double deposition and stripping steps: Application of a new approach in the course of lead ion determination, *Talanta,* **2017**, *171*, 321-326.

4. S. Erarpat, G. Özzeybek, D. S. Chormey, and S. Bakırdere. Determination of lead at trace levels in mussel and sea water samples using vortex assisted dispersive liquid-liquid microextraction-slotted quartz tube-flame atomic absorption spectrometry, *Chemosphere*, **2017**, *189*, 180–185.

5. K. E. Murphy, E. S. Beary, M. S. Rearick, and R. D. Vocke. Isotope dilution inductively coupled plasma mass spectrometry (ID ICP-MS) for the certification of lead and cadmium in environmental standard reference materials, *Fresenius Journal of Analytical Chemistry,* **2000**, *368*(4), 362-370.

6. B. Beltrán, L. O. Leal, L. Ferrer, and V. Cerdà. Determination of lead by atomic fluorescence spectrometry using an automated extraction/pre-concentration flow system, *Journal of Analytical Atomic Spectrometry*, **2015**, *30*(5), 1072-1079.

7. E. L. Pui Mun Lee, Z. Wang, X. Liu, Z. Chen. Glassy carbon electrode modified by graphene-gold nanocomposite coating for detection of trace lead ions in acetate buffer solution, *Thin Solid Films*, **2015**, *584*, 85-89.

8. S. Lee, S. Bong, J. Ha, M. Kwak, S. K. Park, and Y. Piao. Electrochemical deposition of bismuth on activated graphene-nafion composite for anodic stripping voltammetric determination of trace heavy metals, *Sensors and Actuators B: Chemical*, **2015**, *215*, 62-69.

9. J. V. Piovesan, C. A. de Lima, E. R. Santana, and A. Spinelli. Voltammetric determination of

condensed tannins with a glassy carbon electrode chemically modified with gold nanoparticles stabilized in carboxymethylcellulose, *Sensors and Actuators B: Chemical,* **2017**, *240*, 838-847.

10. D. Valera, P. J. Espinoza-Montero, J. Alvarado, P. Carrera, P. Bonilla, L. Cumbal, L. Fernández. Development and evaluation of a glassy carbon electrode modified with silver and mercury nanoparticles for quantification of cysteine rich peptides, *Sensors and Actuators B: Chemical,* **2017**, *253*, 1170-1179.

11. L. Q. Hoa, Y. Sugano, H. Yoshikawa, M. Saito, and E. Tamiya. Structural assembly effects of Pt nanoparticle-carbon nanotube-polyaniline nanocomposites on the enhancement of biohydrogen fuel cell performance, *Electrochimica Acta*, **2011**, *56*(27), 9875-9882.

12. P. K. Kalambate, B. J. Sanghavi, S. P. Karna, and A. K. Srivastava. Simultaneous voltammetric determination of paracetamol and domperidone based on a graphene/platinum nanoparticles/ nafion composite modified glassy carbon electrode, *Sensors and Actuators B: Chemical*, **2015**, *213*, 285-294.

13. G. G. Gerent and A. Spinelli. Magnetite-platinum nanoparticles-modified glassy carbon electrode as electrochemical detector for nitrophenol isomers, *Journal of Hazardous Materials*, **2017**, *330*, 105-115.

14. T. L. Nguyen, V. H. Cao, T. H. Y. Pham, and T. G. Le. Platinum nanoflower-modified electrode as a sensitive sensor for simultaneous detection of lead and cadmium at trace levels, *Journal of Chemistry*, **2019**, 1-10.

15. S. Lee, S. K. Park, E. Choi, and Y. Piao. Voltammetric determination of trace heavy metals using an electrochemically deposited graphene/ bismuth nanocomposite film-modified glassy carbon electrode, *Journal of Electroanalytical Chemistry*, **2016**, *766*, 120-127.

16. Y. Dong, Y. Ding, Y. Zhou, J. Chen, and C. Wang. Differential pulse anodic stripping voltammetric determination of Pb ion at a montmorillonites/ polyaniline nanocomposite modified glassy carbon electrode, *Journal of Electroanalytical Chemistry*, **2014**, *717-718*, 206-212.

17. M. L. Yola, N. Atar, M. S. Qureshi, Z. Üstündag, and A. O. Solak. Electrochemically grafted etodolac film on glassy carbon for Pb(II) determination, *Sensors and Actuators B: Chemical*, **2012**, *171-172*, 1207-1215.

18. A. K. N. S, S. Ashoka, and P. Malingappa. Nano Zinc ferrite modified electrode as a novel electrochemical sensing platform in simultaneous measurement of trace level lead and cadmium, *Journal of Environmental Chemical Engineering*, **2018**, *6*(6), 6939 - 6946.

19. D. F. Tibbetts, J. Davis, and R. G. Compton. Sonoelectroanalytical detection of lead at a bare copper electrode, *Fresenius Journal of Analytical Chemistry*, **2002**, *368*(4), 412-414.

Nâng cao hiệu quả giao thức LEACH trong mạng cảm biến không dây

Nguyễn Ngọc Dũng[1,*], Phùng Văn Minh[1], Đoàn Thị Minh Hạnh[2]

[1]Khoa Công nghệ thông tin, Trường Đại học Quy Nhơn, Việt Nam
[2]Phòng Đào tạo Đại học, Trường Đại học Quy Nhơn, Việt Nam

TÓM TẮT

Trong những năm gần đây, mạng cảm biến không dây (Wireless Sensor Network – WSN) được nghiên cứu và ứng dụng trong nhiều lĩnh vực trong cuộc sống như cứu hộ, giám sát môi trường, tích hợp các ứng dụng IoT… Đặc biệt, trong các trường hợp mà nguồn năng lượng bị giới hạn thì việc duy trì thời gian hoạt động của các nút cảm biến trong hệ thống mạng trở nên quan trọng. Trong bài báo này, chúng tôi tìm hiểu hoạt động giao thức LEACH (Low Energy Adaptive Clustering Hierarchy) – một giao thức tương thích với nguồn năng lượng thấp và đề xuất giải pháp cải tiến để nâng cao hiệu quả sử dụng trong mạng cảm biến không dây. Các kết quả mô phỏng cho thấy, giải pháp của chúng tôi đề xuất tốt hơn về số lượng gói tin đến được trạm gốc và thời gian sống trung bình của các nút cảm biến.

Từ khóa: *Mạng cảm biến không dây, phân cụm, năng lượng trong mạng cảm biến không dây, giao thức định tuyến.*

───────────────

*Tác giả liên hệ chính.

Email: nguyenngocdung@qnu.edu.vn

Improve the efficiency of LEACH protocol in Wireless Sensor Networks

Nguyen Ngoc Dung[1,*], Phung Van Minh[1], Doan Thi Minh Hanh[2]

[1]Department of Information Technology, Quy Nhon University, Vietnam
[2]Undergraduate Training Office, Quy Nhon University, Vietnam

ABSTRACT

In recent years, Wireless Sensor Network (WSN) has been researched and applied in many fields such as rescuing, environmental monitoring, and IoT applications, etc. Especially, when the power source is limited, maintaining the working status of the sensor nodes in the network becomes more and more important. In this article, we explore the operation of the LEACH (Low Energy Adaptive Clustering Hierarchy) protocol - a protocol compatible with low-energy sources and propose a solution to improve efficiency in wireless sensor networks. The simulation results show that our solution is better in terms of the number of packets reaching the base station and the average lifetime of the sensor nodes.

Keywords: *Wireless Sensor Network, clustering, energy in wireless sensor networks, routing protocols.*

1. INTRODUCTION

A Wireless Sensor Network (WSN) consists of wireless sensor nodes scattered in a given space to collect data of the physical signals at the sensor node and send it to the Base Station (BS).[1] The BS will aggregate the data and send it back to the user via the Internet. A wireless sensor node is equipped with components such as a sensor, microprocessor, memory, radio transmitter/receiver, and limited battery power. BS has an unlimited energy source. Wireless sensor networks are often deployed in places with complex terrain, so recharging or replacing batteries for sensor nodes is not possible.

Therefore, the research on solutions to increase the lifetime of the sensor nodes

is always of interest. One of the solutions to improve the efficiency and increase the lifetime of the wireless sensor network is to design a routing protocol for transferring sensor data to the BS.[2,3]

LEACH (Low Energy Adaptive Clustering Hierarchy) is a distributed routing protocol used in wireless sensor networks based on the cluster proposed by Heinzelman, which allows data within a cluster to be processed locally to remove redundant data before transmission.[4] Since the publication of LEACH, various solutions have been proposed by the research community based on LEACH to save energy consumption further and increase network lifetime.[6-9]

*Corresponding author.
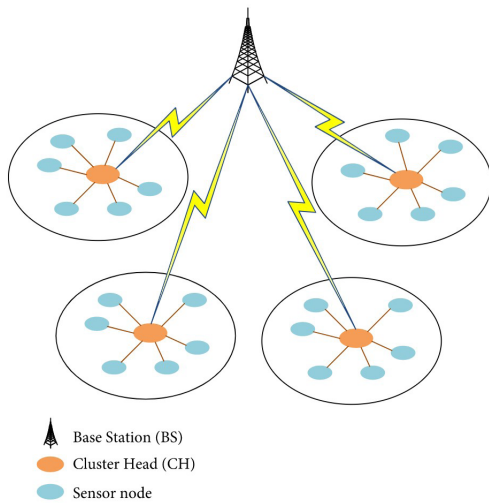*Email: nguyenngocdung@qnu.edu.vn*

Figure 1. WSN architecture under LEACH protocol.

The LEACH protocol has many disadvantages in selecting cluster heads and assigning sensor nodes to clusters, causing unnecessary energy consumption.[5] We study the operation of the LEACH protocol and consider its limitations, thereby proposing a solution based on LEACH to improve some parameters such as network lifetime, the amount of data received by the BS, and the energy consumed by the network. This paper consists of five parts. First, we introduce the wireless sensor networks and issues to be researched. Part 2 presents the LEACH routing protocol and power consumption model. Part 3 proposes solutions to improve LEACH. Part 4 simulates and analyzes the results. Finally, concluding remarks are made in part 5.

2. LEACH PROTOCOL

2.1. Two phases of LEACH

The operation of LEACH is divided into rounds. Each round consists of two phases: the set-up phase and the steady phase.

2.2.1. Set-up phase

In the setup phase, the clusters are organized and CHs are selected. The CH creates a TDMA (Time Division Multiple Access) schedule for member nodes. Thus, the sensor nodes send their data to CH in time slots allocated by the CH node.

Selection of cluster head

At the beginning of each round, LEACH chooses a few nodes in the network to be the cluster head. A sensor node chooses a random number, r, between 0 and 1. If this random number is less than a threshold value, T(n), the node becomes a cluster head for the current round. T(n) is defined:

$$T(n) = \begin{cases} \frac{P}{1-P(r \bmod \frac{1}{P})} & if\ n \in G \\ 0 & if\ n \notin G \end{cases} \quad (1)$$

Where:

 − P is the percentage of cluster heads

 − r is the selected rounds

 − G is the set of non-cluster heads in the last 1/P rounds

According to the threshold equation, each node can be a cluster head only once in an interval (*1/P* rounds). The threshold value *T(n)* increases with each round in *1/P* rounds, which means that the probability of a node becoming a CH increases after rounds. In the last round of a cycle, the threshold *T(n) = 1*, so all nodes that are not selected as CH will become CH in this round. After this round, LEACH will move to a new cycle and all live nodes in the network have an equal chance of becoming CH.

Cluster formation: The cluster heads will send a broadcast packet to the entire network to announce that it is a cluster head, all non-CH nodes will receive information from the CHs and select the nearest CH node to join the cluster based on the signal strength. At this point, the network has formed clusters, each with a CH and member nodes.

Schedule data transmission: After the clusters have been formed, the CH schedules the member nodes to send sensor data to the CH

node using the Time Division Multiple Access (TDMA) method. TDMA schedule helps nodes know when it sends data to the CH to reduce communication conflicts with other nodes in the cluster.

2.1.2. Steady-state phase

In the Steady-state phase, sensor nodes use their allocated TDMA slot to send the collected data to the CH. After receiving the data from its cluster members, CH aggregates and compresses them into a packet, and transfers it to the BS. This process reduces the amount of data that needs to be sent to the base station to reduce the energy consumption of the sensor nodes.

After the CH nodes send data to the base station, the network will move on to the next round.

2.2. Radio energy model

Sensor nodes use radio waves to transmit broadcast data. Therefore, each cluster uses a code to filter the signal according to the CDMA (Code-Division Multiple Access) technique to avoid conflicts with other clusters. The energy usage model[1] is depicted in Figure 2.
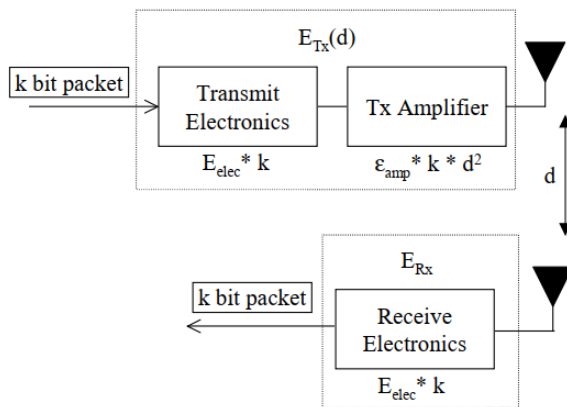

Figure 2. Radio energy consumption model.

The energy to transmit k bits of data between two sensor nodes with a distance of d using radio waves as shown above is calculated by the following formula:

$$E_{Tx}(k, d) = E_{elec} * k + \varepsilon_{amp} * k * d^2 \qquad (2)$$

Where E_{elec} is the energy to run transceiver circuitry; ε_{amp} is the energy consumption of the amplifier.

The energy to receive k bits of data:

$$E_{Rx} = E_{elec} * k$$

3. IMPROVEMENT OF LEACH

In LEACH, the remaining energy of the CH plays an important role in aggregating data from the member nodes and transmitting it to the base station. It is easy to see that a node with less residual energy can still be selected as the CH node. With a low-power CH node, the possibility of running out of energy while aggregating and transmitting data to the BS is very high, causing sensor packet loss.

The E-LEACH[3] solution has partially overcome the disadvantages of the LEACH protocol with a new approach for cluster head selection based on residual energy. When the remaining energy of a node is lower than 50% of the initial energy then the E-LEACH algorithm is used as in Equation (3).

$$T(n) = 2P * \frac{E_{residual}}{E_{inittial}} \qquad (3)$$

Where, P is the percentage of nodes that can become cluster head; $E_{residual}$ is remaining energy; $E_{inittial}$ is initial energy of a sensor node.

Another disadvantage of the LEACH protocol is that member nodes select the nearest CH to join the cluster, which is the case where a sensor node can send data back to the CH in the opposite direction towards BS wasting energy.

To overcome the above two disadvantages, we propose an improvement of the LEACH protocol, called LEACH-MODI as follows:

Cluster head selection

We use the same solution as E-LEACH[3] in selecting the CH node, when the remaining energy of the node is greater than or equal to 50%,

we use the threshold value *T(n)* as formula (1). Otherwise, we apply the cluster head selection as shown in formula (3). Thus, nodes with a larger remaining power source have a greater probability of becoming a CH node.

After selecting the CH node, it will send a broadcast packet HEAD_ADV to announce that it is the cluster head and its location to the entire network. Other sensor nodes receive HEAD_ADV packets from CH nodes and decide to join a cluster in the following way.

Non-CH node joins a cluster

Non-CH node CMj will join the cluster that contains CH_i with the smallest *f(i)* according to formula (4) and send a request packet to join the cluster CH_i.

$$f(i) = 2*d(j, CH_i) + d(CH_i, BS) \qquad (4)$$

Where:

− $d(j, CH_i)$: distance between node CM_j and node CH_i

− $d(CH_i, BS)$: distance between node CH_i and BS

The distance from node a to node b is calculated according to the formula (5).

$$d(a,b) = \sqrt{(x_a - x_b)^2 + (y_a - y_b)^2} \qquad (5)$$

Building the cluster according to formula (4) helps the sensor node to choose the CH node with the closer sensor packet path length, but the number of sensor nodes between the clusters is not too different.

LEACH_MODI is depicted in diagram Figure 3.

4. SIMULATION AND ANALYSIS

We perform a simulation with 100 sensor nodes randomly distributed in the simulation area of 100m x 100m. The base station position is (50,150). The above number of sensor nodes and simulation areas can be applied to the monitoring water environment (e.g., shrimp ponds) or monitoring the health of patients of a department in the hospital. The coverage range of HEAD_ADV and JOIN_Cluster packets is 50m. In case a sensor node cannot find a cluster to join, it sends the sensor packet directly to the base station. In each round, all sensor nodes send a 32-bit packet to CH and then aggregate and send it to the base station.

The simulation parameters[1] are presented in the following table:

Table 1. Simulation parameters.

Number of nodes	100
Network size	100m x 100m
Base station location	(50,150)
Initial energy	0.75J
Data packet size	32 bit
Desired percentage of CH	5%
E_{elec}	50 nJ/bit
ε_{amp}	100 pJ/bit/m^2

The simulation is performed until 70% of the network nodes run out of energy. The simulation scenario is built on NS3 software and uses the following parameters to evaluate the effectiveness of the proposed protocol:

− Number of sensor packets that reach the base station

− Number of sensor nodes that run out of energy

− Average power consumption of the network

− Average lifetime of network nodes

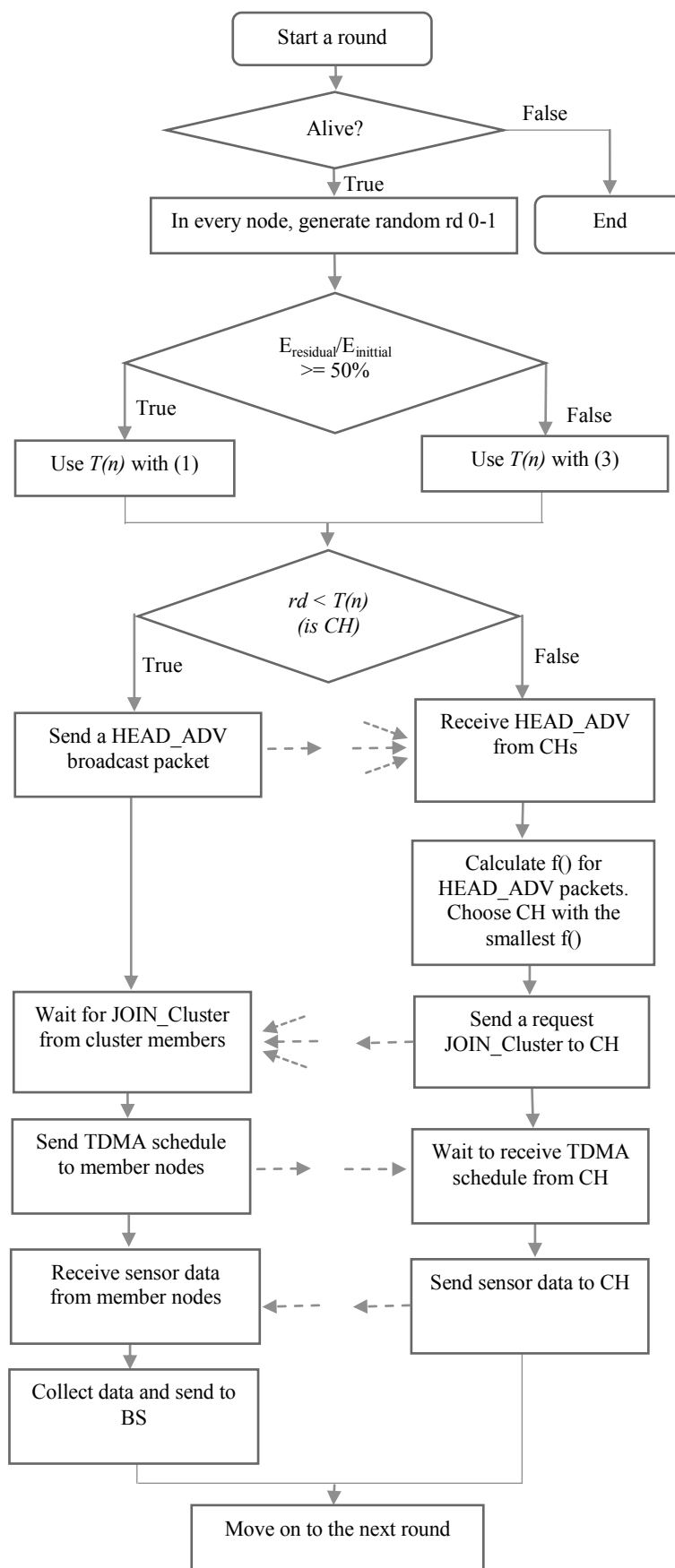The location of the 100 sensor nodes and the base station locations are shown in Figure 4.

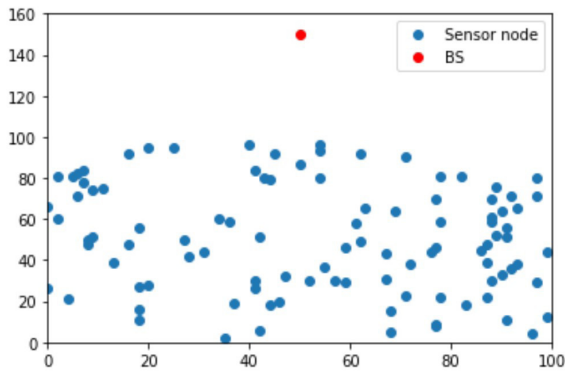**Figure 3.** Flow chart of the LEACH-MODI.

Figure 4. Location of sensor nodes.

We present the simulation result in the form of graphs (Figure 5, Figure 6, Figure 7) and a data table (Table 2).

According to Figure 5, LEACH-MODI and E-LEACH protocols are better than LEACH protocols in maintaining the number of live nodes. This result is obtained by changing the threshold value T(n) according to formula (3) when the nodes have the remaining energy less than 50% of the initial energy. Therefore, nodes with more energy have a higher probability of becoming CH, so energy consumption is more uniform between nodes. Because of the more even distribution of energy between nodes in the LEACH-MODI and E-LEACH protocols, the number of nodes running out of energy increases rapidly in the last period. The LEACH-MODI protocol maintains the number of alive nodes better than the E-LEACH protocol for the duration of the simulation because of the way a member node joins the cluster.
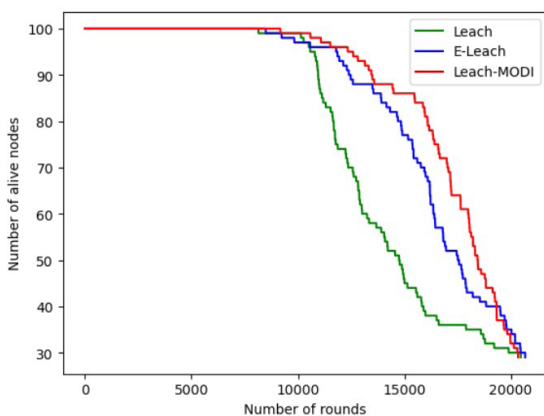

Figure 5. Number of live nodes.

The power consumption in a wireless sensor network is shown in Figure 6. The LEACH and E-LEACH protocols consume the same power for the first half of the time. Because the operation of the protocols is the same when the power is more than 50% of the initial energy. The LEACH-MODI protocol consumes less power than the other two protocols in the first period because of the way the member node selects the cluster leader node according to formula (4) instead of selecting the nearest cluster leader node to join the cluster. This approach avoids the case of sending sensor packets to the CH in the opposite direction to the BS. Round 15000 and later, the average remaining energy of the LEACH-MODI protocol decreases rapidly because its number of live nodes is much more than the other two protocols.

Figure 6. Average remaining energy.
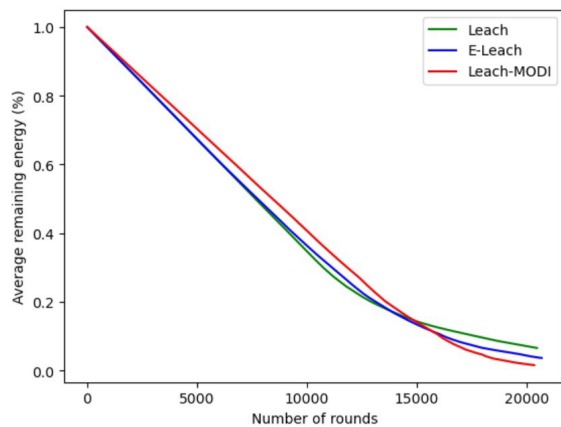
Figure 7 shows the number of packets that reached the base station. The three protocols have the same number of packets arriving at the BS as no node runs out of power. The LEACH protocol is less efficient at the end time because CH nodes run out of energy while aggregating data from member nodes. Furthermore, the number of nodes alive is less than in the other two protocols.
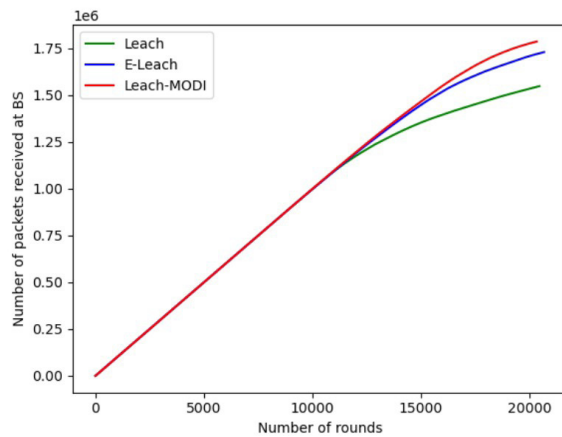
Figure 7. Number of sensor packets reached by BS.

The lifetime of the sensor nodes and the number of packets arriving at the BS are shown in Table 2, showing that the LEACH-MODI protocol is better than the LEACH and E-LEACH protocols.

Table 2. Summary of simulation results.

	Leach	E-Leach	Leach-MODI
The first round has a dead node	8.145	8.487	9.174
Average number of rounds of dead nodes	13.457	15.938	16.838
Number of data packets reaching the base station	1.548.120	1.729.970	1.786.580

Simulation results show that the LEACH-MODI protocol is better than the other two protocols in some evaluation parameters but still has many disadvantages. For example, the selection of cluster heads without considering the geographical location of the nodes affects the network's energy consumption. Moreover, LEACH-MODI has not considered the case of complex network environments such as many obstacles. In a transmission environment with many obstacles, the sensor node transmitting a signal with signal strength based on distance is no longer suitable.

5. CONCLUSION

Energy efficiency and energy load balancing in wireless sensor networks are issues of great concern today. In this paper, we have proposed a LEACH-MODI solution based on LEACH by changing the way a cluster head node is selected and how a cluster is selected for the joining of a member node. The results of the paper show that our proposed protocol is better than the LEACH protocol in maintaining the average lifetime of the network nodes and the number of packets reaching the base station. However, the LEACH-MODI protocol has some disadvantages in selecting cluster heads and when the network operates in complex environments. Therefore, we will focus on research to overcome the disadvantages of LEACH-MODI in the coming time.

REFERENCES

1. W. B. Heinzelman, A. P. Chandrakasa, and H. Balakrishnan. *Energy-efficient communication protocol for wireless microsensor networks*, Published in the Proceedings of the Hawaii International Conference on System Sciences, January 4-7, 2000, Maui, Hawaii.

2. W. B. Heinzelman, A. P. Chandrakasa, and H. Balakrishnan. An application-specific protocol architecture for wireless microsensor networks, *IEEE Transactions Wireless Communications*, **2002**, *1*(4), 660-670.

3. M. Abdurohman, Y. Supriadi, and F. Z. Fahmi. A modified E-LEACH routing protocol for improving the lifetime of a wireless sensor network, *Journal of Information Processing Systems*, **2020**, *16*(4), 845-858.

4. P. Manjunatha, A. K. Verma, A. Srividya. *Multi-sensor data fusion in cluster based wireless sensor networks using fuzzy logic method*, IEEE Region 10 and the Third international Conference on Industrial and Information Systems, 2008.

5. G. Samara, M. Al-okour. Optimal number of cluster heads in wireless sensors networks based on LEACH, *International Journal of Advanced Trends in Computer Science and Engineering*, **2020**, *9*(1).

6. S. K. Singh, M. P. Singh and D. K. Singh. Routing protocols in wireless sensor networks a survey, *International Journal of Computer Science & Engineering Survey*, **2010**, *1*(2).

7. R. K. Patel, P. Kaushal, J. Doshi. Improved performance of LEACH using better CH selection by weighted parameters, *International Journal for Scientific Research & Development*, **2013**, *1*(3).

8. S. Kumari. Performance analysis of LEACH, SEP and ZSEP under the influence of energy, *International Journal of Advanced Engineering Research and Science*, **2017**, *4*(4).

9. S. Lindsey and C. Raghavendra. *PEGASIS: Power-efficient gathering in sensor information systems,* IEEE Aerospace Conference Proceedings, **2002**, *3*, 9-16.

10. M. K. Khan, M. Shiraz, Q. Shaheen, S. A. Butt, R. Akhtar, M. A. Khan, W. Changda. Hierarchical routing protocols for wireless sensor networks: Functional and performance analysis, *Journal of Sensors*, **2021**, 7459368, 1-18.

Xác định hàm lượng verbascosid trong củ Địa hoàng 19 bằng phương pháp sắc ký lỏng hiệu năng cao

Phạm Thanh Loan*

Viện Nghiên cứu Ứng dụng và Phát triển, Trường Đại học Hùng Vương, Phú Thọ, Việt Nam

TÓM TẮT

Nghiên cứu nhằm xây dựng quy trình định lượng verbascosid trong củ của giống Địa hoàng 19 bằng sắc ký lỏng hiệu năng cao (HPLC) để phục vụ công tác đánh giá chất lượng dược liệu. Kết quả đã lựa chọn được điều kiện sắc ký phù hợp là sử dụng cột gemini C18 (250 × 4,6 mm, 5 µm), detector UV 334 nm, pha động acetonitril - acid phosphoric 0,1%, tốc độ dòng 0,8 mL/phút. Diện tích pic và nồng độ verbascosid có tương quan tuyến tính chặt (r = 0,9997), dạng hàm Y = 2349X + 7259,6. Quy trình có độ đúng, độ lặp lại tốt với RSD < 2%. Quy trình này được áp dụng để định lượng verbascosid trong củ của giống Địa hoàng 19 trồng tại 2 tỉnh Vĩnh Phúc, Phú Thọ cho kết quả lần lượt là 0,027% và 0,028%.

Từ khóa: *Verbascosid, HPLC, định lượng, Địa hoàng 19.*

*Tác giả liên hệ chính.
Email: Loandhhv@gmail.com

Determination of verbascoside in the root of *Rehmannia glutinosa* varieties 19 by high performance liquid chromatography

Thanh Loan Pham*

Institute of Applied Research and Development, Hung Vuong University, Vietnam

ABSTRACT

This study aimed to validate a procedure for the quantification of verbascoside in the root of *Rehmannia glutinosa* varieties 19 by high performance liquid chromatography (HPLC) to serve the assessment of medicinal quality. The results have selected suitable chromatographic conditions, using the gemini C18 column (250 × 4.6 mm, 5 µm), detector at 334 nm, mobile phase acetonitrile - phosphoric acid 0.1%, and the flow rate at 0.8 mL/min. Peak area and verbascoside concentration are strongly correlated (r = 0.9997), Y = 2349X + 7259.6. The procedure has good accuracy and repeatability with RSD < 2%. This procedure was applied to quantify verbascoside in the root of *Rehmannia glutinosa* varieties 19, which is grown in Vinh Phuc, Phu Tho provinces, and the results determination of verbascoside were 0.027% and 0.028%, respectively.

Keywords: *Verbascoside, HPLC, quantification, Rehmannia glutinosa varieties 19.*

1. INTRODUCTION

Most of the *Rehmannia glutinosa* materials used in Vietnam are imported from China, and the samples assigned to evaluate the quality of this medicinal plant are made on imported samples. *Rehmannia glutinosa varieties 19* has been recognized as a new variety and circulated in Vietnam from August, 2020.[1] Currently, there is no published evaluation of its quality in Vietnam. The active ingredient verbascoside is an important chemical component in the root of the *Rehmannia*, which is regulated by the Vietnam Pharmacopoeia V as a marker to test the quality of medicinal herbs.[2] Verbascoside has strong biological activities such as antibacterial, anti-inflammatory, and re-epithelialization[3-5] and has diuretic, antioxidant, wound healing,

cell autoimmunity, and protective effects on the nervous system.[3,6,7] Active ingredient verbascoside is being researched and developed by pharmaceutical companies for medicinal ingredients and health foods. The research results contribute to the assessment of this variety of quality grown in Vietnam.

2. RESEARCH METHODS

2.1. Material

The research sample is tubers grown from the *R. glutinosa varieties 19* harvested at 2 locations: Bach Luu commune - Song Lo - Vinh Phuc (code DH2102) and Dan Quyen commune - Tam Nong - Phu Tho (code DH2104) in March 2021, processed according to the Vietnam Pharmacopoeia V in 2017, treatise *Rehmannia*.[5]

---

*Corresponding author.
Email: Loandhhv@gmail.com

The sample was created by Dr. Nguyen Van Huy, Center for Medicinal Materials, Institute of Applied Research and Development. The scientific name is *Rehmannia glutinosa*, the family of snout flowers (Scrophulariaceae). The specimen is kept at the Center for Medicinal Materials, Institute of Applied Research and Development, code VNC/DH192101.

2.2. Chemicals, raw materials

Standard substance verbascoside with a purity of 98.14% (lot number RFS-M01101910014) was purchased from Chengdu Herbpurify, China. Other chemicals included acetonitrile (Merck), phosphoric acid (Merck), methanol (Merck), and double-distilled water as standard for high-performance liquid chromatography (HPLC).

2.3. Appliances

Shimadzu HPLC meter, LC-20AD pump, SPD-20A UV Vis detector, SIL-20A automatic sample injection system, CTO-20A thermostat, Electronic analytical balance (Switzerland), and reflux extraction device were deployed.

2.4. Chromatographic conditions

Using a gemini column C18 (250 × 4.6 mm, 5 μm) and chromatographic conditions such as selection of detection wavelength, mobile phase composition, flow rate, and injection volume were referenced based on the previous studies.[2,8-10]

2.5. Standard solution

Standard verbascoside was dissolved in methanol to obtain a solution containing 1000 μg/mL.

2.6. Test solution

Accuratedly weighted 0.8 g of medicinal powder were dissovled in a flask containing 50 ml of methanol (MeOH). The soltion was then placed in a reflux extraction for 1.5 h for cooling. A 20 mL of the obtained filtrate was collected and recovered in the solvent under vacuum condition to nearly dry. The mobile phase then dissolved and transfered entirely so a 5 mL volumetric flask, made up to the mark with the mobile phase before being filtered through a 0.45 μm filter.

2.7. Quantitative process appraisal

Verification of the verbascoside quantification process, including criteria: relevance, specificity, repeatability, linear correlation, precision, the limit of detection (LOD) and limit of quantitation (LOQ) was accorded to the Guidelines No. 32/2018/TT-BYT of the Ministry of Health, Decision No. 07/2013/QD-QLD of the Drug Administration of Vietnam and refered to the regulations of the International Conference on Harmonisation, 2005 (ICH).[11-13]

2.7.1. Suitability

Standard verbascoside solution (concentration 80 μg/ml) and chromatography were prepared six times. The parameters of retention time (t_R), peak area (S_{peak}), mean value, and relative standard deviation (RSD) of S_{peak} were determined. If RSD < 2%, the system is highly relevant.[11-13]

2.7.2. Specificity

Specificity was tested by analyzing the blanks, standard verbascoside solutions, and test solutions. Blank samples shall not give an analytical signal.[11-13]

2.7.3. Repeatability

Chromatography was performed six times for the test solution. If the RSD of verbascoside is ≤ 2%, then the procedure has good repeatability.[11-13]

2.7.4. Linear correlation

From the standard solution of 1000 μg/ml, 5 samples were prepared with concentrations of 20 μg/mL, 40 μg/mL, 80 g/mL, 160 μg/mL and 320 μg/mL for conducting HPLC analysis. The correlation of S_{peak} with verbascoside concentration according to the function $Y = aX + b$ by the method of least squares was investigated. If the correlation coefficient r ≥ 0.9990, the quantitative process has good linearity.[11-13]

2.7.5. Accuracy

Solution without standard addition: the test solution used in the experiment.

Standard addition solution: Take the test solution and add 25 µg/mL, 50 µg/mL and 100 g/mL verbascoside standard quantities to the test sample. Each level of titration was repeated six times.

The verbascoside content is calculated based on the function $Y = aX + b$. The accuracy must be in the range of 98 ÷ 102%, and the range has RSD ≤ 2%.[11-13]

2.7.6. Limit of detection (LOD) and limit of quantification (LOQ)

The test solution is gradually diluted into samples LOD1, LOD2, LOD3, LOD4, etc. In turn, 20 µL of each sample is injected into the HPLC system. The S/N ratio (Signal to Noise ratio) was determined. S is the signal height of verbascoside, and N is the background noise. LOD is accepted at a concentration with S/N = 3. LOQ is accepted at a concentration with S/N = 10.[11-13]

2.8. Data processing

The data were processed using Microsoft Excel 2016 and SPSS statistic 20.0 software for correlation function and statistical processing.

3. RESULTS

3.1. Results of selection of chromatographic conditions

The quantification process of verbascoside was conducted to investigate the chromatographic conditions of the HPLC analytical system. The result was that the suitable chromatographic conditions were selected using a gemini column C18 (250 × 4.6 mm, 5 µm), UV detector 334 nm, mobile phase MeCN - phosphoric acid 0.1% (16/84, v/v), flow rate 0.8 mL/min, injection volume 20 µL, analyte retention time 4, 16 minutes.

3.2. Quantitative process appraisal

3.2.1. Suitability

The results of the suitability assessment of the procedure are presented in Table 1, showing that the relative standard deviations of t_R (RSD = 0.29) and S_{peak} (RSD = 0.30) are both < 2%, so the HPLC system has high suitability and ensures the stability of the verbascosid[12,13] quantification procedure.

Table 1. Results of HPLC system suitability verification.

No	Retention time (Minute)	Peak area (mAU.s)
1	4,15	206159
2	4,16	207190
3	4,17	207115
4	4,15	207103
5	4,18	208113
6	4,17	207201
Xtb	4,16	207146,8
RSD (%)	0,29	0,30

3.2.2. Specificity

The results of the specificity evaluation of the procedure are shown in the chromatogram (SKD) (Figure 1). The blank sample (1) did not give any peak on the SKD. On the test solution (3), a peak with a corresponding retention time compared to the verbascoside tR on the standard solution (2) shows that the verbascoside tR in the two samples (2 and 3) is similar (approx. 4.16 minutes). High specificity HPLC system and test procedure were confirmed.[12,13]

3.2.3. Linear correlation

The results of the correlation evaluation between S_{peak} and verbascoside concentrations showed that they had a very tight linear correlation (r = 0.9997 > 0.9990) and were simulated by

the function $Y = 2349X + 7259.6$. The results of testing the existence of correlation coefficients and parameters show a linear correlation between concentration and peak area ($p \approx 0 < 0.05$).[12,13]
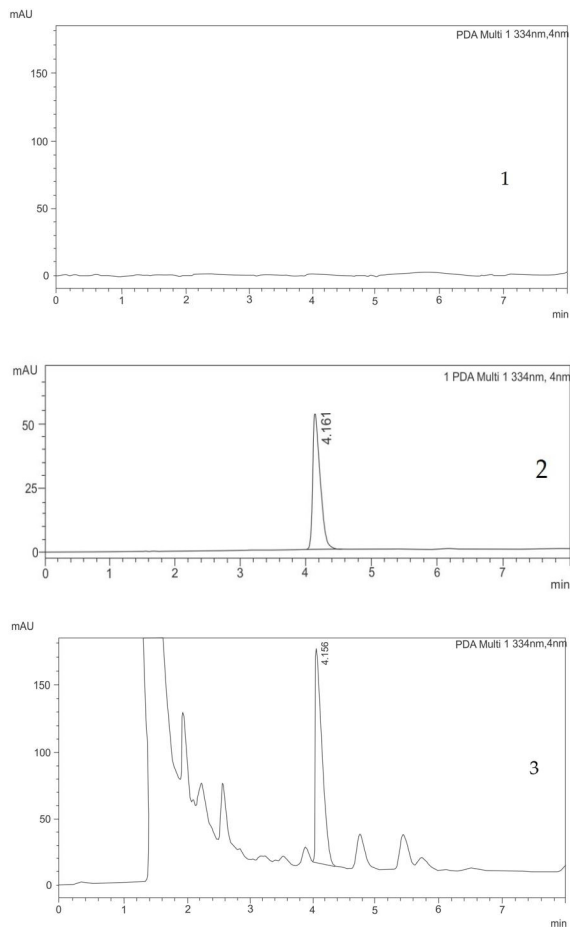

Figure 1. Process specificity assessment chromatogram: (1) White pattern, (2) Standard solution verbascosid, (3) Solution for testing sample.

Table 2. Correlation between S_{peak} and verbascoside concentration.

Concentration (µg/ml)	20	40	80	160	320
S_{pic} (mAU.s)	46870	98620	207103	383595	756511
$Y = 2349X + 7259{,}6$					
$R^2 = 0{,}9994; r = 0{,}9997$					
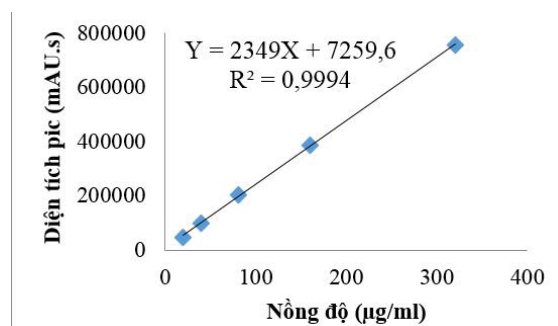
Figure 2. Correlation between S_{peak} and verbascoside concentration.

3.2.4. Repeatability

The repeatability of the procedure was evaluated through 6 replicate tests. The results showed that the average content of verbascoside in the test sample was 0.032%, with RSD = 1.63% < 2%, so the procedure has high repeatability.[12,13]

Table 3. Test solution repeatability evaluation results.

Parameters	Lặp 1	Lặp 2	Lặp 3	Lặp 4	Lặp 5	Lặp 6	Statistics
Weight of sample (g)	0,806	0,815	0,812	0,803	0,819	0,814	Mean (g) = 0,812 RSD (%) = 0,73
Verbascosid content (%)	0,031	0,032	0,032	0,031	0,032	0,032	Mean (%) = 0,032 RSD (%) = 1,63

3.2.5. Accuracy

The results of the procedure correctness evaluation showed that the recovery rate of verbascoside was from 98.24 ÷ 99.64% and within the allowable limit (98 ÷ 102%) with RSD from 1.37 ÷ 1.87% (RSD ≤ 2%), indicating that the procedure has high accuracy.[12,13]

Table 4. Process accuracy.

Time	The concentration of the additional standard (μg/ml)	Recovery concentration (μg/ml)	Accuracy (%)	RSD (%)
Within a day ($n = 6$)	25	24,91	99,64	1,87
	50	49,12	98,24	1,53
	100	98,67	98,67	1,37
Consecutive days ($n = 6$)	25	24,82	99,28	1,84
	50	49,62	99,24	1,65
	100	99,40	99,40	1,51

3.2.6. LOD and LOQ verbascosid

The LOD and LOQ values of verbascoside in the test solution were determined, at a concentration of 1.5 μg/mL producing an S/N ratio of 3 (LOD = 1.5 μg/mL), at a concentration of 4.9 μg/ml producing an S/N ratio of 10 (LOQ = 4.9 μg/mL).

3.2.7. Quantitative results of verbascoside in samples grown in Vinh Phuc, Phu Tho

Applying the validated procedure to quantify verbascoside in the root samples obtained from the *R. glutinosa* varieties 19 grown in Bach Luu - Song Lo - Vinh Phuc and Dan Quyen - Tam Nong - Phu Tho. The results are summarized in Table 5.

Table 5. Results of quantification of verbascoside in the samples grown in Vinh Phuc, Phu Tho.

No	Locations	Verbascosid content (%)
1	Bach Luu - Song Lo - Vinh Phuc	0,028
2	Dan Quyen - Tam Nong - Phu Tho	0,027

The verbascoside content in the *R. glutinosa* varieties 19 samples obtained at all locations was comparable to that of the Vietnam Pharmacopoeia V (verbascoside content $\geq$ 0.02%).

4. DISCUSSION

Verbascoside is a major active ingredient in the *R. glutinosa* and has important biological activities such as anti-inflammatory, re-epithelialization,[3-5] diuretic, antioxidant, wound-healing, and nervous system-protective effects.[3,6,7] This active ingredient is being interested in the development of medicines and supplement foods. Determining verbascoside content in medicinal herbs grown in different locations contributes to assessing the quality of medicinal herbs according to the soil conditions of each region.

The quantification process of verbascoside by the HPLC method has the advantages of high sensitivity, accuracy, reliability, and reasonable cost. Most of the laboratories in Vietnam are equipped with HPLC analysis systems; therefore, this process is easy to apply, it has high popularity in practice testing and evaluating the quality of medicinal herbs. The study was conducted to verify the quantification process of verbascoside in the tubers of the *R. glutinosa* varieties 19. The results showed that the procedure achieved the suitability of the system, good specificity, and a strong linear correlation (r = 0.9997), high recovery rate (99.1%) and high accuracy and repeatability (RSD < 2%), meeting the requirements of the Ministry of Health.[11,12] This result is similar to the research results of some authors, such as Gu et al. (2021), who evaluated the verbascoside content in 33 samples of *R. glutinosa* collected in six provinces of China (Henan, Anhui, Sichuan, Zhejiang, Shandong, Shanxi) by HPLC method that gave the results from 0.020 ÷ 0.26%.[10] The study of Tae et al. quantified verbascoside in 21 samples in Korea and China by HPLC with an average content of 0.07%.[8] Thus, using the HPLC method is suitable for the quantification of verbascoside.

In this study, chromatographic conditions of the HPLC system were used such as the selection of mobile phase acetonitrile (MeCN) - phosphoric acid 0.1% (16/84, v/v), flow rate

0.8 mL/min., an injection volume of 20 µL, measured at 334 nm, is suitable, simple and efficient for determining the presence of verbascoside by HPLC. The process has some different chromatographic conditions compared with some procedures for the quantification of verbascoside described in the Vietnam Pharmacopoeia V, which used the mobile phase solvent system MeCN - acetic acid 0.1%.[2] While the study of Gu. et al. used MeCN - aqueous phosphate system of 0.02%, a flow rate of 1 ml/min, injection volume of 10,[1] measured at wavelength 205 nm,[10] Tae et al. used MeCN–water solvent system, flow rate 0.3 mL/min, injection volume 10 µL, measured at 205 nm,[8] and Li et al. (2020) used a flow rate of 0.5 mL/min.[9]

The process applied in this study to analyze *R. glutinosa* varieties 19 samples grown in Vinh Phuc, Phu Tho gave high suitability. The results of the analysis of real samples showed that the verbascoside content was from 0.027% ÷ 0.028%, the result met the requirements of the Vietnam Pharmacopoeia V (the minimum required verbascoside content was 0.02%).[2] Thus, the *R. glutinosa* varieties 19 planted in Vinh Phuc and Phu Tho produces good quality medicinal herbs, serving as a basis for expanding cultivation in this area.

There are no other publications on the quality evaluation of the *R. glutinosa* varieties 19 grown in Vietnam. The results in this paper will contribute to the development of a quantitative process for verbascoside for the medicinal plant – the *R. glutinosa* varieties 19 grown in Vietnam.

5. CONCLUSION

The study has established a procedure for the quantification of verbascoside in root grown from *R. glutinosa* varieties 19 by HPLC. The results of the process validation showed that there was a strong linear correlation (r = 0.9997) between S_{pic} and verbascoside concentrations, the functional form Y = 2349X + 7259.6. Quantitative results

of verbascoside in the medicinal samples of *R. glutinosa* varieties 19 grown in Vinh Phuc, Phu Tho reached 0.027% ÷ 0.028%, the result met the requirements as prescribed by the Vietnam Pharmacopoeia V.

REFERENCES

1. Department of Crop Production, Ministry of Agriculture and Rural Development. Notice No. 909/TB-TT-CLT dated 31 July 2020 about the announcement of circulation of the variety Dia Hoang 19, 2020.

2. Ministry of Health. *Vietnam Pharmacopoeia V*, Medicine Publishing House, 2017.

3. R. X. Zhang, M. X. Li, Z. P. Jia. *Rehmannia glutinosa:* a review of botany, chemistry and pharmacology, *Journal of Ethnopharmacology,* **2008**, *117*, 199-214.

4. J. H. Lee, J. Y. Lee, H. S. Kang, C. H. Jeong, H. Moon, W. K. Whang. The effect of acetonide on histamine release and arachidonic acid release in RBL-2H3 mast cells, *Archives Pharmacal Research,* **2006**, *29*, 508-513.

5. O. Nigro, A. Tuzi, T. Tartaro, A. Giaquinto, I. Vallini, G. Pinotti. Biological effects of verbascoside and its anti-inflammatory activity on oral mucositis: a review of the literature, *Anti Cancer Drugs*, **2020**, *31*(1), 1-5.

6. W. T. Li, R. X. Deng, X. S. Jing, J. P. Chen, D. Yang, J. G. Shen. Acteoside ameliorates experimental autoimmune encephalomyelitis by inhibiting peroxynitrite-mediated mitophagy activation, *Free Radical Biological Medicines*, **2020**, *146*, 79-91.

7. A. Kalina, K. Liudmila, E. O. Ilkay, I. G. Milen. Verbascoside - A review of its occurrence, (bio) synthesis and pharmacological significance, *Biotechnology Advances*, **2014**, *32*, 1065-1076.

8. H. W. Tae, K. R. Sung, S. K. Sam, S. Jongheon. Simultaneous Analysis of Bioactive Metabolites from *Rehmannia glutinosa* by HPLC-DAD-MS/MS, *Natural Product Sciences,* **2010**, *16*(2), 116-122.

9. H. Y. Li, J. J. Fang, H. D. Shen, X. Q. Zhang, X. P. Ding, J. F. Liu. A quantity-effect research strategy for comparison of antioxidant activity and quality of Rehmanniae Radix and Rehmannia Radix Praeparata by online HPLC-UV-ABTS assay, *BMC Complementary Medicine and Therapies*, **2020**, *20*(16), 1-10.

10. M. Gu, Y. P. Yuan, Z. N. Qin, N. N. Shi, Y. P. Wang, H. Q. Zhai, Z. Z. Qian. A combined quality evaluation method that integrates chemical constituents, appearance traits and origins of raw Rehmanniae Radix pieces, *Chinese Journal of Natural Medicines,* **2021**, *10*(7), 551-560.

11. Ministry of Health. ASEAN guidelines on appraisal of analytical process, Circular 32/2018/TT-BYT Regulating the registration of circulation of drugs and medicinal ingredients, 2018.

12. Drug Management Department. Appendix 8 - Appraisal of analytical procedures by high-performance liquid chromatography (HPLC), decision No. 07/QD-QLD dated 11 January 2013, on the issuance of the Drug Registration Manual.

13. International Conference on Harmonization of Technical Requirements for Registration of Pharmaceuticals for Human Use. Validation of analytical procedures: Text and Methodology, 2005.

Thành phần loài cá rạn san hô vùng biển ven bờ Bắc Hải Vân - Sơn Chà, tỉnh Thừa Thiên Huế

Lê Nguyễn Thới Trung[1], Võ Điều[2,*], Nguyễn Ngọc Hòa[1]

[1]Bảo tàng thiên nhiên Duyên hải miền Trung, Việt Nam
[2]Khoa Thủy sản, Trường Đại học Nông Lâm, Đại học Huế

TÓM TẮT

Nghiên cứu thành phần cá rạn san hô vùng biển ven bờ Bắc Hải Vân - Sơn Chà, tỉnh Thừa Thiên Huế được thực hiện từ tháng 01 năm 2020 đến tháng 10 năm 2022 nhằm mục đích cập nhật dữ liệu, góp phần xây dựng luận chứng khoa học - kỹ thuật cho việc thiết lập khu bảo tồn biển. Vị trí thu mẫu gồm 4 điểm là Bãi Cả, Bãi Chuối, Sũng Rau Câu và đảo Sơn Chà. Mẫu được thu bằng lưới, lừ, vợt và súng bắn tên/xiên theo định kỳ 2 tháng/lần. Kết quả nghiên cứu đã xác định được 142 loài thuộc 94 chi, 48 họ, 23 bộ cá rạn san hô. Trong đó, 5 bộ có số lượng loài cao gồm Perciformes (36 loài), Ovalentaria (20 loài), Kurtiformes (14 loài), Labriformes (13 loài) và Tetraodontiformes (8 loài). Các bộ còn lại chỉ có từ 1 đến 5 loài. Kết quả nghiên cứu cũng cho thấy độ phong phú về thành phần loài cá ở các điểm khảo sát có sự khác nhau. Trong đó, đảo Sơn Chà có độ phong phú về loài cao nhất với 71 loài thuộc 48 chi, 28 họ và 16 bộ; thấp nhất là Bãi Cả với 51 loài thuộc 35 chi, 24 họ và 13 bộ.

Từ khóa: *Cá rạn san hô, Hải Vân - Sơn Chà, đa dạng thành phần loài cá.*

*Tác giả liên hệ chính.
Email: vodieu@huaf.edu.vn hoặc vodieu@hueuni.edu.vn

Species composition of coral reef fish
in the coastal areas of North Hai Van - Son Cha,
Thua Thien Hue province

Le Nguyen Thoi Trung[1], Vo Dieu[2,*], Nguyen Ngoc Hoa[1]

[1]Central Coast Nature Museum, Vietnam
[2]Faculty of Fisheries, University of Agriculture and Forestry, Hue University, Vietnam

ABSTRACT

The study on coral reef fish species composition in the coastal areas of North Hai Van - Son Cha, Thua Thien Hue province was carried out in the period from January, 2020 to October, 2022 at 4 sites, namely Bai Ca, Bai Chuoi, Sung Rau Cau, Son Cha island to update scientific data to contribute to establishing the marine reserve. Fish were collected using fish nets, fish traps, scoops and spears every two months. 142 coral reef fish species belonging to 94 genus, 48 families and 23 orders were found. There were 5 orders with large number of species such as Perciformes (36 species), Ovalentaria (20 species), Kurtiformes (14 species), Labriformes (13 species) and Tetraodontiformes (8 species). Other orders had from 1 to 5 species. Fish species composition abundance was different between the study sites, of which the highest diversity was found at Son Cha island, with 71 species belonging to 48 genus, 28 families and 16 orders while the poorest composition was recorded at Bai Ca, with 51 species belonging to 35 genus, 24 families and 13 orders.

Keywords: *Coral reef fish, Hai Van - Son Cha, fish species composition diversity.*

1. INTRODUCTION

Thua Thien Hue is one of the central provinces with a long coastline and high marine biodiversity, of which North Hai Van - Son Cha is a typical area. According to Nguyen Van Tien and Nguyen Huy Yet,[1] Hai Van - Son Cha (from Lap An lagoon to South Hai Van) has high biodiversity with 245 microalgae species, 74 zooplankton species, and 135 seaweed species, 3 seagrass species, 14 mangrove species, 142 coral species, 303 benthic animal species, 162 coral reef fish species and 4 sea turtle species. Coral reefs are typical ecosystems of this area and are

mostly located at Bai Ca, Bai Chuoi, Bai Dau Heo, Sung Rau Cau, West Son Cha, Northwest Son Cha and South Hai Van.

Based on the high biodiversity, Hai Van - Son Cha was proposed to establish a marine protected area in 1998 (Nguyen Chu Hoi et al.).[2] In this proposal, Hai Van - Son Cha marine reserve composes three areas in the south of Phu Loc district, Thua Thien Hue province, namely Son Cha island, Lang Co lagoon and North Hai Van. The total area of the proposed reserve is about 6,000 - 7,000 ha. Then, Nguyen Van Tien and Nguyen Huy Yet[1] investigated

---

*Corresponding author.

Email: vodieu@huaf.edu.vn or vodieu@hueuni.edu.vn

to collect scientific evidence and submitted the People's Committee of Thua Thien Hue province the proposal to establish Hai Van - Son Cha as marine reverse with a total area of 9,503 ha (from Lap An lagoon to South Hai Van). Throughout additional surveys, Hai Van - Son Cha was officially involved in the list of 16 marine reserves approved by the Prime Minister in 2010 (Decision No. 742/QĐ-TTg).[3] The total area of this reserve is 17,039 ha, of which the marine area is 7,626 ha. Up to now, most of the marine protected areas in the central region in the list approved by the Prime Minister have been established such as Con Co, Cu Lao Cham, Ly Son, Nha Trang Bay, Nui Chua, Hon Cau but not for Hai Van - Son Cha.

The coastal areas of North Hai Van - Son Cha is an important fishing ground for 38.5% of households living in Lang Co and the surrounding areas (Le Thi Nguyen and Nguyen Bac Giang).[4] In addition, this area is also the fishing ground of many fishermen in Lien Chieu district, Da Nang city (Nguyen Van Tien and Nguyen Huy Yet).[1] Therefore, the pressure from exploitation on biodiversity and ecosystems in general and on coral reef fish resource of this sea in particular is very large. However, because Hai Van – Son Cha has not been established as a conservation area, biodiversity in this area in general and coral reef fish in particular has not been properly managed and exploited.

This study aimed to update data and contribute to building scientific evidences to establish the Hai Van – Son Cha marine reserve in Thua Thien Hue province.

2. METHODS

2.1. Study sites and period

Study period: This study was conducted in the period of 01/2020 - 10/2022.

Study sites: Fish were collected at 4 sites in the coastal areas of North Hai Van, Thua Thien Hue province (Table 1 and Figure 1).

Table 1. Sample collection sites.

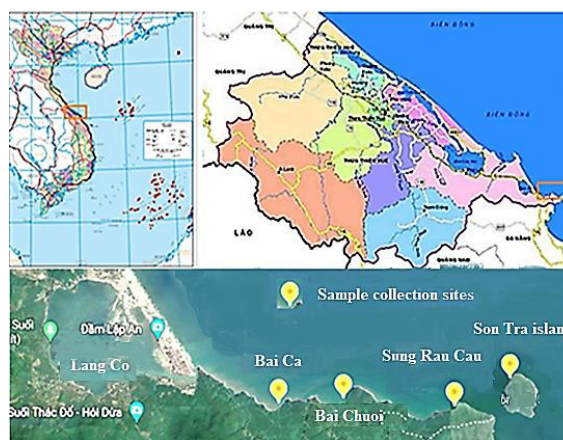| No.	Sites	Longitude	Latitude
1	Bai Ca	108,12152°	16,21450°
2	Bai Chuoi	108,14370°	16,21628°
3	Sung Rau Cau	108,18161°	16,21332°
4	Son Cha island	108,20192°	16,22358°

Figure 1. Sample collection sites.

2.2. Sample collection

Fish were collected at the study sites every 2 months (total of 16 times of sampling) using fishing gears such as gillnets, scoops, spears. A total of 726 fish individuals were collected.

After collection, fish were washed and kept into the frozen containers and transferred to the preliminary sample analysis site in the field. Here, fish were preliminarily classified according to their morphology. Then 6-8 individuals were selected to take pictures and tag the sample code. Then, these fish were fixed in 10% formalin solution and transferred to the Central Coast Nature Museum, KQH7 (Diem Phung Thi Street, Vy Da ward, Hue city, Thua Thien Hue Province) for analysis.

2.3. Sample analysis

Fish were classified using morphological methods. The fish classification documents of

authors as Nguyen Huu Phung et al.,[5-8] Mansor et al.,[9] Rainboth et al.[10] and Nelson[11] were used.

In addition, the website http://www.fishbase.org was also used to update fish classification information. The fish taxon was based on the method of Nelson.[11]

3. RESULTS AND DISCUSSION

3.1. Fish species composition diversity

In the study period, 142 coral reef fish species belonging to 94 genus, 48 families and 23 orders were found in North Hai Van – Son Cha (Table 2).

Table 2. The list of coral reef fish species in the coastal areas of Hai Van – Son Cha.

Number	Order/ Subseries	Number	Species
I	**Anguilliformes**	1	*Pisodonophis boro* (Hamilton, 1822)
		2	*Gymnothorax undulatus* (Lacepède, 1803)
II	**Clupeiformes**	3	*Encrasicholina punctifer* (Fowler, 1938)
		4	*Stolephorus* sp.
		5	*Stolephorus commersonnii* (Lacepède, 1803)
		6	*Sardinella gibbosa* (Bleeker, 1849)
III	**Siluriformes**	7	*Plotosus* sp.
		8	*Plotosus lineatus* (Thunberg, 1787)
IV	**Aulopiformes**	9	*Synodus dermatogenys* (Fowler, 1912)
		10	*Trachinocephalus myops* (Forster, 1801)
V	**Holocentriformes**	11	*Myripristis pralinia* (Cuvier, 1829)
		12	*Sargocentron praslin* (Lacepède, 1802)
		13	*Sargocentron rubrum* (Forsskål, 1775)
		14	*Sargocentron melanospilos* (Bleeker, 1858)
VI	**Kurtiformes**	15	*Apogon imberbis* (Linnaeus, 1758)
		16	*Apogonichthyoides taeniatus* (Cuvier, 1828)
		17	*Cheilodipterus macrodon* (Lacepède, 1802)
		18	*Jaydia melanopus* (Weber, 1911)
		19	*Lepidamia kalosoma* (Bleeker, 1852)
		20	*Ostorhinchus aureus* (Lacepède, 1802)
		21	*Ostorhinchus cookii* (Macleay, 1881)
		22	*Ostorhinchus doederleini* (Jordan & Snyder, 1901)
		23	*Ostorhinchus endekataenia* (Bleeker, 1852)
		24	*Ostorhinchus lateralis* (Valenciennes, 1832)
		25	*Ostorhinchus semilineatus* (Temminck & Schlegel, 1842)
		26	*Ostorhinchus compressus* (Smith & Radcliffe, 1911)
		27	*Ostorhinchus fasciatus* (White, 1790)
		28	*Taeniamia fucata* (Cantor, 1849)

VII	Gobiiformes	29	*Butis butis* (Hamilton, 1822)
		30	*Oxyurichthys* sp.
		31	*Glossogobius giuris* (Hamilton, 1822)
VIII	Ovalentaria	32	*Ambassis kopsii* (Bleeker, 1858)
		33	*Chromis margaritifer* (Fowler, 1946)
		34	*Chromis xanthura* (Bleeker, 1854)
		35	*Dascyllus trimaculatus* (Rüppell, 1829)
		36	*Neoglyphidodon melas* (Cuvier, 1830)
		37	*Neoglyphidodon nigroris* (Cuvier, 1830)
		38	*Neopomacentrus azysron* (Bleeker, 1877)
		39	*Neopomacentrus cyanomos* (Bleeker, 1856)
		40	*Plectroglyphidodon leucozonus* (Bleeker, 1859)
		41	*Pomacentrus brachialis* (Cuvier, 1830)
		42	*Pomacentrus coelestis* (Jordan & Starks, 1901)
		43	*Pomacentrus flavioculus* (Allen, Erdmann & Pertiwi, 2017)
		44	*Pomacentrus moluccensis* (Bleeker, 1853)
		45	*Pomacentrus simsiang* (Bleeker, 1856)
		46	*Stegastes obreptus* (Whitley, 1948)
		47	*Stegastes* sp.
		48	*Abudefduf saxatilis* (Linnaeus, 1758)
		49	*Abudefduf sexfasciatus* (Lacepède, 1801)
		50	*Abudefduf sordidus* (Forsskål, 1775)
		51	*Amphiprion clarkii* (Bennett, 1830)
IX	Mugiliformes	52	*Osteomugil cunnesius* (Valenciennes, 1836)
		53	*Upeneus sulphureus* (Cuvier, 1829)
X	Blenniiformes	54	*Aspidontus* sp.
		55	*Aspidontus taeniatus* (Quoy & Gaimard, 1834)
		56	*Cirripectes filamentosus* (Alleyne & Macleay, 1877)
		57	*Istiblennius edentulus* (Forster & Schneider, 1801)
		58	*Meiacanthus* sp.
XI	Atheriniformes	59	*Atherinomorus lacunosus* (Forster, 1801)
XII	Beloniformes	60	*Hemiramphus lutkei* (Valenciennes, 1847)
		61	*Hyporhamphus quoyi* (Valenciennes, 1847)
XIII	Carangiformes	62	*Alepes apercna* (Grant, 1987)
		63	*Alepes djedaba* (Forsskål, 1775)
		64	*Selaroides leptolepis* (Cuvier, 1833)
		65	*Trachinotus mookalee* (Cuvier, 1832)

XIV	**Istiophoriformes**	66	*Sphyraena barracuda* (Cuvier, 1832)
		67	*Sphyraena obtusata* (Cuvier, 1829)
XV	**Pleuronectiformes**	68	*Brachirus niger* (Macleay, 1880)
		69	*Solea elongata* (Day, 1877)
		70	*Cynoglossus bilineatus* (Lacepède, 1802)
XVI	**Syngnathiformes**	71	*Fistularia commersonii* (Rüppell, 1838)
		72	*Dactyloptera orientalis* (Cuvier, 1829)
XVII	**Labriformes**	73	*Cheilinus trilobatus* (Lacepède, 1801)
		74	*Halichoeres bicolor* (Bloch & Schneider, 1801)
		75	*Halichoeres hortulanus* (Lacepède, 1801)
		76	*Halichoeres marginatus* (Rüppell, 1835)
		77	*Labroides dimidiatus* (Valenciennes, 1839)
		78	*Macropharyngodon meleagris* (Valenciennes, 1839)
		79	*Stethojulis interrupta terina* (Jordan & Snyder, 1902)
		80	*Stethojulis* sp.
		81	*Stethojulis terina* (Jordan & Snyder, 1902)
		82	*Thalassoma lunare* (Linnaeus, 1758)
		83	*Leptoscarus vaigiensis* (Quoy & Gaimard, 1824)
		84	*Scarus rivulatus* (Valenciennes, 1840)
		85	*Scarus psittacus* (Forsskål, 1775)
XVIII	**Perciformes**	86	*Gerres oyena* (Forsskål, 1775)
		87	*Parupeneus heptacanthus* (Lacepède, 1802)
		88	*Upeneus tragula* (Richardson, 1846)
		89	*Pempheris oualensis* (Cuvier, 1831)
		90	*Therapon jarbua* (Forsskål, 1775)
		91	*Rhynchopelates oxyrhynchus* (Temminck & Schlegel, 1842)
		92	*Cephalopholis boenak* (Bloch, 1790)
		93	*Aethaloperca rogaa* (Forsskål, 1775)
		94	*Diploprion bifasciatum* (Cuvier, 1828)
		95	*Epinephelus merra* (Bloch, 1793)
		96	*Epinephelus sexfasciatus* (Valenciennes, 1828)
		97	*Hyporthodus septemfasciatus* (Thunberg, 1793)
		98	*Siganus guttatus* (Bloch, 1787)
		99	*Monodactylus argenteus* (Linnaeus, 1758)
		100	*Eubleekeria* sp.
		101	*Karalla daura* (Cuvier, 1829)
		102	*Leiognathus equulus* (Forsskål, 1775)
		103	*Chaetodon auriga* (Forsskål, 1775)
		104	*Chaetodon auripes* (Jordan & Snyder, 1901)

		105	*Chaetodon speculum* (Cuvier, 1831)
		106	*Chaetodon trifascialis* (Quoy & Gaimard, 1825)
		107	*Chaetodon wiebeli* (Kaup, 1863)
		108	*Lutjanus argentimaculatus* (Forsskål, 1775)
		109	*Lutjanus johni* (Bloch, 1792)
		110	*Lutjanus* sp1.
		111	*Lutjanus* sp2.
		112	*Lutjanus vitta* (Quoy & Gaimard, 1824)
		113	*Lutjanus* sp3.
		114	*Lutjanus fulviflamma* (Forsskål, 1775)
		115	*Caesio cuning* (Bloch, 1791)
		116	*Siganus canaliculatus* (Park, 1797)
		117	*Siganus javus* (Linnaeus, 1766)
		118	*Siganus spinus* (Linnaeus, 1758)
		119	*Siganus virgatus* (Valenciennes, 1835)
		120	*Sigunus canaliculatus* (Park, 1797)
		121	*Scatophagus argus* (Linnaeus, 1766)
XIX	**Scorpaeniformes**	122	*Parascorpaena mossambica* (Peters, 1855)
		123	*Scorpaenodes evides* (Jordan & Thompson, 1914)
		124	*Scorpaenopsis cirrosa* (Thunberg, 1793)
		125	*Sebastapistes cyanostigma* (Bleeker, 1856)
		126	*Minous inermis* (Alcock, 1889)
XX	**Moroniformes**	127	*Drepane punctata* (Linnaeus, 1758)
XXI	**Acanthuriformes**	128	*Zanclus cornutus* (Linnaeus, 1758)
		129	*Ctenochaetus striatus* (Quoy & Gaimard, 1825)
XXII	**Spariformes**	130	*Sillago aeolus* (Jordan & Evermann, 1902)
		131	*Sillago sihama* (Forsskål, 1775)
		132	*Scolopsis ciliata* (Lacepède, 1802)
		133	*Scolopsis vosmeri* (Bloch, 1792)
		134	*Lethrinus nebulosus* (Forsskål, 1775)
XXIII	**Tetraodontiformes**	135	*Ostracion cubicus* (Linnaeus, 1758)
		136	*Cantherhines pardalis* (Rüppell, 1837)
		137	*Cantherhines* sp.
		138	*Pervagor alternans* (Ogilby, 1899)
		139	*Monacanthus chinensis* (Osbeck, 1765)
		140	*Arothron immaculatus* (Bloch & Schneider, 1801)
		141	*Rhynchostracion nasus* (Bloch, 1785)
		142	*Diodon hystrix* (Linnaeus, 1758)

Of 23 orders, Perciformes was most dominant in all taxon levels, taking account 25% in family, 24.5% in genus and 25.7% in species level, followed by Ovalentaria (13.9%), Kurtiformes (10.4%), Labriformes (9.2%), Tetraodontiformes (5.6%) in total of species. Number of species of Blenniiformes, Scorpaeniformes and Spariformes took account 3.5%. The lowest percentage in species (0.7%) was found in orders Moroniformes and Atheriniformes. Other orders held 1.4% to 2.8% in total of species (Table 3).

Table 3. Number of orders, families, and genus of fish in the coastal areas of North Hai Van – Son Cha.

Number	Order	Family		Genus		Species	
		n	Percentage	n	Percentage	n	Percentage
1	Anguilliformes	2	4.2	2	2.1	2	1.4
2	Clupeiformes	2	4.2	3	3.2	4	2.8
3	Siluriformes	1	2.1	1	1.1	2	1.4
4	Aulopiformes	1	2.1	2	2.1	2	1.4
5	Holocentriformes	1	2.1	2	2.1	4	2.8
6	Kurtiformes	1	2.1	6	6.4	14	9.9
7	Gobiiformes	2	4.2	3	3.2	3	2.1
8	Ovalentaria	2	4.2	9	9.6	20	14.1
9	Mugiliformes	1	2.1	2	2.1	2	1.4
10	Blenniiformes	1	2.1	4	4.3	5	3.5
11	Atheriniformes	1	2.1	1	1.1	1	0.7
12	Beloniformes	1	2.1	2	2.1	2	1.4
13	Carangiformes	1	2.1	3	3.2	4	2.8
14	Istiophoriformes	1	2.1	1	1.1	2	1.4
15	Pleuronectiformes	2	4.2	3	3.2	3	2.1
16	Syngnathiformes	2	4.2	2	2.1	2	1.4
17	Labriformes	2	4.2	8	8.5	13	9.2
18	Perciformes	12	25.0	23	24.5	36	25.4
19	Scorpaeniformes	2	4.2	4	4.3	5	3.5
20	Moroniformes	1	2.1	1	1.1	1	0.7
21	Acanthuriformes	2	4.2	2	2.1	2	1.4
22	Spariformes	3	6.3	3	3.2	5	3.5
23	Tetraodontiformes	4	8.3	7	7.4	8	5.6
	Total	**48**	**100**	**94**	**100**	**142**	**100**

There have been many studies on coral reef fish composition diversity in Vietnam in general as well as in Central Vietnam in particular, but there has been no such records in the coastal areas of North Hai Van – Son Cha. Compared to other studies, the species abundance of fish in our study areas is lower than that in Cu Lao Cham island (Nguyen Van Long et al.),[12] Ly Son island (Hoang Xuan Ben et al.),[13] but higher than that in Con Co (Tran Van Huong et al.).[14] Cu Lao Cham and Ly Son have been establishes as the marine reserves so organism resource can be well protected and this can be one of reasons leading to the high diversity of coral reef fish here (Table 4).

Table 4. The comparison of number of species of coral reef fish in the coastal areas in Central Vietnam.

Number	Areas	Number of species	References
1	Hai Van – Son Cha	142	This study
2	Cu Lao Cham	267	Nguyen Van Long et al. [12]
3	Con Co	104	Tran Van Huong et al. [14]
4	Ly Son	232	Hoang Xuan Ben et al. [13]

There were 142 species of coral reef fish found in our study that is less than records of Nguyen Van Tien and Nguyen Huy Yet[1] (162 species were found in Hai Van – Son Cha, of which there were 21 species not identified). This difference can be due to different study areas. We just investigated in the North Hai Van – Son Cha while Nguyen Van Tien and Nguyen Huy Yet[1] collected samples in the North Hai Van – Son Cha and 5 sites in the South Hai Van belonging to Da Nang city.

3.2. The coral reef fish composition distribution at the study sites

The results showed that number of orders, families, genus and species of fish was different between the study sites (Figure 2).

Figure 2. The coral reef fish composition distribution in the North Hai Van – Son Cha.

The abundance of coral reef fish composition at Son Cha island was highest (Figure 2), with 71 species belonging to 48 genus, 28 families and 16 orders. There were 61 species belonging to 49 genus, 32 families and 17 orders found at Sung Rau Cau, 52 species, 36 genus, 19 families and 14 orders found at Bai Chuoi. The lowest abundance of fish was recorded at Bai Ca, with 51 species, 35 genus, 24 families and 13 orders.

Nguyen Van Tien and Nguyen Huy Yet[1] reported that the highest diversity of fish species composition was at Sung Rau Cau (84 species), followed by Bai Chuoi (54 species) and the abundance of fish composition at the areas around Son Cha island was low, with 23 species (Northwest Son Cha) and 49 species (West Son Cha). However, our results (Table 5 and Figure 2) show the rich fish composition at the areas around Son Cha (71 species), Sung Rau Cau (61 species) and Bai Chuoi (52 species). It is speculated that Son Cha has been well managed so illegal fishing activities are reduced, leading to the ecosystems are better protected in comparison to other areas. However, this is our preliminary speculation and it is necessary to do surveys on coral reef coverage and fishing status in this area in order to give accurate evidences.

4. CONCLUSION AND SUGGESTION

There were 142 coral reef fish species belonging to 94 genus, 48 families and 23 orders found in the coastal areas of North Hai Van – Son Cha. Among them, Perciformes was dominant, with 36 species, 23 genus and 12 families.

In the North Hai Van – Son Cha, the most abundant composition of coral reef fish was at Son Cha island, with 71 species, 48 genus, 28 families and 16 orders.

REFERENCES

1. N. V. Tien and N. H. Yet. *Scientific and technical argument for establishing Son Cha - Hai Van marine reserve*, Department of Science and Technology of Thua Thien Hue, 2004.

2. N. C. Hoi, N. H. Yet and D. N. Thanh. *Scientific basis for marine protected areas planning*, Hai Phong: Hai Phong Institute of Oceanography, in Vietnamese, 1998.

3. Decision No. 742/QĐ-TTg of the Prime Minister for approving the planning of the system of marine reserves of Vietnam until 2020, issued on May 26, 2010.

4. L. T. Nguyen and N. B. Giang. The aquatic resources exploitation status in the coastal waters of North Hai Van and the consequences of establishing Son Tra marine reserve, *Journal of Geology*, **2006**, *296*, 119-124.

5. N. H. Phung and N. N. Thi. *The list of Vietnamese marine fish. Volume II. Class of bony fish (Osteichthyes). From the order Elopiformes to the order Mugiliformes,* Hanoi Science and Technology Publishing House, 1994.

6. N. H. Phung, L. T. Phan, N. N. Thi, N. P. Dinh, D. T. N. Nhung and N. V. Luc. *The list of Vietnamese marine fish. Volume III. Order Perciformes. Suborder Percoidei and Echeneoidei,* Hanoi Science and Technology Publishing House, 1995.

7. N. H. Phung, N. N. Thi, N. P. Dinh, D. T. N. Nhung. *The list of Vietnamese marine fish. Volume IV. Order Perciformes. Suborder Percoidei. From Labroidei to Stromateoidei,* Hanoi Science and Technology Publishing House, 1997.

8. N. H. Phung. *The list of Vietnamese marine fish. Volume V. Order Scorpaeniformes, Pleuronectiformes, Tetraodontiformes, Lophiformes, Batrachoidiformes and Pegasiformes,* Hanoi Science and Technology Publishing House, 1999.

9. M. I. Mansor, H. Kohno, H. Ida, H. T. Nakamura, Z. Aznan and S. Abdullah. *Field Guide to Important Commercial Marine fish of the South China sea*. SEAFDEC/MFRDMD, 1998.

10. W. J. Rainboth, C. Vidthayanon and M. D. Yen. *Fish of the greater Mekong ecosystem with species list and photographic Atlas*, Miscellaneous Publication Museum of Zoology University of Michigan, 2012.

11. J. S. Nelson, T. C. Grande, and M. V. H. Wilson. *Fishes of the World* (Fifth Edition), Wiley & Sons, Hoboken, New Jersey, USA, 2016.

12. N. V. Long, V. S. Tuan, N. V. Vu. Species diversity and the status of some typical ecosystems in Cu Lao Cham marine reserve, Quang Nam province, *Journal of Marine Science and Technology*, **2021**, *21*(2), 201–213.

13. H. X. Ben, N. V. Long, H. T. Tuyen, P. K. Hoang and T. M. Quang. Biodiversity and characteristics of coral reef communities in Ly Son marine reserve, Quang Ngai, *Journal of Marine Science and Technology*, **2018**, *18*(2)*,* 150-160.

14. T. V. Huong, D. A. Duy, N. V. Long and T. M. Quang. The status of biodiversity and coral reef fish density in Con Co marine reserve, Quang Tri province, *Journal of Agriculture and Rural Development,* **2020**, 122-131.

MỤC LỤC